NASA Technical Memorandum 104749

Comparison of Continuous and Discontinuous Collisional Bumpers: Dimensionally Scaled Impact Experiments into Single Wire Meshes

Friedrich Hörz
Mark Cintala
Lyndon B. Johnson Space Center
Houston, Texas

Thomas See
Ronald Bernhard
Frank Cardenas
William Davidson
Jerry Haynes
Lockheed Engineering and Sciences Company
Houston, Texas

National Aeronautics and Space Administration
Lyndon B. Johnson Space Center
Houston, Texas

April 1992

ABSTRACT

An experimental inquiry into the utility of discontinuous bumpers was conducted with the objective to investigate the collisional outcomes of impacts into single grid-like targets and to compare the results with more traditional bumper designs that employ continuous sheet stock. We performed some 35 experiments using 6.3 and 3.2 mm diameter (D_p) spherical soda lime glass projectiles at low velocities (< 2.5 km/s), and 13 experiments at velocities between 5 and 6 km/s, using 3.2 mm spheres only. The thrust of the experiments related to the characterization of collisional fragments as a function of target thickness (T) or areal shield mass (m_A; g/cm^2) of both bumper designs. The primary experimental variables were target thickness T, scaled to projectile dimensions via the parameter D_p/T that ranged from 2 to 12, and impact velocity (1 to 6 km/s). We also started to explore the utility of multiple, successive wire meshes; the latter are expected to comminute all collisional fragments.

The primary product of these experiments were witness plates that faithfully record the resulting population of collisional fragments. The largest crater on such plates reflects the single, most kinetic fragment (F_{max}), that is transmitted (or caused) by the bumper; the continuous and discontinuous bumpers yield comparable F_{max}. The discontinuous bumper produces, however, fewer numbers of debris particles, a favorable property. On the other hand, the areal distribution of these particles is distinctly lumped for grid-like bumpers, reflecting the target's heterogeneous mass-distribution; the latter leads to localized energy concentrations on the witness plates that is distinctly undesirable for any bumper. However, the few experiments which employed multiple meshes demonstrate that they accomplish additional comminution and dispersion of the debris cloud. A pictorial summary-comparison between continuous, single- and multiple grid targets is shown in Figures 31 and 32 at the end of this report.

The mass displaced from the target (m_T) was determined by difference from the weights measured before and after each experiment. Also, the experiments were designed to permit physical collection and weighing of loose debris, separated into "uprange" ("ejecta" of mass m_E) and "downrange" ("spall products" of mass m_S) components. The discontinuous, single grids yielded consistently smaller dislodged masses m_T, m_E and m_S at equivalent experimental conditions, frequently outperforming the continuous bumper by mass-differences approaching factors of 5, if not order of magnitude (see Figures 24-28).

Substantial interpretative and predictive insights into bumper performance were obtained. All qualitative observations (on the witness plates) and detailed measurements of displaced masses seem simply and consistently related only to total bumper mass (m_A) available for interaction with the impactor. This renders the grid bumper into the superior shield design, due to its favorable areal mass (g/cm^2) at equivalent thickness D_p/T. The use of multiple meshes accomplishes additional debris comminution, and will also lead to sufficient dispersion of the newly discovered and undesirable, highly localized fragment distributions produced by the first grid. These findings present evidence that discontinuous bumpers are a viable concept for collisional shields, possibly superior to continuous geometries, and that they deserve additional, concerted study.

INTRODUCTION

This work takes off from the viewpoint that there is no theoretical need to have an effective meteorite bumper constructed from contiguous metal or any other sheet-like, quasi-infinitive material, the traditional approach in ongoing bumper developments (*e.g.*, Anderson, 1987, 1989 or Christiansen, 1990). Instead this study suggests that the lateral extend of the bumper can be limited and may be scaled to projectile dimensions. It specifically argues that the lateral extend of any bumper must not be greater than its thickness. This concept then leads to the suggestion that any regular grid or mesh may be suitable. If this premise were correct, substantial bumper-mass may be saved, which in turn could lead to significant cost savings, due to decreased launch mass, to provide collisional protection of flight systems in space.

Ongoing bumper developments primarily evaluate the thickness (T) per any given material that may lead to a desired degree of projectile deceleration, fragmentation and dispersion, such that the energy density (ergs/cm^2) of the resulting debris cloud is lower than some threshold value acceptable to a specific flight system (see Christiansen, 1990, or Anderson, 1990). Regular grids or any other discontinuous solid will also decelerate, fragment and disperse any hypervelocity impactor provided they satisfy certain geometric constraints as schematically illustrated in Figure 1. Mesh opening (M) must be related to the diameter (D_p) of a prospective projectile against which protection is sought by $M < D_p$; this assures that the projectile makes contact with a solid. This condition results naturally from any grid fabricated from a material of thickness T and when center-to-center mesh distances (M_c) are $M_c = D_p$. This geometry generates the condition $M = (M_c - T)$ and therefore the condition $M < D_p$. Any impactor of diameter D_p or larger must therefore interact with the grid.

It is furthermore suggested -- as illustrated in Figure 1 -- that any number of meshes, of successively smaller mesh-openings and thicknesses, may be stacked to interact with the debris cloud generated by the first, most massive grid. The idea here is that multiple interaction of high-speed debris with successive grids will lead to additional comminution, deceleration and dispersion of projectile fragments. Cour-Palais and Crews (1990) demonstrate the effects of successive penetrations of stacked, thin films, and similar effects were observed in space-exposed, thermal blankets retrieved from the Solar Maximum satellite (*e.g.*, Warren *et al.*, 1989) and the Long Duration Exposure Facility (*e.g.*, see *et al.*, 1990).

The above patent suggests, however, that stacked grids have variable thickness and mesh-openings, starting with a most massive mesh and then decreasing continually as per Figure 1. Ideally, the last stack-member, having the smallest mesh-opening (M_{min}), defines the largest fragment size (F_{max}) that may pass the entire bumper (*i.e.*, $F_{max} < M_{min}$). As a consequence, F_{max}, may be engineered commensurate with the protection-requirement of a specific flight system. Successive grids of systematically decreasing mesh-openings are, of course, also needed to protect against the wide range of impactor masses existing in space. The above requirement of $F_{max} < M_{min}$ applies to primary impactors as well (*i.e.*, $D_{Pmin} = F_{max}$ or $D_{Pmin} < M_{min}$).

The crucial question for discontinuous bumpers -- as it is for continuous bumpers -- relates to its absolute thickness T, because the latter defines the absolute mass available for interaction with the impactor to produce some desired degree of fragmentation, and it defines, ultimately, the ballistic limit of a continuous bumper (*e.g.*, Cour-Palais, 1987). Bumper-thickness (or mass) determined from experiments that employ contiguous metal sheets will directly apply also to the grid solids. If both discontinuous and continuous bumpers are made from the same material of thickness T, identical shock-stresses will be set up in the projectile at any given encounter velocity and shock-pulse duration will be identical as well. Identical shock-stress and pulse durations should therefore yield identical fragmentation products of any model impactor.

The above equivalence of T in both continuous and discontinuous bumpers is correct as far as initialization of the shock wave is concerned, but there are differences in how this shock wave propagates and how material flow fields in the target may be set in motion. The shock is permitted to freely expand centrosymmetrically in the case of continuous bumpers, including radial ranges $>> D_p$. In contrast, this is not the case for the discontinuous bumpers, where flows are inhibited by free surfaces of typical distances $< D_p$. As a consequence, energy partitioning between continuous and discontinuous bumpers may differ.

Also, the idealized equivalence of T in both continuous and discontinuous bumpers is valid only for vertical impacts that occur on the center-line of any solid grid element of thickness T. Typical impacts will not occur at this idealized site, but at any arbitrary location with regard to the specific profile constituting a mesh bumper. This, de facto, causes a shock-geometry consistent with oblique impact; the latter may decrease the shock stress and pulse duration, yet details are poorly understood.

It is difficult to predict how the above deviations from the ideal equivalence of T in both bumper designs affect the phenomenology of the collisional event. An experimental study was therefore initiated with the objective to determine the degree of projectile fragmentation and dispersion upon collisions with single grids, and to compare the results with equivalent experiments into contiguous membranes. This experimental comparison constituted the objective of this report; the effects of multiple stacked meshes were to comprise the major thrust for year two.

Embedded in this study is the concept of "dimensional scaling" which has been successfully applied to a wide variety of impact phenomena (*e.g.*, Holsapple and Schmidt, 1982; Gurson, 1990). It fundamentally states that linear dimensions of impactor and targets may be used to predict collisional outcomes at scales beyond those practical in the laboratory. Within the context of this study, the diameter of a prospective projectile becomes the most crucial dimension, because it controls all geometric elements of the target, owing to the requirement of $M<D_p$.

It is important to note, that the suggestion of dimensionally scaled, stacked meshes as illustrated in Fig. 1, differs from the utilization of a single mesh advocated by Christiansen (1990) to provide effective shielding. The latter concept envisions the use of a single mesh of $M << D_p$ to accomplish projectile disintegration, yet a solid shield is employed towards the rear for additional fragmentation, dispersion and deceleration of the impactor. As per Fig. 1, we do not include such contiguous solids in our shield-design. It is nevertheless clear that parametric experimentation with a single mesh -- the subject of this study -- will be beneficial to both shield concepts.

BACKGROUND EXPERIMENTS

Figure 2 illustrates schematically the objectives of background experiments in contiguous targets that explored the style and degree of projectile fragmentation during penetration of single foils that have systematically decreasing thicknesses (T). Because these experiments are well analyzed, they constitute the major rationale and empirical framework for the multiple mesh-concept; they are therefore summarized briefly in this chapter.

The dimensions of penetration holes produced by projectiles of 50 μm, 150 μm, 1000 μm (1 mm) and 3200 μm (1/8") projectiles upon impact, at a nominal 6 km/s, with aluminum (series 1100; annealed) membranes of decreasing thickness (D_p/T) are illustrated in Figure 3. Note that penetrations at massive target plates resemble in essence truncated craters. Also, it generally takes $D_p/T > 30$ to produce a comparatively small hole that approaches projectile diameter. The general morphology of all penetration holes seems sensitively related to absolute foil thickness and morphologic changes are gradual, such as effective hole size or relative width of the crater lip. The morphologic similarity at any given D_p/T, regardless of impactor size and other absolute dimensions, seems strikingly evident, adding substantial credence to the concept of dimensional scaling embodied in the multiple mesh bumper concept.

The quantitative diameter measurements of penetration holes (D_h) and their relation to projectile diameter and absolute foil thickness are illustrated in Figure 4. Note, that D_h and T can be measured on any space exposed membrane and that this graph, therefore, may serve as a (new) "calibration" plot to solve for the initial projectile diameter, D_p, from a measured hole diameter (*e.g.*, Carey *et al.*, 1985). More important in the context of this report, however, is again the conclusion, that "dimensional" scaling seems to work for impactor sizes that vary by almost 2 orders of magnitude. The latter include, at the large end, direct observations of impactors > 1 mm and they, therefore, directly apply to impactors considered a substantial threat to spacecraft.

Following the diameter measurements and knowing the absolute target thickness, we calculated the volume of the penetration holes (V_t). The results are illustrated in Figure 5, grouped by projectile size and with V_t normalized to

projectile volume (V_p). The dashed lines represent interpolations at constant D_p/T. The purpose of this figure is to demonstrate that volumes substantially larger than projectile volumes are being generated at essentially all $D_p/T < 5$. This, also suggests, that substantially more mass is displaced from the target itself, relative to the incoming projectile, for all targets of $D_p/T < 5$. However, the relation between penetration hole volume and total mass displaced is not known exactly and not necessarily linear proportional to the relative volume: the target is being plastically deformed and there are substantial lip areas (*e.g.*, Fig. 3) that accommodate unknown fractions of the displaced volume or mass. This is especially the case at massive targets, where wholesale plastic deformation of the target, in the immediate vicinity of the penetration hole, is observed. At thinner foils, substantial mass movement and plastic deformation subsides, *e.g.*, for the condition of $D_h = D_p$, close correspondence results between relative volumes and relative displaced mass.

The purpose of Fig. 5 is to demonstrate that "massive" bumpers typically shed more mass than that represented by the impactor itself, clearly an undesirable characteristic. There are thus technical arguments as well, that make relatively thin bumpers desirable, in addition to fiscal concerns related to launch cost of massive bumpers and which also decrease the effective payload mass that may be launched. Nevertheless, some mass is needed to fragment and decelerate the impactors, and bumpers of effective thickness $D_p/T > 5$ are rarely considered in current bumper developments (*e.g.*, Christiansen, 1990). Clearly compromise solutions must be found for bumper thicknesses that shed a minimum of mass while providing the desired degree of collisional protection.

The requirement for thin foils raises the question of what threshold thickness suffices to sufficiently decelerate and fragment the impactors? Figures 6 and 7 illustrate witness plates, mounted to the targets' rear, that received the full brunt of all downrange debris. Obviously, this debris would interact with a flight system if it were to be protected by a continuous bumper of specific D_p/T values.

It is important to note that the spray patterns illustrated in Figures 6 and 7 are caused by a mixture of projectile fragments as well as by materials dislodged from the test-foil. Indeed at values of $D_p/T < 0.7$ all witness plate damage is caused exclusively by target debris; the flow-fields of these truncated cratering events are such, that the projectile is quantitatively ejected uprange. As foil thickness decreases, increasingly larger fractions of the projectile will exit the target's rear and at $D_p/T > 10$, the spray patterns tend to be dominated by impactor fragments. The effects of still thinner foils manifest themselves in increasingly smaller angles of dispersion and the generation of fewer, yet relatively large fragments, as evidenced by clusters of overlapping, relatively large craters. Such conditions are undesirable for any bumper design, because the kinetic energy seems not sufficiently distributed over a wide enough area.

Knowing the stand-off distance for each experiment, measurement of the diameters of these spray patterns will yield the dispersion angles of the debris cloud. Such angles are illustrated in Figure 8 for the four impactor sizes employed. We distinguished and measured the following cone angles: the diameter of the entire spray reflects all dislodged material (angle α) and is, in most cases, demonstrably the result of target debris; the projectile fragments can be identified on the basis of dark colored crater interiors and their diameters define angle β; at very small T the projectile is fragmented, yet dispersion is small and a "central cluster" is formed that contains most of the impactor (angle τ), but not all. Therefore, angle β and τ can differ.

Knowledge of these dispersion angles is an important consideration in any collisional bumper design, because it enables predictions of the kinetic energy density suffered by a flight system that is protected by a bumper of a given thickness and stand-off distance. Once again we note and stress the similarity in witness plate spray patterns (Figures 6 and 7) and associated characteristics of debris dispersion, regardless of impactor size. Clearly, scaled foil thickness utterly dominates the collisional outcomes, rather than absolute impactor size. We demonstrate again that dimensional scaling is a useful and valid approach to learn about collisional fragmentation processes.

In summarizing these background experiments we conclude that substantial fragmentation of impactors during penetration of relatively thin foils is demonstrated. Also, the experimental approach of dimensional scaling seems validated. Clearly, these findings constitute basic constraints and guides in formulating the most diagnostic

experimental conditions to address the feasibility of discontinuous targets as collisional bumpers, the subject of the present effort. In the following these conditions are detailed and rationalized.

EXPERIMENTAL SET UP AND PROCEDURES

THE TARGETS

The design of the experiments called for the (dimensional) "scaling" of thickness T to projectile dimensions (see Figure 1). The largest projectile that can be launched in our two-stage Light-Gas Gun, of 5 mm bore, is 1/8" (3.2 mm) in diameter. We thus needed grids that employed wires ideally 1/16", 1/32" and 1/64" in thickness to yield D_p/T ratios of 2, 4, and 8; we also employed grids with wire thickness of 0.012", yielding a $D_p/T = 10$. A few experiments were conducted with 1/4" projectiles at low velocities employing the powder-propellant Vertical Gun and the latter employed targets as thick as 1/8". "Continuous" membrane targets were manufactured from commercially available sheet-stock and their thicknesses duplicated those of the wire grids, permitting direct comparisons of continuous and discontinuous bumpers at identical D_p/T.

All thicknesses employed were substantially thinner than projectile dimensions. On the massive side, absolute T has a geometric cut-off: grids of $D_p/T < 1$ either touch or overlap each other and are, de facto, "solid" membranes that have no transparency. The cut-off at the thin end was intuitively placed at D_p/T of approximately 10. Thinner grids and foils are expected to be unsuitable to sufficiently fragment metal impactors (see below).

We manufactured our test grids from straight welding rod stock that was inserted through suitably spaced and dimensioned holes in a massive metal target holder as illustrated in Figure 9. Each grid wire was fastened by set screws at either end. The vertical separation between "rows" and "columns" of grid-elements was ideally T, such that the wires were permitted to loosely touch at intersections without being strained. True wire-weaves or welding at intersections would most likely increase the rigidity of the grids; the grids employed in our experiments represent, therefore, some form of "worst" case in which each grid element was permitted to deform freely. The T = 0.012" was an exception to this rule; it was the only commercially available wire-weave employed in this study; in addition, this weave had double strands in one direction (T = 0.012") and a single strand in the other direction (T = 0.010").

The material of choice for the grid targets would be aluminum 6061-T6, because it is a strong candidate for continuous bumpers (E. Christiansen, pers. communication, 1991). However, alloy 6061 is not available in wire form, while the alloys used for wires are not employed in the manufacture of sheet stock. The metallurgy and attendant physical properties of wire and sheet-materials are seemingly exclusive. We employed aluminum 5365 for the grids, the alloy with the highest tensile strength among welding rod materials. We did employ, however, aluminum 6061-T6 for the continuous membranes to facilitate comparison and generalization with existing bumper experiments (Cour-Palais, 1987). As a consequence, the target materials employed in this study differ, by design, from those utilized in the above background experiments which employ aluminum 1100.

All experiments were principally set up to compare scaled target thickness and the experimental matrix was driven by the parameter D_p/T. The latter controlled all other dimensions and it, therefore, dictated the specific, areal shield mass (m_A; g/cm^2). This parameter constitutes all target mass per unit surface area available to interact with an impactor. We obtained m_A for the various target configurations by direct weighing of relatively large surfaces that represented the diverse D_p/T values or by volume calculations of specific geometries.

WITNESS PLATE ARRANGEMENT

The background experiments provided some realistic expectations about the geometric variability of the debris clouds and provided evidence that ejecta emanating from the targets' front surface may be significant, especially at massive T, where truncated craters are being produced. In the context of evaluating diverse bumper-designs, a *complete* assessment of all displaced mass seems mandatory. The crater-ejecta or "uprange" mass constitute additional debris in free flight and thus a long term threat, while the "downrange" debris defines the effective mass and energy that

represents the immediate threat to a flight system. As a consequence, we employed a target-set up and witness plate geometries unlike the background experiments.

As illustrated in Figures 10 and 11, the entire target was enclosed by flat and cylindrical witness plates, all mounted inside a sturdy Plexiglass-box. The latter was physically subdivided at the target plane into a "front" and "rear" section by means of a massive aluminum plate which also accommodated the target-holder. Illustrative experiments that illuminate the damage suffered by these witness plates are shown in Figures 12 and 13. Figure 12 is the continuous bumper case, while Figure 13 is a grid, with all other initial conditions essentially identical. Both figures show the typical products per experiment, provide some first order comparison of continuous versus grid-bumpers, and demonstrate unambiguously that full characterization of both uprange and downrange debris is paramount for general comparisons of bumper efficiency.

We employed four witness plates (see Figures 10-13) which are defined as follows:

1. The "ENTRANCE PLATE" collected all uprange mass of high ejection angles. It was a 1/8" plate of Al 1100 (identical to the background experiments) with an entrance hole for the projectile in its center.

2. The "EXIT PLATE" was identical in dimensions and material to the Entrance Plate. It was mounted to the rear of the target. It monitored the major debris cloud, however, over a diameter of 8" only, because cylindrical witness plates truncated larger diameter sprays. As a consequence, the Exit Plates frequently display spray patterns, in the illustrations to follow, that portray seemingly constant dispersion diameters, which of course is an incorrect perception.

3. The "FRONT PLATE" consisted of 0.004" (100 μm) aluminum foil (1100 series) that was conveniently wrapped into a cylinder of 8" diameter and which was sufficiently stiff to maintain a cylindrical shape. It was readily penetrated by most ejecta and the primary record is composed of penetration holes, rather than secondary craters as is the case for the massive Entrance and Exit plates.

4. The cylindrical "REAR PLATE" was made from identical material as the front plate.

All witness plates were blued with water-based layout ink for optical contrast and to facilitate relatively easy recognition and documentation of very small impact features (see Figures 12 and 13). All plates were photographed in a single session under what was perceived as "optimum" lighting and other conditions. However, due to the large size of the cylindrical witness plates that formed an 8" (20.5 cm) diameter cylinder and that were therefore some 63 cm long, some loss of detail was unavoidable in the resulting photos and additional detail was lost during subsequent photographic reproductions and reductions of the illustrative art work, which required the assembly of any number of photos for ready comparison of diverse experiments. Most information lost, however, refers to small features that do not seem to represent a substantial mass-fraction of the debris clouds.

POST-MORTEM DOCUMENTATION AND MEASUREMENTS

Following each experiment, the witness plates were removed after careful shaking and other assurances, that all loose debris had fallen off and remained in the proper "uprange" or "downrange" box-compartment for physical collection and subsequent weighing. Consistent with their dominant mode of formation, the mass collected in the uprange volume is termed "EJECTA" (m_E) throughout this report and the material collected in the rear compartment is identified as "SPALL" mass (m_S). Clearly, this loose debris is but a fraction of all mass dislodged, as many fragments terminated and lodged in the witness plates; on the other hand, some loose material may have been generated during the debris impacts on the witness plates resulting in some "excess" mass. It is not possible to distinguish among these primary and secondary sources; we simply documented/measured total, cumulative mass of the loose debris, separated into uprange (m_E) and downrange (m_S) components, regardless of specific source or origin.

The grids were photodocumented following each experiment on both the projectile "entrance" and "exit" side. The target fixture was then disassembled by removing all broken and deformed wires, including one additional grid

element to either side of the last, macroscopically deformed element. These wires were then weighed and the total displaced "TARGET MASS" (m_T) was determined by difference with the pre-experiment wire mass, obtained during assembly of the grid. The thinnest grid employed prefabricated wire mesh, in which case the total target mesh (~10 x 10 cm) was weighed before and after the experiment. Similarly, m_T for continuous membranes was obtained by weighing the round target discs before and after the experiment.

Following documentation of the targets, the witness plates were disassembled. Depending on experimental conditions, they may contain hundreds if not thousands of debris impacts. No doubt, these witness plates are the primary products of the experiments as they contain a faithful record of the number of fragments produced as well as their geometric dispersion. Unfortunately, characterization of such large numbers of debris impacts is a rather time-consuming effort, that was not practical within the limited scope of this effort. We will therefore present images only of witness plates in this report. They should suffice, however, to convey some qualitative sense of impactor fragmentation and dispersion and to test the relative merits of discontinuous and continuous bumpers.

THE PROJECTILES

Throughout this study we employed spherical soda-lime glass projectiles, either 1/4" (6.4 mm) or 1/8" (3.2 mm) in diameter in the Vertical Gun, or 1/8" diameter exclusively for all experiments at >4 km/s, which required the Light-Gas Gun. Such silicate impactors are rarely used in traditional bumper studies; the latter generally employ metal projectiles, most commonly aluminum or stainless steel. The physical properties, such as compressive and tensile strength of the impactor, are crucial in affecting its collisional fragmentation. Silicate impactors undoubtedly rupture and fragment with greater ease than metal impactors. The choice of silicate impactors in this study is justified by two major considerations: (1) the "background" experiments were conducted with soda lime glass impactors, thereby providing an internally consistent context for some interpretations. (2) Many mm sized impactors in LEO are silicates, indeed most, based on the analysis of Solar Max and LDEF surfaces.

Clearly, both silicate and metal impactors are needed to design meaningful bumpers; there simply is not a single material that would adequately simulate the diversity of prospective impactors in LEO. The present simulations merely started with silicates and duplicate experiments employing metal impactors will have to be conducted at a later time.

EXPERIMENTAL MATRIX

Figure 14 illustrates, essentially in parametric matrix form, the major experimental variables and their ranges. Table 1 lists detailed initial conditions per each experiment, sorted by experiment number, for convenient consultation. Three major variables, in order of increasing significance, make up this matrix:

a. Scaled Target Thickness (D_p/T)
We ranged in D_p/T from 2 to 12.5 for reasons detailed above and which are largely based on the background experiments.

It is important to note that the range in D_p/T is linearly related to areal shield mass (m_A) only in the case of continuous bumpers, but not for grids, on simple geometric grounds. Table 1 lists the exact, empirical D_p/T values as well as associated areal shield mass; note that D_p/T is not always an exact integer as portrayed in the illustrations throughout this report. It is important to keep the distinction between equivalent shield thickness (T) and equivalent shield mass (m_A) in mind.

b. Impact Velocity
Impact velocity ranks among the most important variables to extrapolate the laboratory simulations to the real conditions in LEO. Projectile speed in both guns is measured by redundant systems that monitor the occultation -- by the projectile -- of IR-laser-beams via photodiodes or the generation of an impact flash on the target, also monitored by photodiodes. Velocity measurement is accurate to <1%.

c. Projectile Size
Detailed experimental set-up and arrangements were developed in the Vertical Gun where 1/4" diameter projectiles are launched with greatest ease. The use of such large impactors was continued, however, into the actual test program, fully realizing that the largest projectile available for the higher velocity Light-Gas Gun simulations can only be 1/8". The use of 1/4" projectiles must be viewed as a first step for (limited) dimensional scaling of effects which depend on impactor size.

EXPERIMENTS EMPLOYING MULTIPLE MESHES

We performed a few exploratory experiments employing multiple meshes. The purpose of these experiments was primarily to develop suitable target configurations and to determine whether the target-box and witness plate arrangements developed for single-grid experiments are suitable for multiple meshes as well. The current hardware seems suitable. The target holder was equipped with 4 threaded spacer rods, onto which the actual spacers were inserted, such that a 1" (2.5 cm) separation distance between successive meshes resulted. We exposed 2, 3 and 5 identical grids of the commercially available, thinnest mesh at $D_p/T = 10$.

RESULTS

The results are described in two major chapters, one presenting photographic documentation of targets and witness plates, the other relating to measured or calculated masses that were dislodged.

As already stated and for scale in the photographic documentation to follow: the debris pattern on the exit and entrance plates can not be more than 8" (20 cm) in diameter, and the cylindrical witness plates are 63 cm long. Also, attempts were made to assure constant, internally self-consistent, reduction factors of individual photos that were assembled into specific plates. Absolute reductions between plates may vary by factors of 5, yet it is hoped that they convey, nevertheless, some sense of absolute scale and frequency of secondary impact features on various witness plates. Also, most individual photographs contain the experiment number for cross-reference with Table 1 that contains explicit experimental detail.

PHOTODOCUMENTATION

Targets

A representative suite of continuous and discontinuous targets are shown in Figure 15 with the intent to display the effects of scaled target thickness and impact velocity, employing 3.2 mm projectiles, except shots 3262 and 3263 (6.3 mm impactors). The continuous targets (Figure 15A) effectively duplicate the background experiments, yet note that two different aluminum alloys were employed (Al 1100 (annealed) for Figure 3 etc. and 6061-T6 for Figure 15). Penetration-hole morphology in 6061 aluminum follows the trends detailed by the background experiments; hole-diameter increases with increasing target thickness (right to left). Also, hole diameter increases sympathetically with velocity (top to bottom), a dependence that was not investigated by background experiments.

The penetrations of the grid-targets (Figure 15B) may be characterized as follows: the degree of deformation for individual grid elements seems to decrease with increasing thickness (right to left). Note that the $D_p/T = 10$ mesh (809 and 813) was the commercial, double-stranded weave. The effects of velocity are substantial, yet acerbated by target thickness. Thicker targets display more sensitivity (*i.e.*, more relative deformation) to velocity compared to thin grids. Note the increasing severity of grid damage for the $D_p/T = 2$ case: at 1.6 km/s the grid damage is limited to those single rods that took the direct blow, but increasing deformation of neighboring grid elements is observed at higher velocities.

Interpretation and understanding of these trends relates strongly to the background data illustrated in Figures 3 and 5: the area of damage (*i.e.*, hole diameter in Figure 3) is relatively invariant for thin foils, because the impactor simply punches through the target to generate a hole of approximate dimensions $D_h = D_p$. While no detailed experiments exist to address the velocity scaling of these relations, it seems reasonable to suggest that the condition of $D_h = D_p$

applies to a wide velocity range because the projectile simply punches out its own effective cross section, no matter what velocity. This situation, however, is different for thick targets, where the penetration must be viewed as truncated cratering event. Crater dimensions and volume are strongly controlled by total kinetic energy and, therefore, by velocity effects. Crater dimensions in aluminum scale with $V^{2/3}$ according to Cour-Palais (1987). By analogy, the degree and style of deformation of "massive" grids displays relatively strong velocity dependence. These observations and interpretations constitute evidence of analogous processes during penetration of continuous and discontinuous bumpers, the basic premise of this work.

Exit Witness Plates

Among all witness plates, the Exit Witness plate is considered the most important, as it intercepts that debris which will do immediate damage to the underlying flight system. Indeed, many collisional shield developments employ this plate only; frequently its absolute thickness simulates by design a real flight system, such as a spacecraft hull, to directly obtain information under what conditions a specific flight component may or may not be punctured or damaged otherwise. Note that our background experiments also employed a single exit plate only.

A few general comments apply to all witness plates. Many plates were coated and dusted by fine, high albedo powder, presumably projectile related, typically manifesting itself as white halo or streaks in the photographic products below. On occasion, a brownish stain is observed, that attests to heating and oxidation of the blue lay-out ink. Unfortunately, a realistic perception of the depth of craters and of other damage to the witness plates can not be portrayed photographically. Also note the initial problems with stabilization of the cylindrical witness plates that obviously bulged, jiggled and moved in the early phases of this study (Figure 16) until we learned how to immobilize them with enclosing rings (Figure 17).

Figures 16 and 17 compare the exit plates of continuous and discontinuous bumpers at "low" (1 and 2.3 km/s) and "high" (5 and 6 km/s) impact velocities, respectively, as a function of scaled foil thickness (vertical position). Note that 6.3 mm projectiles were used for the low-velocity experiments, but 3.2 mm impactors at high velocities. We structure observations and discussions of the experiments illustrated in Figures 16 and 17 in terms of three distinct features:

1. Largest witness plate crater produced
2. Absolute number of craters
3. Areal distribution of craters

Largest Crater - The largest crater (D_{max}) is of substantial interest, because it reflects the most kinetic fragment (F_{max}) produced per any given experiment and it constitutes, therefore, the most serious threat to an underlying flight system. Careful inspection of the original plates reveals that there is no discernable, systematic difference in F_{max} -- at all experimental conditions -- between continuous and discontinuous bumpers. However, F_{max}, depends on T and is -- not surprisingly -- largest for the thinnest bumpers, because the impactor is marginally ruptured into a few, large fragments only. Also most experiments contain any number of craters with relatively large diameters. There is no single, exceptionally large crater that would stand out as the obvious largest event in any given experiment, but instead an ensemble of large fragments, all of comparable sizes, is being produced. Inspection of the entrance plates and all cylindrical witness plates are consistent with these observations, although the latter generally received debris of smaller sizes than the exit plate. Without exception, the largest fragments are part of the exit debris. Nevertheless, the important observation is that F_{max} does not systematically depend on specific bumper type, but it relates sensitively to absolute bumper thickness and impact velocity only. As a consequence, these observations substantiate the equivalence of T in producing the largest fragment via continuous and discontinuous bumpers.

Absolute Number of Craters - The total number of craters and associated size frequency distributions are a measure of the total mass impinging onto a flight system that is being simulated by the witness plate. If combined with a velocity distribution of these fragments, one could define the total kinetic energy that results from a given collisional event. As demonstrated in Figure 5, this mass can greatly exceed the impactor mass. It follows, that the downrange-debris is obviously a mixture of projectile and dislodged bumper material as also demonstrated by

Pietkutowski (1990) and Schonberg (1990). Generally, the number of exit plate craters is higher for the continuous bumpers under all experimental conditions (compare the pairs 3266 & 3267 or 809 & 810 or 805 & 807 in Figures 16 and 17). This simply reflects bumper-geometry and volume, which is higher for continuous bumpers compared to grids. We have not developed a clear sense for the dependence of T and V on the absolute number of fragments produced, yet crater frequency seems to increase with increasing T and V, because those conditions are amenable to dislodge increasing amounts of target volume. We refer, however, to Figure 2 where we identified specific boundary conditions that produce "0" fragments on the exit plate (the "crater" case in infinite halfspace target and the case of "intact" projectile passage at ultra-thin foils). In consequence, there must be specific D_p/T conditions that yield maximum numbers of either target or projectile fragments. We do not know what those D_p/T ratios are. Note, however, that variable numbers of fragments are observed in Figure 6; distinctly fewer fragments were produced at very thick ($D_p/T < 1$) and relatively thin foils ($D_p/T > 20$), compared to intermediate D_p/T values.

Areal Distribution of Craters - Because areal density of craters is a measure of the specific kinetic energy (ergs/cm^2) experienced by a flight system, it represents an important criterion to evaluate bumper performance. Even cursory inspection of Figures 6, 7, 12, 13, 16 and 17 reveals that dramatically different geometries of spray patterns are produced by continuous and discontinuous bumpers. These figures also demonstrate that surprisingly systematic and reproducible collisional outcomes result from well characterized target configurations. Subtle and major differences depend sensitively on T and the specific distribution of mass within the bumper. All continuous bumpers produce a largely centrosymmetric spray pattern at the D_p/T simulated, but the discontinuous bumpers generate sprays that are dominated by linear elements, depending whether single or multiple grid elements were involved in the direct collision. The grid-sprays of the thinnest targets have affinities to equivalent membrane penetrations (*e.g.*, pairs 3264 & 3265 or 809 & 810). As T and V increase, the grids deviate increasingly from continuous bumpers. Specifically the grids produce highly localized concentrations of secondary craters of distinctly linear alignment(s) (*e.g.*, 799, 803 or 3267).

Although no quantitative crater counting was performed on any of these exit plates, the qualitative impression is that the absolute number of craters is higher for the continuous bumpers at equivalent D_p/T. This entails that more total, cumulative energy (E_{cum}) will have to be absorbed by an underlying flight system in the case of continuous bumpers compared to discontinuous bumpers. Continuous bumpers, however, cause generally wide dispersion angles and relatively even distribution of witness plate craters. This makes for substantially more favorable conditions regarding average specific energy per unit surface area which a flight system would have to tolerate. The crater clusters produced by discontinuous bumpers are a distinctly undesirable feature, because they represent local maxima in specific energy that are difficult to protect against.

We rearranged, in Figure 18, the exit witness plates to directly convey a sense of the velocity-dependent effects. Some of these effects were already described above. Effects of velocity are less pronounced with thin targets than they are with massive bumpers, which simply is yet another way of stating that target volume and mass are dominant and that -- in principle -- most of the spray patterns of thick targets are utterly dominated by target debris. Clearly, the continuous bumpers produce debris clouds that disperse increasingly with increasing velocity and the latter is true also for thin grids. The trend to produce linear concentrations of secondary impacts in the case of grid-bumpers increases sympathetically with increasing velocity and target thickness.

In summarizing the exit plate observations, we conclude that the debris clouds of grid penetrations are distinctly more lumpy than those of continuous membranes. This translates into localized maxima of energy deposition (ergs/cm^2) on the witness plate (flight system), unlike the continuous target. Such energy concentrations are a severe short-coming of single grid penetrations, despite the fact that the latter produce fewer numbers of debris fragments compared to membranes. For the purposes of this work, however, the most significant observation is that the largest or most kinetic fragments (F_{max}) do not differ measurably between the two bumper designs.

Ultimately, any bumper performance must be judged by criteria that relate to specific kinetic energy content that is suffered per unit surface area of a flight system. It seems obvious, that this energy may vary substantially, depending on the definition of "surface area." Clearly, the single F_{max} fragment is the most prominent threat, because it delivers its energy onto a very "small" area (E_{max}); the lumped and clustered grid impacts represent highly

localized energy highs (E_{loc}), which are, however, smaller than E_{max} ($E_{loc} < E_{max}$); finally the cumulative mass contains E_{cum} and $E_{cum} < E_{loc} < E_{max}$. No doubt, any bumper must be designed to minimize E_{max}. Continuous and discontinuous bumpers seem to have similar characteristics in this regard. The continuous bumper, however, outperforms the grid bumper regarding E_{loc}, yet it is inferior in terms of E_{cum}.

ENTRANCE WITNESS PLATE

Spray patterns on the entrance plates are shown in Figures 19 and 20, with Figure 19 illuminating the effects of velocity and Figure 20 the effects of target thickness; note that Figure 20B illustrates the entrance plates corresponding to the exit plates of Figure 17B.

Very generally, only small ejecta were observed on all entrance plates compared to the substantially more massive "exit" fragments. Under many conditions, no discernable craters, pits, or other damage occurred on the entrance plates. A circular, hued area is common, however, that seems to be due to thermal discoloration and possible deposition of vapors, rather than to the arrival of small fragments. Although poorly visible on the photographs, most any continuous bumper target produced some fragments, the population of which increased, until photographically documentable at thick plates and high velocities (*e.g.*, 802 and 805). While Figure 20 concentrates on the high-velocity experiments, Figure 19 presents entrance plates from low-velocity grid experiments also. Note again the presence of discoloration, yet the lack of discernable pits and other damage over a wide variety of initial impact conditions, including< 2.5 km/s velocities.

Summarizing Figures 19 and 20, we conclude that only small ejecta pieces, at best, take off at sufficiently steep angles to encounter the entrance plate. The mass fraction represented by these ejecta seems small in all cases. It is nevertheless substantially higher for continuous bumpers than it is for grids. The latter can not be entirely due to differences in target mass, especially at $D_p/T = 2$, but most likely relates also to modified take-off angles caused by flat versus curved target surfaces. All in all, the entrance plates are not terribly informative, yet they demonstrate that a small mass fraction escapes along steep trajectories and in relatively fine-grained form; penetrations of continuous bumpers produce more damage on the entrance plate than do discontinuous bumpers, yet total damage is insignificant compared to that on the exit plates.

CYLINDRICAL WITNESS PLATES

The relatively large cylindrical witness plates are particularly difficult to document photographically. We nevertheless illustrate in Figure 21 both plates for the high-velocity experiments for comparative purposes. Note: all plates were rotated 90°, with (arbitrary) 0° in the upper left-hand corner and, consequently, 360° in the lower left-hand corner. The position of the target is to the left side of the Front plate (thinner strip), yet to the right side of the Rear plate (thicker strip), so as to preserve the potential geometry of two cones that originate in the target plane. Note that Figure 21A corresponds to those experiments illustrated in Figures 17B and 20B.

We observe an increase in cylindrical plate penetrations with increasing target thickness (*e.g.*, 798, 807 & 810) and the substantially more even and centrosymmetric distribution from membrane penetrations (*e.g.*, 798 & 802) compared to the lumpy nature of grid-debris (*e.g.*, 803 & 806). The latter correspond to the localized debris concentrations that characterize the exit plates.

Enlarged views of the FRONT plates are offered for the high-velocity experiments in Figure 22. The target is towards the bottom of each plate. Note that the continuous bumpers (Figure 22A) tend to produce more penetrations than do discontinuous targets (Figure 22B) and that the continuous bumper ejecta are substantially centrosymmetric, whereas the grid ejecta are not. The continuous bumper ejecta also have distinct mass concentrations at relatively shallow angles, primarily produced by numerous, small fragments (possibly melt droplets?), while somewhat larger ejecta, albeit in small numbers, may occur at substantially higher take-off angles. The salient observation of Figure 22, however, relates to the difference in total ejecta mass between the two bumper designs, which is overwhelmingly in favor of the discontinuous bumper. The latter simply contains little mass, to start with, for displacement.

Figure 23 represents the cylindrical REAR plates of the same experiments shown in Figure 22 and illustrates again that massive targets simply displace more mass. The target surface (cone-apex) is towards the bottom of each plate. At small thicknesses, the grid bumper seems to out perform the continuous target, yet the direct hit of a grid element in experiment 803 demonstrates, that grid-bumpers may also cause undesirable, local concentrations of debris that have higher areal densities than those of any continuous target. The latter observations render the continuous bumper of superior utility, as already discussed via the exit plate observations, and the damage observed on the rear plates is simply evidence for the geometric extension of lumpy debris clouds, to high dispersion angles, that characterize the penetrations of massive grid targets.

WITNESS PLATES: SUMMARY

The total mass of debris that is produced during penetration of targets that are substantially thinner than the ballistic limit depends sensitively on target thickness and, therefore, on available mass within the target itself. Projectile fragments may be of secondary importance, possibly insignificant, when employing massive targets of $D_p/T < 2$. By necessity, the latter view entails that multiple projectile masses are contained in the debris clouds. It seems also evident that most of this mass emanates to the targets' rear to interact with the exit plate, and thus with a prospective flight-system.

This major exit-mass in the case of continuous bumpers displays substantial sensitivity to the parameter P_d/T; the latter also controls its geometric dispersion onto an underlying flight system to the degree that dispersion angles become predictable. The exit cloud from continuous bumpers is also fairly evenly dispersed, producing favorable energy densities (ergs/cm^2) on an underlying substrate. In contrast, the major exit-mass from discontinuous bumpers mimics the heterogeneous mass distribution of the bumper itself by producing distinct lumping and clustering of secondary craters that are difficult to predict, and some of which produce substantially higher ergs/cm^2 than continuous bumpers. Such lumping is also observed on the cylindrical Rear witness plate and therefore applies to all dispersion angles. The number of individual downrange fragments is larger for continuous bumpers. Very importantly, however, there seems to be no difference in the size of the largest or most kinetic fragment (F_{max}) exiting continuous and discontinuous bumpers. Nevertheless, the clumping and clustering of secondary craters is an undesirable characteristic of discontinuous bumpers which constitutes a substantial concern. The use of multiple, stacked grids, however, may cause additional dispersion of these lumps.

The mass ejected uprange is distinctly less than the downrange mass in all cases studied. The latter depends strongly on D_p/T also and increases with increasing target thickness. Still more massive targets than those used, undoubtedly, will result in increasingly more crater-like penetrations and, therefore, more uprange ejecta. Ultimately, beyond the ballistic limit, the genuine cratering event produces nothing else but ejecta, while downrange mass becomes nil. For the D_p/T ranges investigated, the discontinuous bumper seems to outperform the continuous target in terms of ejecta mass. However, some clumping and clustering is observed in the ejecta cloud also for the most massive grids used. While this may also be cause for concern, the total mass and size-distribution of ejecta is distinctly smaller than that of the exit cloud. The potential damage done to neighboring flight systems, by direct, secondary ejecta hits, is thus relatively modest in a comparative sense with the exit cloud. However, these ejecta particles may also become free-flying to form an integral part of the orbital debris threat, in which case the difference between continuous and discontinuous bumpers may become important. The grid-targets yield systematically fewer ejecta fragments than do continuous targets.

MASS DETERMINATIONS

The mass determinations offered below relate to total target mass displaced and to the physical recovery of loose fragments in the uprange and downrange compartments of the target box. While such mass determinations assist in bumper evaluation, it must be realized that they represent only part of the total mass consideration(s). In the absence of detailed witness plate analyses, important information is simply lacking, rendering all mass-related arguments somewhat incomplete. Also, mass arguments alone, without associated velocity-assignments, do not permit characterization of the dynamic properties of evolving debris clouds, the ultimate discriminator among various bumper designs. Nevertheless, limited as they may be, we consider measurements of displaced masses an important

ingredient in the complete description, ultimately, of debris clouds. While some dynamic information is available from penetration of continuous bumpers (*e.g.*, Pietkutowsky, 1990), none exist for grid-bumpers, the reason why dynamic information, from direct measurements, is not discussed in this report.

TOTAL TARGET MASS DISPLACED

This mass (m_T) was determined by difference from weight measurements prior to and after an experiment. The absolute target mass lost is listed in Table 1 as is areal shield mass (m_A) which was obtained from a combination of direct measurements and volumetric calculations, using 2.7 g/cm^3 for the density of aluminum. There is some scatter in the empirically determined masses that seems typical for such small scale impact experiments.

Figure 24 summarizes the results with displaced mass normalized to projectile mass mp. Figure 24A depicts the continuous bumpers, and Figure 24B the discontinuous designs. Connecting lines are eyeball fits, intended to illuminate trends, rather than to quantify them. Two overwhelming trends result that apply to both bumper designs: (l) Target thickness T controls the total mass contained in any target; total displaced mass is sensitively related to this target mass, as revealed by vertical position at any given velocity. With T and associated target mass strongly controlling the displaced mass, it is no surprise that continuous bumpers displace much more mass at otherwise identical conditions than do the discontinuous grids. (2) The connecting lines and their slopes portray velocity dependence; at equivalent D_p/T the higher velocity impactors displace more mass.

Clearly, total displaced mass depends on a target's areal shield mass (g/cm^2), the reason for Figure 25. It depicts the displaced target mass as a function of areal shield mass, grouped into low velocity (Figure 25A) and high velocity (Figure 25B) experiments for clarity, yet plotting continuous and discontinuous targets in the same graph (unlike Figure 24). Note that our grid design involved continuous rods, resembling a weave, that leads to overlapping rods and mass duplications at the mesh junctures. This leads to actual shield masses modestly higher than those based on (ideally) non-overlapping grids and is the reason why thinner meshes deviate progressively more in a relative sense from the mass represented by a continuous shield. The overriding trend that we extract from Figure 25 relates to the systematic relationship of displaced mass and areal shield mass, no matter whether the latter is provided by a continuous or discontinuous bumper geometry. This simply verifies the generally similar nature of penetrations in continuous and discontinuous targets, which in both cases dislodge materials over comparable radii, regardless of detailed bumper geometry.

In the context of bumper development, the systematic relationships illustrated in Figures 24 and 25 imply substantial predictive capabilities for displaced mass as a function of (relatively thin) bumper thickness, no matter what its detailed design. The interpretative framework to view penetrations as truncated craters, offered via the background experiments, seems to apply for grid-bumpers as well. Areal shield mass utterly controls the displaced mass at any given velocity and discontinuous bumpers emerge as the superior design, therefore, with regard to parameter m_T.

RECOVERED EJECTA MASS

The total mass of all loose debris collected in the uprange compartment of the target box is illustrated in Figure 26, once again plotted against areal shield mass, and grouped into low- and high- velocity experiments. Clearly, these fragments are a mixture of primary ejecta from the target and debris dislodged from the witness plates. The latter can be demonstrated by the occasionally blue fragment that was recovered, which can only originate from the inked witness plate(s). As a consequence, ejecta mass alone can not be characterized in detail. No doubt, the empirically recovered masses are highly experiment sensitive, such as witness plate location(s), materials, thicknesses, etc., yet the latter were held constant for all experiments, the reason why recovered mass may be a meaningful parameter. It can reflect the energy of the ejecta and their damage inflicted on neighboring flight systems. Clearly, none of the absolute ejecta masses is very meaningful, but their relative magnitudes are of help in bumper comparisons, because they may result from secondary collisions and because they can potentially contribute to free-flying debris.

Within these limitations we note again, substantial dependence of m_E on target mass and modest dependence on velocity, akin to m_T. Once again there is no great sensitivity to specific bumper design, because of the overwhelming control by areal shield mass. The more massive a bumper, the less favorable becomes parameter m_E and discontinuous bumpers emerge more suitable, because of their favorable areal shield mass at a given D_p/T.

RECOVERED SPALL MASS

Much of the discussion pertinent to m_E applies, of course, also to the mass (m_S) recovered from the downrange volume of the target box. These masses are depicted in Figure 27. Generally, these masses are surprisingly similar to the ejecta masses, although increased fragment populations must exit the target based on the exit and rear witness plate spray patterns. Once again, m_S is demonstrably a mixture of primary and secondary fragments that may be viewed as a relative measure of potential damage inflicted directly to an underlying flight system(s); also some of this mass could contribute to the orbital debris population. It is not surprising by now that total spall mass relates once more to areal shield mass and seems independent of specific bumper design. Once again, discontinuous bumpers outperform continuous designs with regard to parameter m_S.

LARGEST FRAGMENT RECOVERED

The largest fragment for each of the recovered ejecta and spall fragments was weighed individually. There is no direct knowledge whether this particle originated from the target or from the witness plates. However, most of these particles must be viewed as originating from the witness plates (crumbled foils, some of them even blued), rather than resembling fragments dislodged from the (unpainted) target.

Figure 28A represents the largest ejecta; Figure 28B, the largest spall fragments. Note that the latter tend to be more massive than the ejecta, especially for thick targets. Also, the largest pieces recovered do not differ systematically between grid-bumpers and continuous membranes, yet the thicker the bumper, the more massive the largest dislodged fragment. Indeed the largest fragments depend on T only; unlike parameters m_T, m_E and m_S, there is no discernable trend as a function of m_A in Figure 28. In summary: neither largest ejecta or spall piece recovered seems sensitive to detailed bumper design and both continuous and discontinuous targets shed/produce approximately the same largest fragment, with absolute fragment size depending on T. Note that visual inspection of the exit witness plates led to similar conclusions, although D_{max}/F_{max} is (demonstrably) not identical to the largest fragments that could be recovered physically. It is nevertheless significant that continuous and discontinuous bumpers result in similar largest fragment populations, regardless of their detailed origin. On the basis of internally consistent criteria, (one by visual judgement, the other by direct mass measurement), the most massive fragments generated by the two principle bumper designs are virtually indistinguishable and, furthermore, depend entirely on T only.

SUMMARY OF MASS CONSIDERATIONS

We demonstrated that most masses measured in this study depend sensitively on absolute areal shield mass, regardless of specific bumper design. As these shield masses are substantially smaller for grids at any given D_p/T compared to continuous bumpers, the grid design outperforms the contiguous bumper in the categories of total displaced target mass, recovered ejecta and spall mass. The largest fragments that could be recovered are comparable for both bumper designs. However, all physically recovered, loose debris and associated masses depend sensitively on specific experiment set up and can only be used in a relative sense, because pertinent experimental conditions were held constant.

This qualification is not necessary, however, for the mass displaced from the target; the latter is not affected by specific arrangements of witness plates and associated (experiment dependent) secondary effects, yet depends only on experimental parameters of interest. The experiments demonstrate that this mass may be predicted from knowledge of areal shield mass no matter what detailed bumper design, clearly a new and significant result.

However, the experiments can only give limited answers, from the visual analysis of the witness plates, where this mass ends up, what its grain-size distribution might be, and especially what is the velocity distribution and

associated kinetic energy of the debris clouds? The latter, ultimately, constitute first order criteria for bumper comparisons, rather than the absolute quantity of mass displaced. While we consider the mass measurements obtained during this study of importance, they must be viewed, nevertheless, as supporting criteria only in comparisons of relative bumper efficiency.

MULTIPLE MESH EXPERIMENTS

We performed a small, exploratory series of experiments that addressed the effect(s) of multiple grids, because the major expectation behind the current work is that successive penetrations of a series of grids would lead to progressive comminution of the debris that is produced by the first grid. Such considerations are also germane to the multi-foil penetration experiments of Cour-Palais and Crews (1989) and the dual-wall bumper concept (*e.g.*, Schonberg, 1990; Christiansen, 1990). These workers demonstrated favorable areal shield masses for a given degree of projectile destruction and deceleration compared to single sheet penetrations. Multi-shock concepts must clearly be favored over single sheet penetrations, as additional comminution and heating results from each successive shock.

Although Fig. 1 suggests that grids of successively smaller mesh opening are desirable to specifically reduce F_{max} in expedient fashion, we performed the exploratory experiments with grids of identical T and M and used the thinnest grid employed in the other experiments (*i.e.*, the readily available, commercial, double-stranded weave of $D_p/T = 10$). We simply stacked one (813), two (822), three (824) and five (826) identical grids, separated by 1" spacers between each of the successive meshes and employed 1/8" projectiles at a nominal 6 km/s. No attempt was made to "register" the meshes; the latter were arbitrarily cut from stock and mounted without concern for relative alignment.

The results of all four experiments are illustrated in Figures 29, 30 and 31. Figure 29 is an overview, while Figure 30 details the mesh deformations and Figure 31, the exit witness plates. Note that the entrance hole on the first grid is essentially the same for all four experiments, yet successive grids suffered massive damage and possess dramatically enlarged penetrations. Where applicable, the second (and third) meshes have similar hole dimensions. The large penetration holes in successive grids are consistent with the dispersion of debris that is sufficiently kinetic to destroy the thin meshes. The five-mesh experiment suggests, however, that the high angle, fine-grained spray is effectively decelerated or comminuted during encounter with the first four meshes, because the penetration hole on mesh 5 is smaller than that of mesh 4. Particles at the outer edges of the dispersion cone were eliminated measurably and only the central part of the debris cloud was able to penetrate mesh 5.

Associated effects on the witness plates are dramatic as well (Figure 31). Compare the substantial number of pits and their localized fragment concentrations from the one-mesh experiment with that employing five grids in Figure 31, which displays highly favorable mass dispersion of relatively fine-grained debris only. The beneficial effects of progressive comminution and the incipient elimination of undesirable, localized fragment/crater clusters, however, is already evident in the two-mesh experiment and extends systematically to the three-mesh case, and ultimately to the five-mesh experiment. These experiments demonstrate that the undesirable fragment clusters characterizing the debris clouds of single grid penetrations may be eliminated readily by use of multiple meshes.

Note in Figure 29 that the cylindrical witness plates display no penetrations of any concern compared to the exit plate damage, particularly that of the one-mesh experiment. The cylindrical rear plates in particular are relatively clean, attesting that multiple meshes inhibit lateral dispersion, a conclusion already suggested by the comparatively small penetration hole of mesh 5 and by the decreased diameter of the spray pattern on the exit plate of experiment 826.

For completeness and in conclusion, we illustrate in Figure 32 the exit plate spray patterns of continuous and single grid-bumpers produced by otherwise identical impact conditions to the mesh experiments and we now identify areal shield-mass explicitly for comparative purposes. The difference at comparable shield mass of approximately 0.05 g/cm^2 is dramatic. It seems self-evident that the multiple mesh-bumper emerges as the vastly superior design.

CONCLUSIONS

We performed experiments that allow comparison of the collisional outcome of hypervelocity penetrations of single grid-targets with those of the more traditional, continuous meteorite-bumper concepts. Also, a few experiments that exposed multiple grids were conducted. The concept of dimensional scaling formed the basis for all experimental conditions and seems validated by the results.

Analysis of these experiments, based on qualitative observations and a limited number of absolute mass measurements, reveals the following:

a. Most collisional outcomes seem to depend on total areal shield mass only and are independent of specific bumper design.

b. There is no discernable difference between continuous and discontinuous bumpers regarding the most energetic fragment produced, as deduced from the size of secondary craters on witness plates and from physically recovered ejecta and spall materials.

c. Dispersion and thus specific energy contents of the debris clouds, however, are superior in the continuous bumpers, compared to grids, because the latter produce distinct crater clusters and localized energy maxima that mimic the target's uneven mass distribution.

In summary we conclude that bumpers made of discontinuous solids are highly promising and deserve further study. Most findings are consistent with expectations derived from dimensional scaling. Adequate fragmentation, deceleration and dispersion of a prospective impactor are largely dependent only on the total, vertical mass-column encountered by an impactor, rather than on the lateral extend of bumpers. Effective collisional bumpers may well have lateral dimensions that are not larger than bumper thickness. Both dimensions can be substantially smaller than typical projectile dimensions and relatively fine grids will be adequate.

Figure 33 represents simple geometric calculations that depict the relative volumes of continuous and discontinuous bumpers as a function of D_p/T. "Unity" is defined as material of $T = D_p$ on both axes. Round symbols represent "weaves," square symbols represent punched grids, without mass duplication at the intersects. If continuous and grid-bumpers were manufactured from identical materials, the relative volumes would, of course, directly correspond to a mass ratio and therefore to relative areal shield mass (g/cm^2) as defined and used throughout this report. It seems obvious, that substantial mass savings seem possible if thin grid-bumpers were used, even more so if one keeps in mind that continuous bumpers seem to require more absolute shield mass to accomplish equivalent degrees of projectile fragmentation relative to successive collisions in multiple grid-bumpers.

The thrust of additional developments must address detailed and optimal geometries of multiple mesh bumpers. Duplicate experiments for single and multiple grids that employ metal impactors are also needed. In addition, it seems highly desirable to develop automated techniques based on image processing, to extract more quantitative information from witness plates (*e.g.*, Klopp *et al.*, 1990).

REFERENCES

Anderson, C.E. ed. (1990), Hypervelocity Impact, *Proc. of the 1989 Symposium on Hypervelocity Impact, Int. J. Impact Eng., V. 10*, 1990, 639 p.

Carey, W.C., McDonnell, J.A.M., and Dixon, D.G. (1985) An Empirical Penetration Equation for Thin Metallic Films used in Capture Cell Techniques, in "*Properties and Interactions of Interplanetary Dust*," Giese, H. and Lamy, P.H. eds., Reidel, 1985, p. 131-136.

CDCF, *Cosmic Dust Collection Facility: Scientific Objectives and Programmatic Relations, Committee Report*, F. Hörz, ed., NASA TM 102169, 1990, 30 p.

Christiansen, E.L. (1990), Advanced Meteoroid and Debris Shielding Concepts, AIAA/NASA/DOD *Orbital Debris Conference, AIAA 90-1336*, 14 p.

Cour-Palais, B.G. (1987), Hypelvelocity Impact in Metals, Glass, and Composites, *Intern. J. Impact Eng., Vol. 5*, p. 221-237.

Cour-Palais, B.G. and Crews, J.L. (1990) A Multishock Concept for Space Craft Shielding, *Int. J. Impact Eng., Vol. 10*, 135-146.

Gurson, A.L. (1990) The Effects of Geometric Scale on Impact Induced Fragmentation, and its Application to the Design of Dual Plate Armor, *Int. J. Impact Eng., Vol. 10*, p. 213-229.

Holsapple, K.A. and Schmidt, R.M. (1990) On the Scaling of Crater Dimensions, Impact Processes, *J. Geophys. Res., Vol . 87*, p. 1849-1870.

Klopp, R.W., Shockey, D.A., Osher, J.E., and Chao, H.H. (1990) Characteristics of Hypervelocity Impact Debris Clouds, *J. Int. Impact Eng., Vol. 10*, p. 323-335.

Pietkutowski, A.J. (1990) A Simple Dynamic Model for the Formation of Debris Clouds, *J. Int. Impact Eng, Vol. 10*, p. 453-471.

See, T.H., Allbrooks, M.K., Atkinson, D.R., Simon, C.G. and Zolensky, M.E. (1990) *Meteoroid and Debris Impact Features Documented on the Long Duration Exposure Facility*, NASA JSC Report #24608 (1990), 561 p.

Schonberg, W.P. (1990) Hypervelocity Impact Response of Spaced Composite Materials Structures, *Int. J. Impact Eng., Vol. 10*, p. 509-523.

Warren, J.L. and 9 Co-Authors (1989) The Detection and Observation of Meteoroid and Space Debris Impact Features on the Solar Maximum Satellite, *Proc. Lunar Planet. Sci Conf. l9th*, p. 641-657.

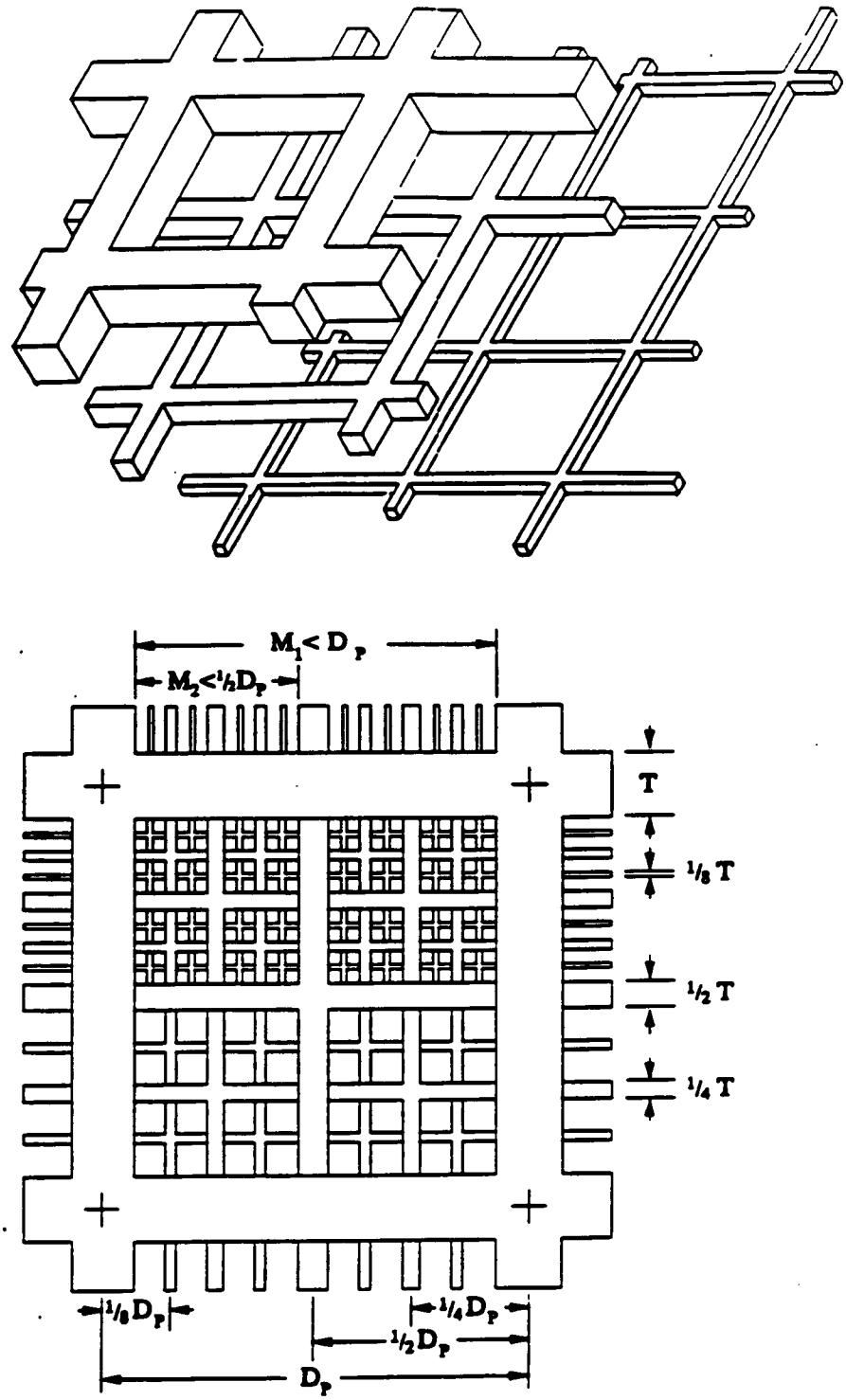

FIGURE 1. Geometric arrangement and requirements for discontinuous meteorite bumpers that employ a series of stacked, dimensionally scaled wire meshes. (A) Isometric view of three meshes and (B) geometric constraints related to dimensional scaling. Note that each successive mesh has mesh distances that are half of the preceding, more massive member. This implies that all fragments half the size of the initial impactor (or of intervening fragmentation products) will encounter a solid. The wire thickness in this illustration represents the $D_p/T = 5$ case; this dimensional ratio is somewhat arbitrary for purposes of conceptual illustration. Indeed, a major objective of the impact experiments described in this report aims at establishing the thinnest T possible that would still provide adequate protection against collisional damage.

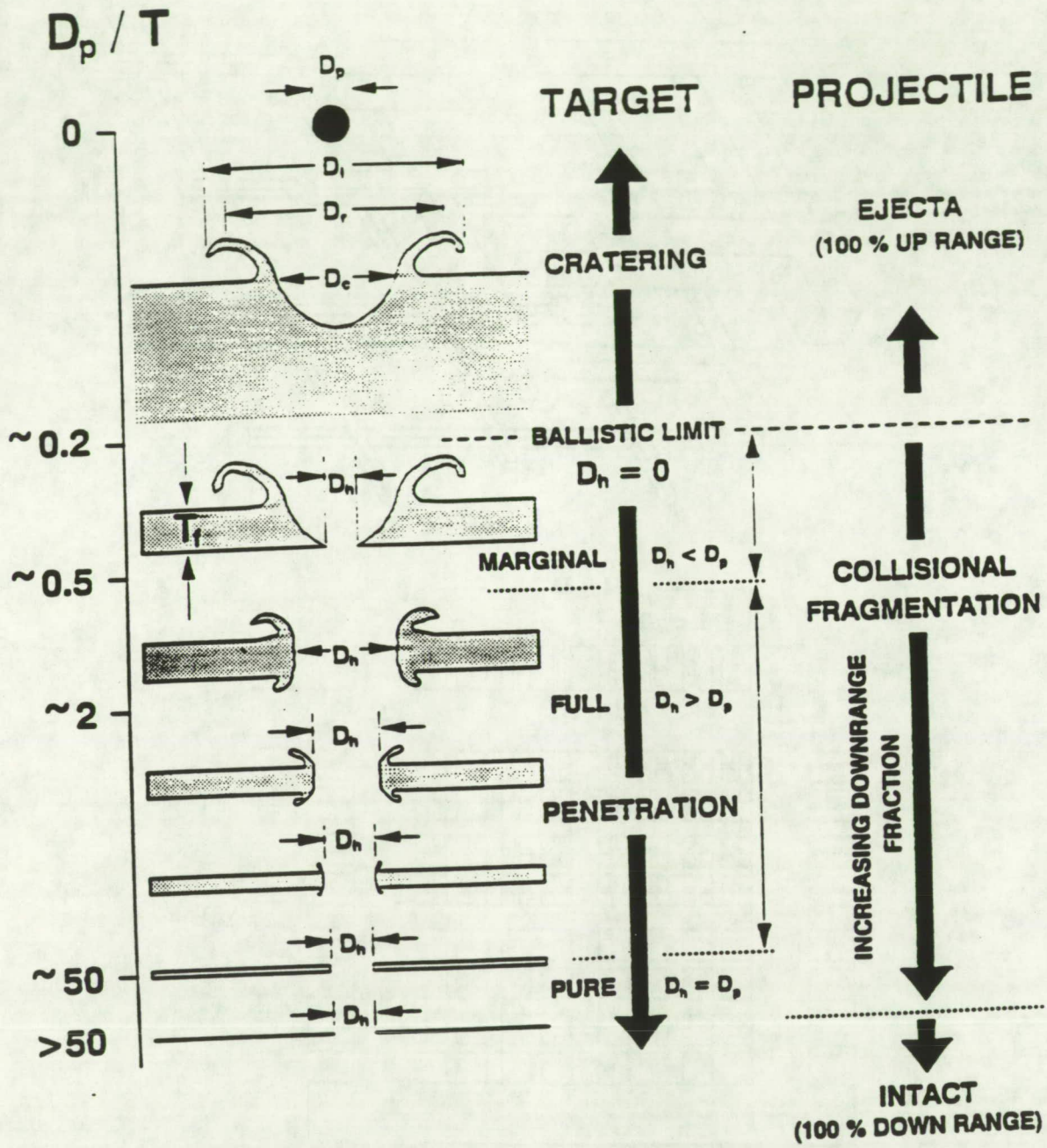

FIGURE 2. Possible penetration scenarios of hypervelocity projectiles encountering laterally continuous targets of ever decreasing thickness (T), the latter scaled to projectile diameter (D_p).

FIGURE 3. (opposite page) Morphology of craters and penetration holes in aluminum targets of systematically decreasing thickness (increasing D_p/T in lower right-hand corner of each image) that were produced by projectiles varying in diameter from 50 to 3200 μm. Note the gradual morphologic changes of the penetration holes as a systematic function of foil thickness. Also note the general similarity of penetration holes at any given D_p/T (in lower right-hand corner), independent of absolute projectile size. These experiments lend strong support to the concept of "dimensional scaling".

Soda Lime Glass → Aluminum 1100-O

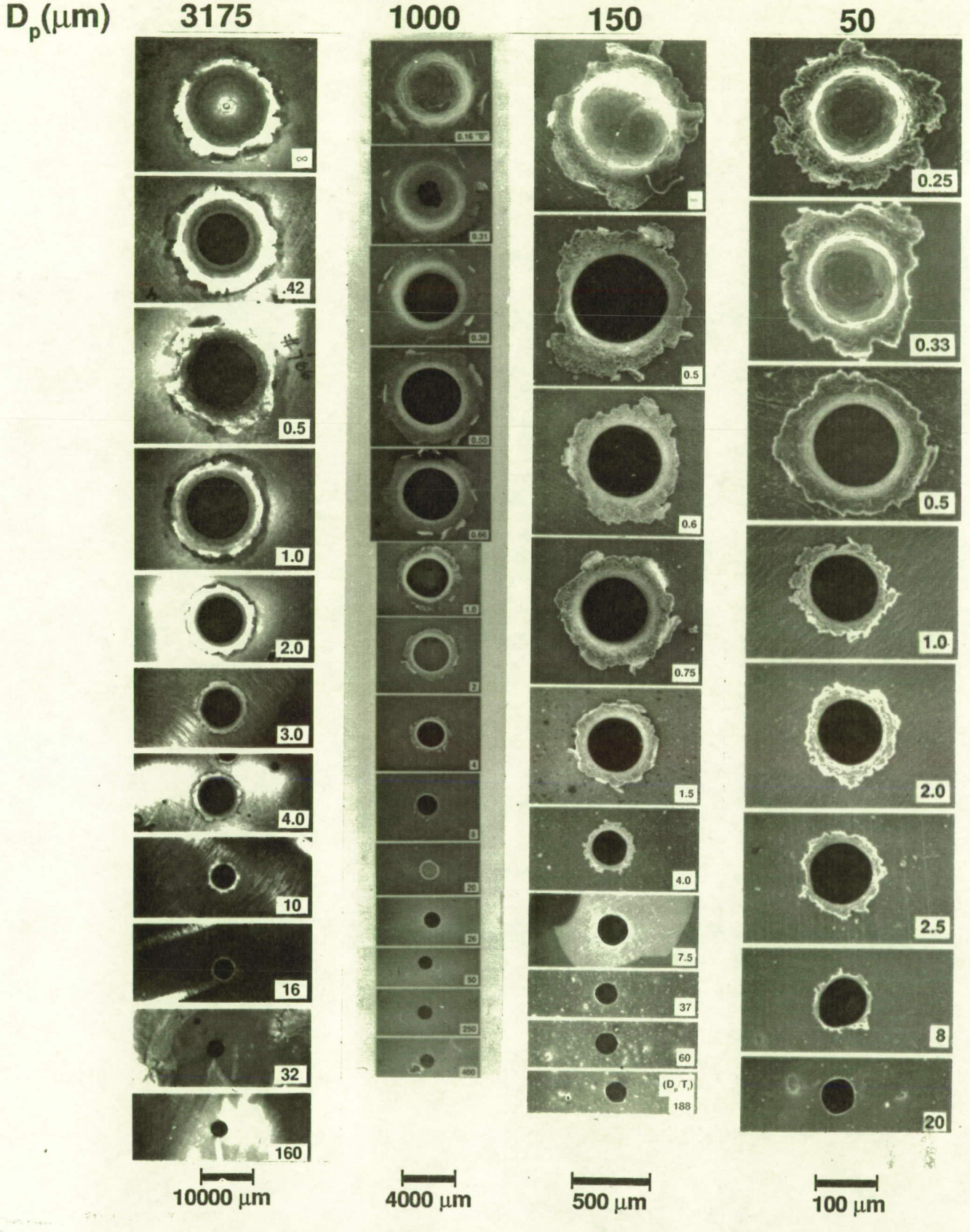

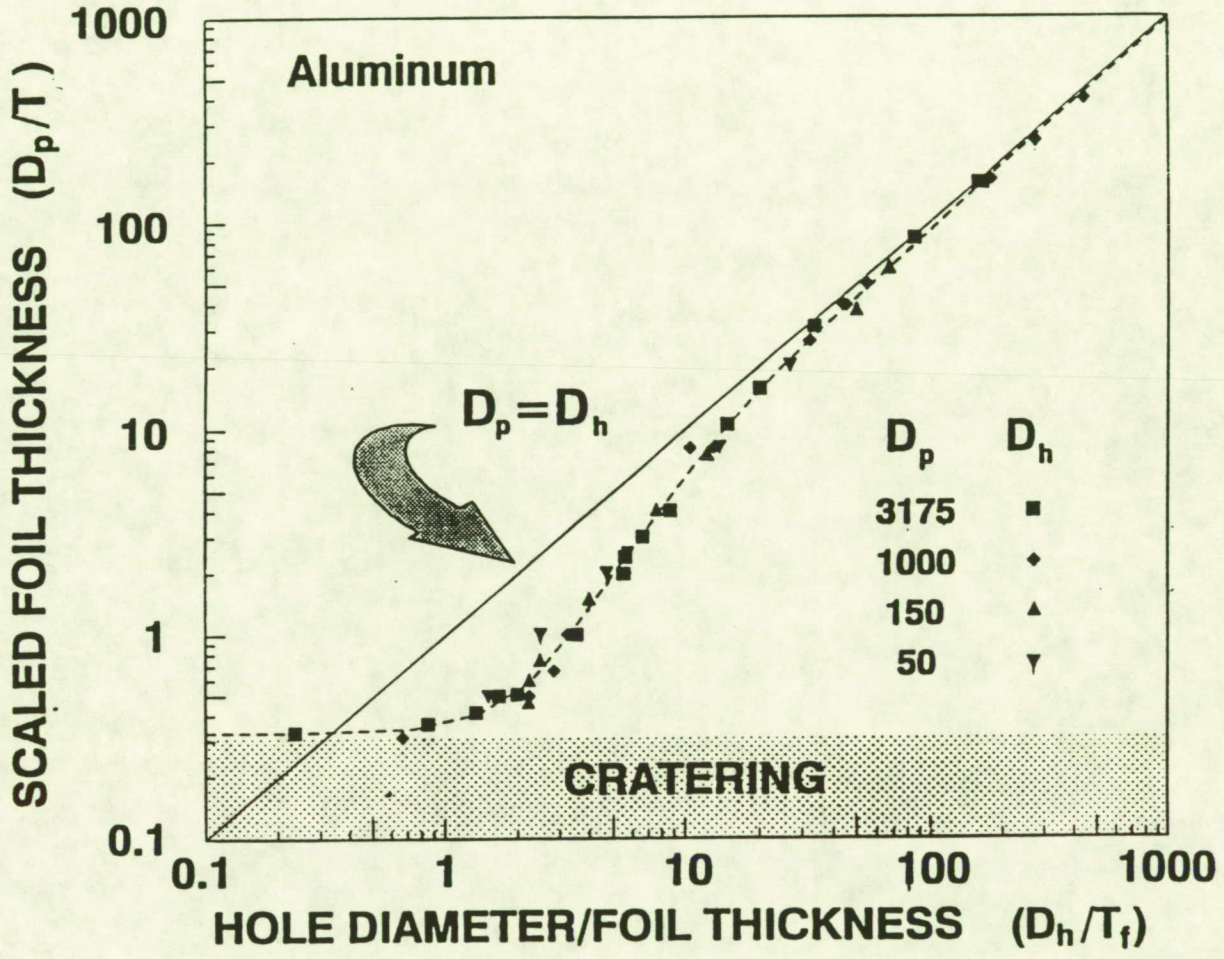

FIGURE 4. Empirically determined relationship of penetration hole diameter (D_h), foil thickness (T) and projectile diameter (D_p) at 6 km/s. Note that these relationships yield unique solutions for D_p from the measurement of D_h and T on space exposed membranes.

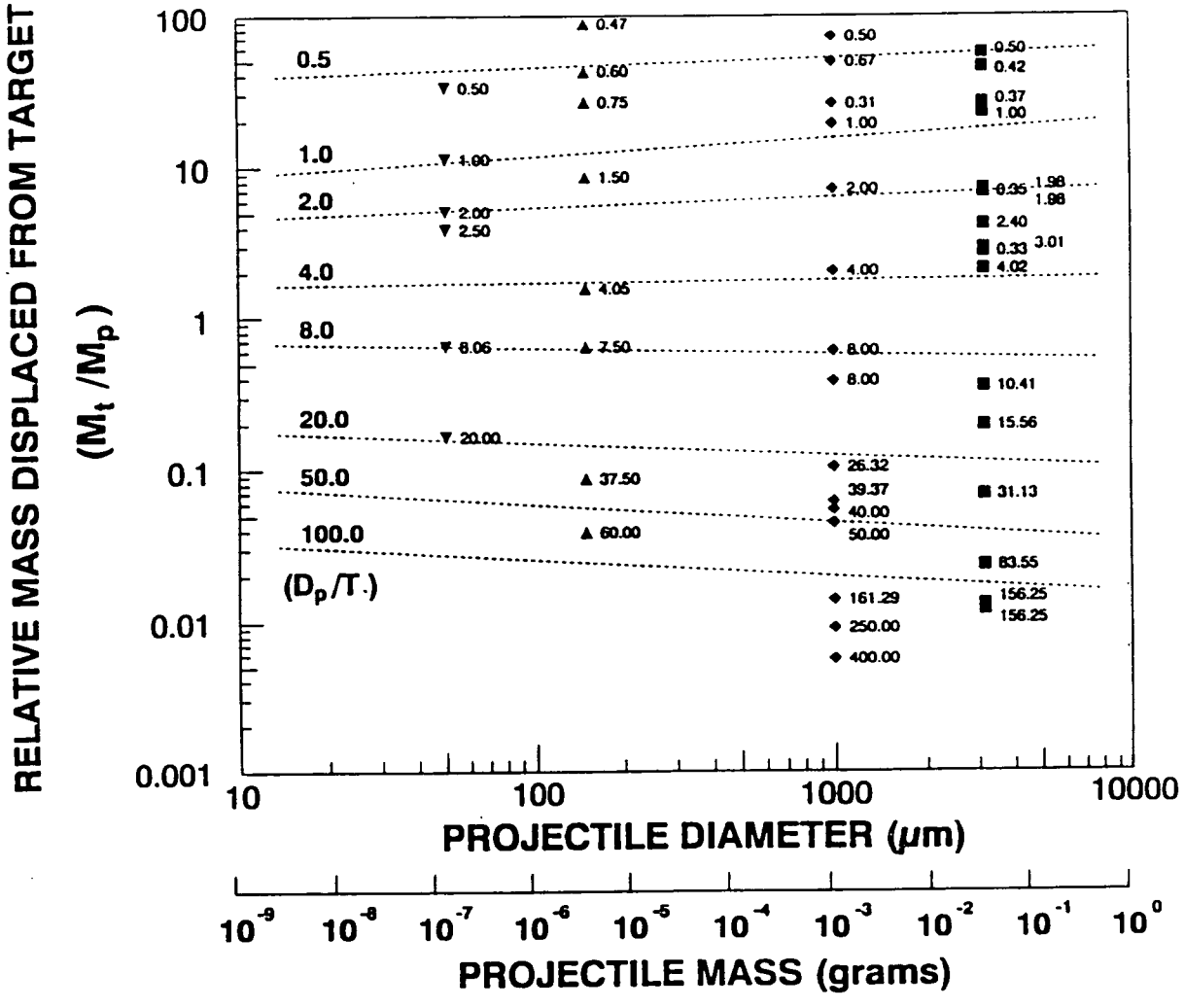

FIGURE 5. Summary of all target mass (m_T=M_t), normalized to impactor mass (m_P = M_p) that was displaced during thin-film penetrations of four different impactors (vertical columns) and as a function of target thickness; D_p/T is arranged in vertical sequence for a given impactor and indicated next to each datum. Dashed lines are visual interpolations for integer, convenient numbers of D_p/T (bold print).

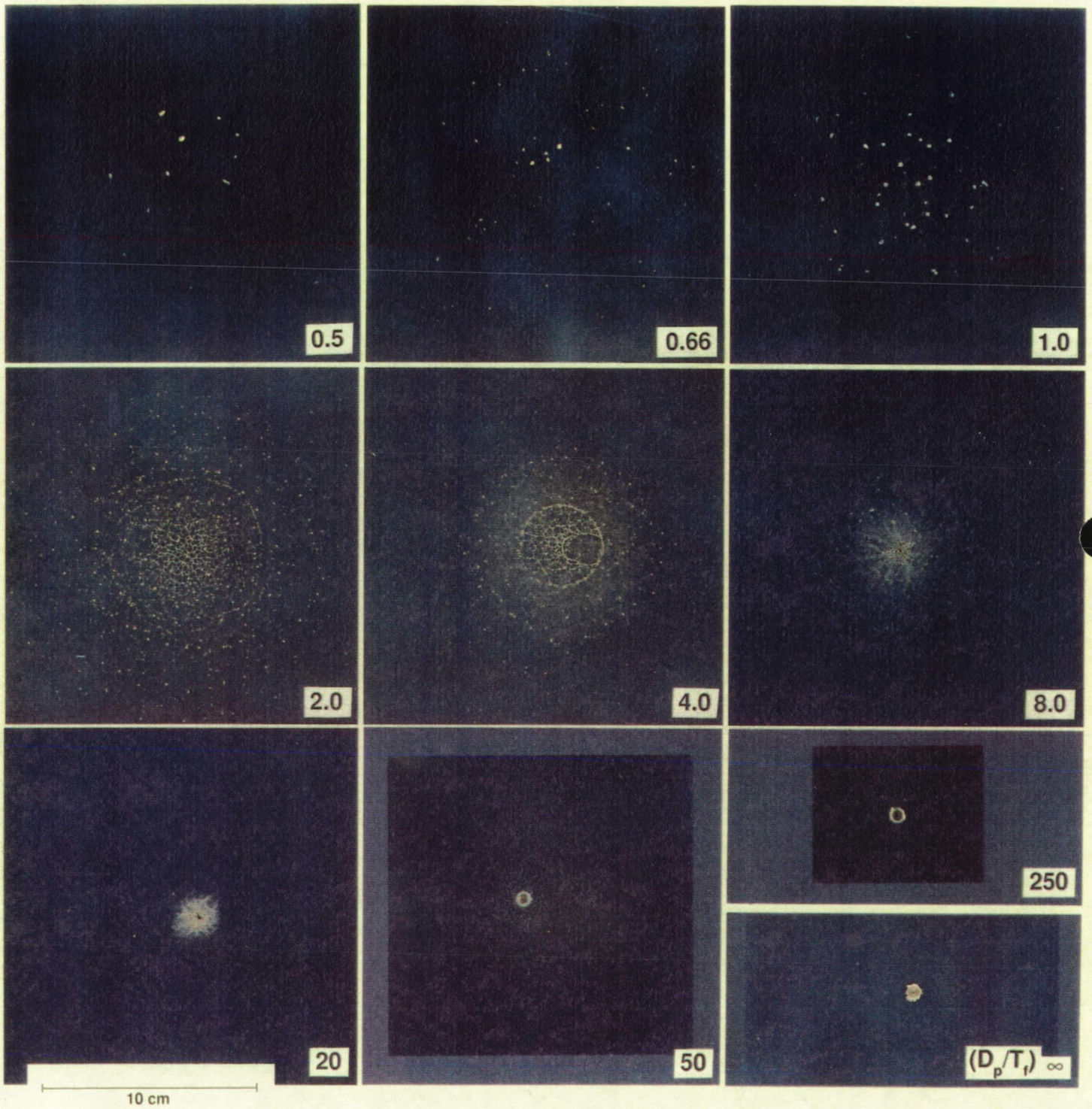

FIGURE 6. Typical patterns of debris spray that resulted from a select set of experiments illustrated in Figure 3, utilizing 1 mm impactors. Note the similarity in spray geometry at equivalent D_p/T with Figure 7, although the latter employed Teflon targets.

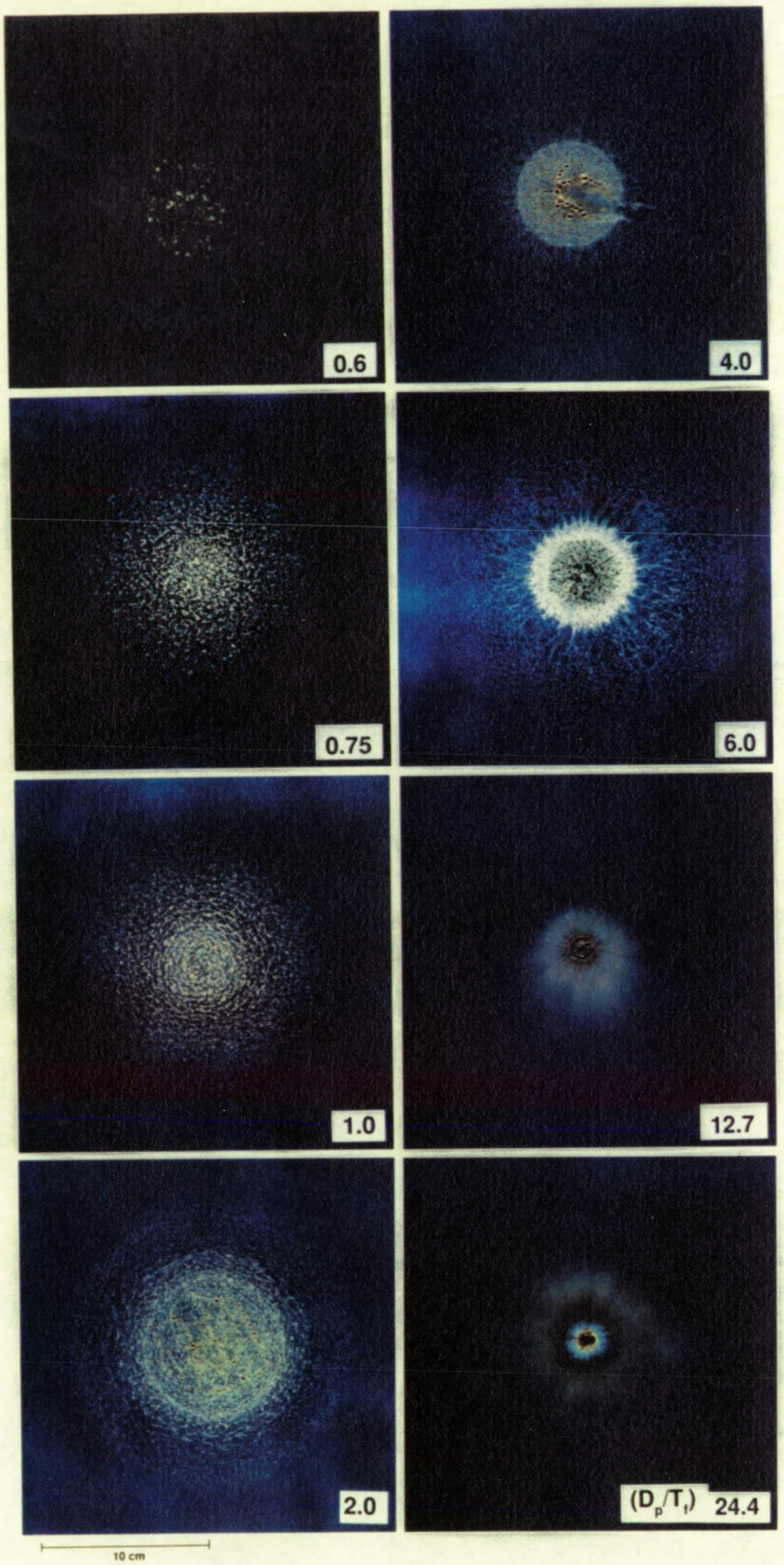

FIGURE 7. Typical patterns of debris spray on witness plates to the targets' rear. The target material was Teflon rather than aluminum; the projectile was the standard 1/8" soda-lime glass sphere. Teflon targets are illustrated here to show that the trends developed for aluminum targets are of a general nature, and because corresponding spray patterns in aluminum (D_p=1/8"; 6 km/s) are presented in detail throughout this report.

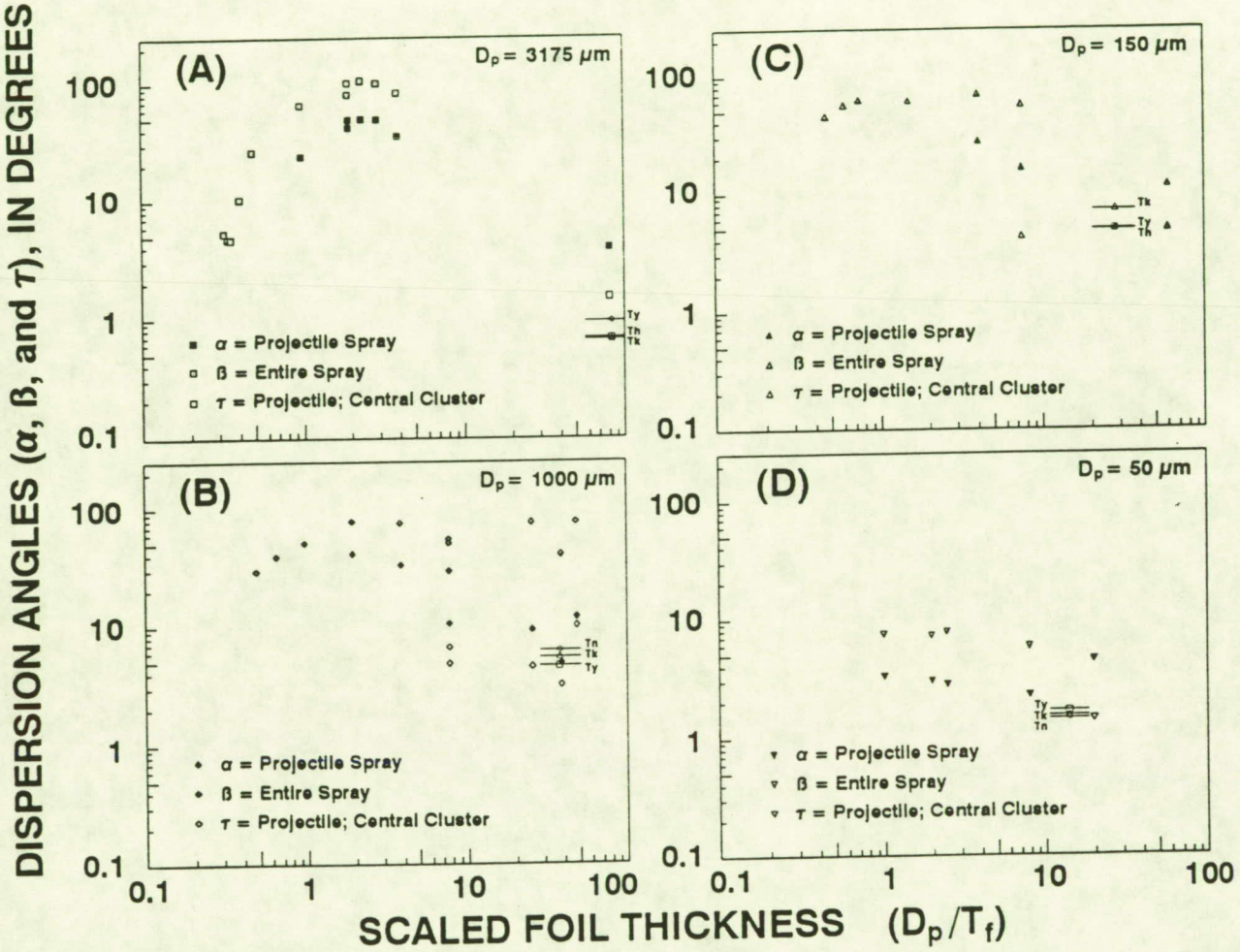

FIGURE 8. The dispersion angles of projectile and target fragments exiting a penetrated foil of scaled thickness D_p/T for each of four projectile sizes, all at some 6 km/s. The horizontal lines at relatively thin foils indicate the generation of an unadulterated crater in the massive witness plates and the corresponding D_p/T thus represents that foil- thickness which permits "intact" projectile passage as defined in Figure 2. Such craters possess finite cone angles in this representation, because it is based on diameter measurements on the witness plate at known stand-off distance. The latter varied from projectile size to projectile size, but was held constant for any specific D_p. Note also that all angles will have to go through some maximum value, because they are demonstrably "0" at $D_p/T<0.2$ (crater in infinite half space target) and they (ideally) are "0" as well for the intact passage of an ultra-thin foil (no projectile dispersion and minimal foil mass available for displacement).

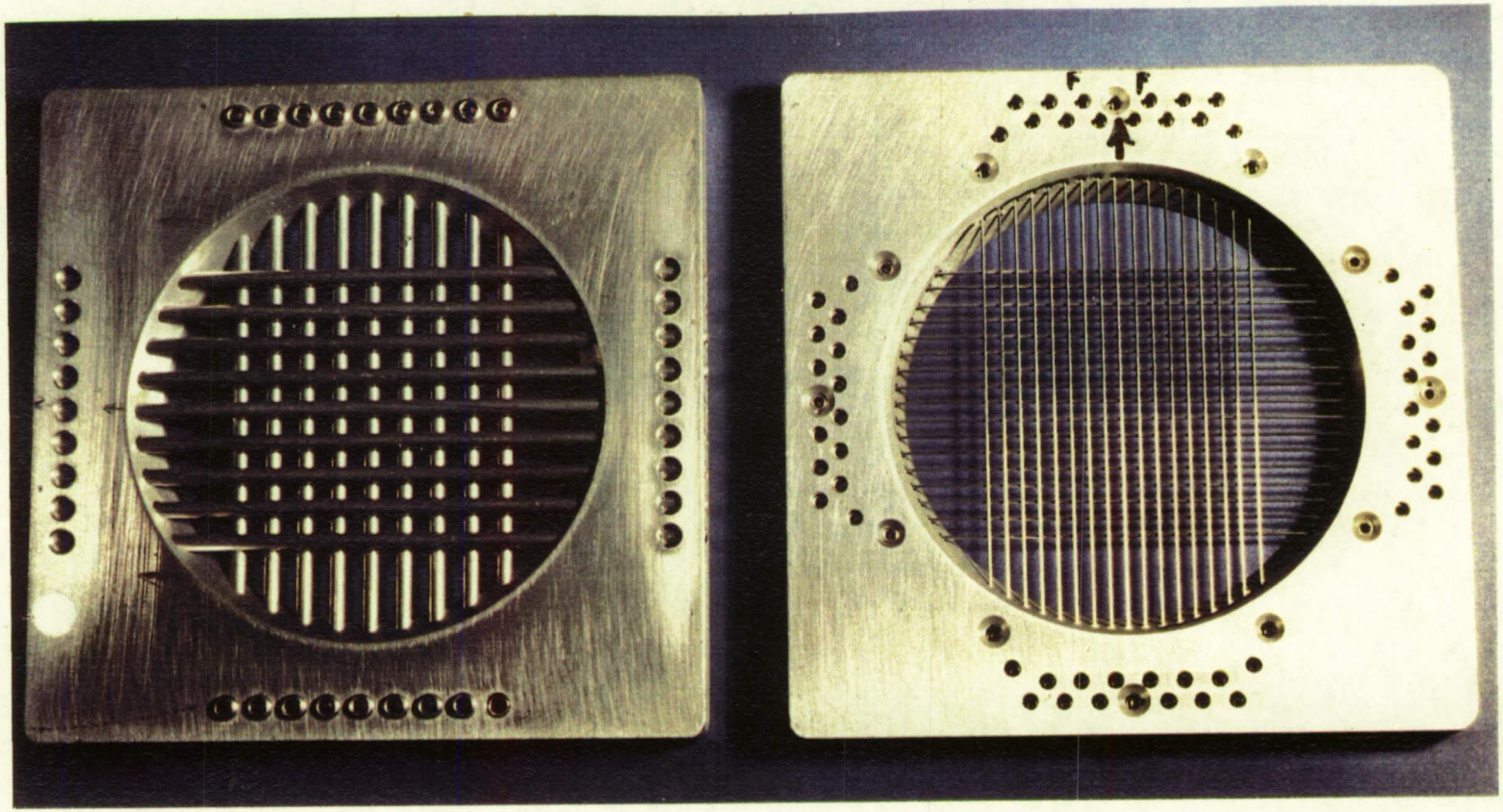

FIGURE 9. Target holder and typical, custom made meshes employed in this study. Note each individual grid wire is held by set-screws and exposed an effective grid some 1.5" x 1.5" on the side (sufficiently large to avoid edge effects). The coarse grid shows 1/8" thick wires, centered at 1/4" distances ($D_p/T=2$ for 1/4" D_p); the fine grid was used with 1/8" diameter impactors and wire thickness is 1/32" in this particular example.

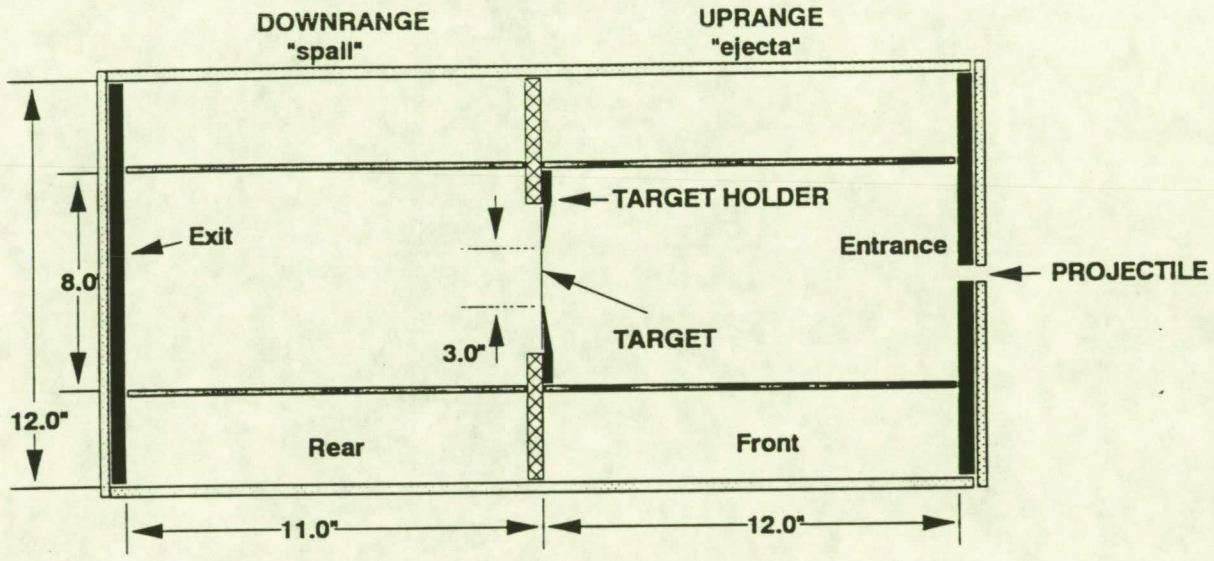

FIGURE 10. Schematic cross-section of target and witness-plate arrangements developed for and employed in this study. Note the sturdy plate that separates the "uprange" and "downrange" volumes and which served as mounting platform for the target holder.

FIGURE 11. (opposite page) The DDF target-box mounted inside the Light-Gas Gun, ready for firing. The entire box was typically removed from the gun-chamber and placed on a clean bench top for removal of the top plate and to quantitatively collect all loose debris in the respective compartments, to retrieve the actual target, to remove all witness plates, and to carefully clean the box interior. A new target and sets of witness plates were installed then and the completely assembled box was returned to the gun chamber for the next experiment.

ORIGINAL PAGE
COLOR PHOTOGRAPH

PRECEDING PAGE BLANK NOT FILMED

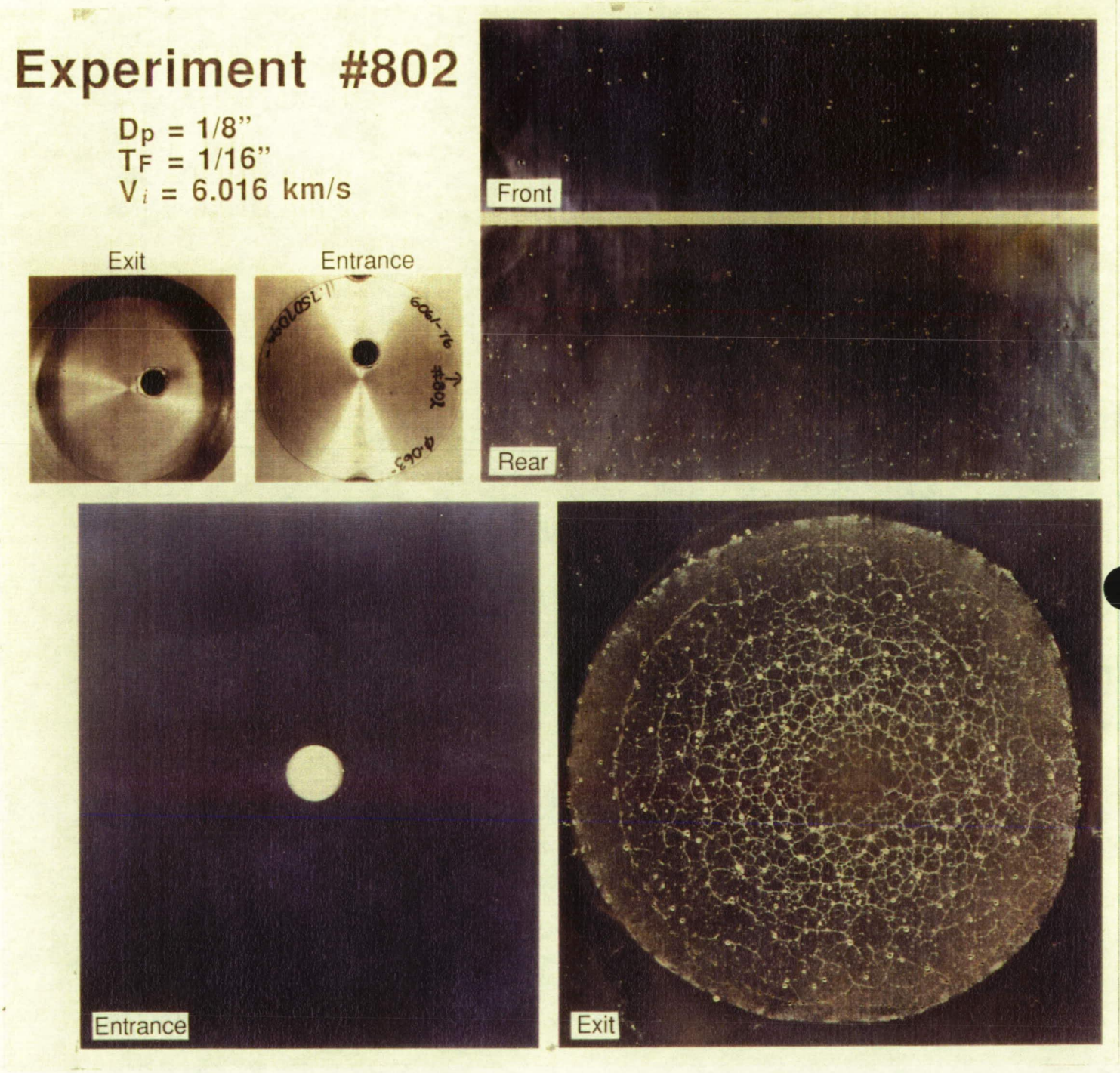

FIGURE 12. Experiment 802, employing $D_p/T=2$; $D_p=3.2$ mm; V=6.016 km/s and a continuous membrane target. A relatively centro-symmetric distribution of debris is observed on the entrance and exit plates. The cylindrical front and rear plates display centro-symmetric distributions of penetration holes as well (penetration hole density in a lateral sense, as total plate length corresponds to 360°); however, vertical gradients in the spatial density of penetrations indicate a conically expanding debris cloud with distinct mass concentrations and associated take-off angles. Clearly, all geometric relations of the debris clouds are preserved on the four witness plates and details could be reconstructed, in principle. Note the similarity of the exit plate spray patterns with those illustrated in Figures 6 and 7, and note specifically, the production of discernable ejecta populations on the uprange witness plates.

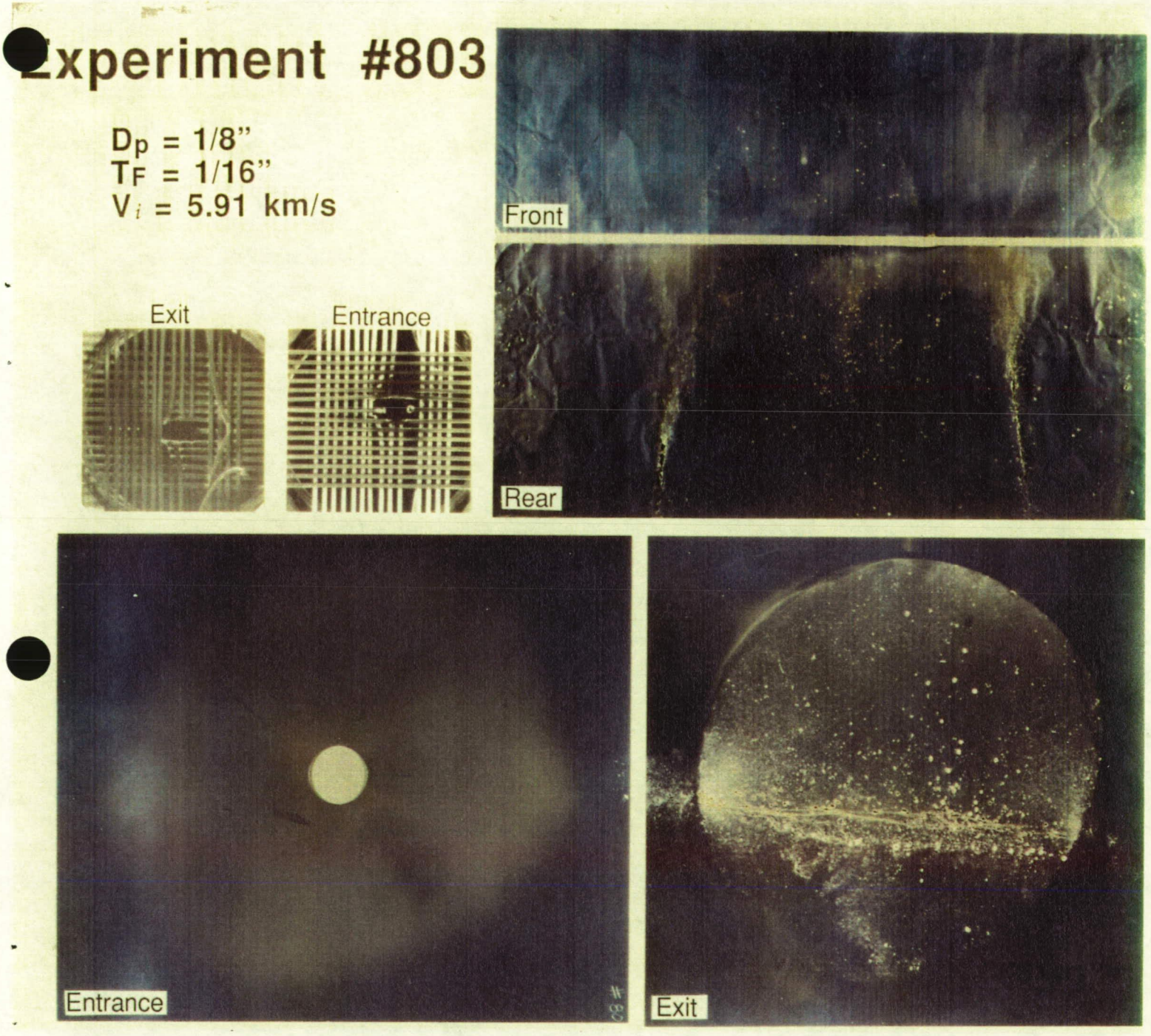

FIGURE 13. Witness plate spray patterns of experiment 803, employing a 3.2 mm impactor at 5.91 km/s and target rods of 1.6 mm thickness ($D_p/T = 2$), thus constituting the dimensional equivalent to Figure 12. Note the linear concentration of impacts on the exit plate which reflects the direct hit of a single target rod, and how this pattern continues on the cylindrical rear plate in the form of two linear concentrations, approximately 180° apart. Some evidence for impact with a second wire is manifested by two arched sprays on the cylindrical front plate, which are also 180° apart, but that are at approximately 90° from the linear spray of the rear plate; the secondary concentration of penetrations (in the middle) of the rear plate seems to be related to the destruction of the second wire as well. Note the substantially decreased number of uprange impacts relative to Figure 12, indicating that significantly less mass was ejected. On the other hand, the highly localized impacts on the cylindrical rear plate caused substantially more severe damage compared to the downrange debris of Figure 12.

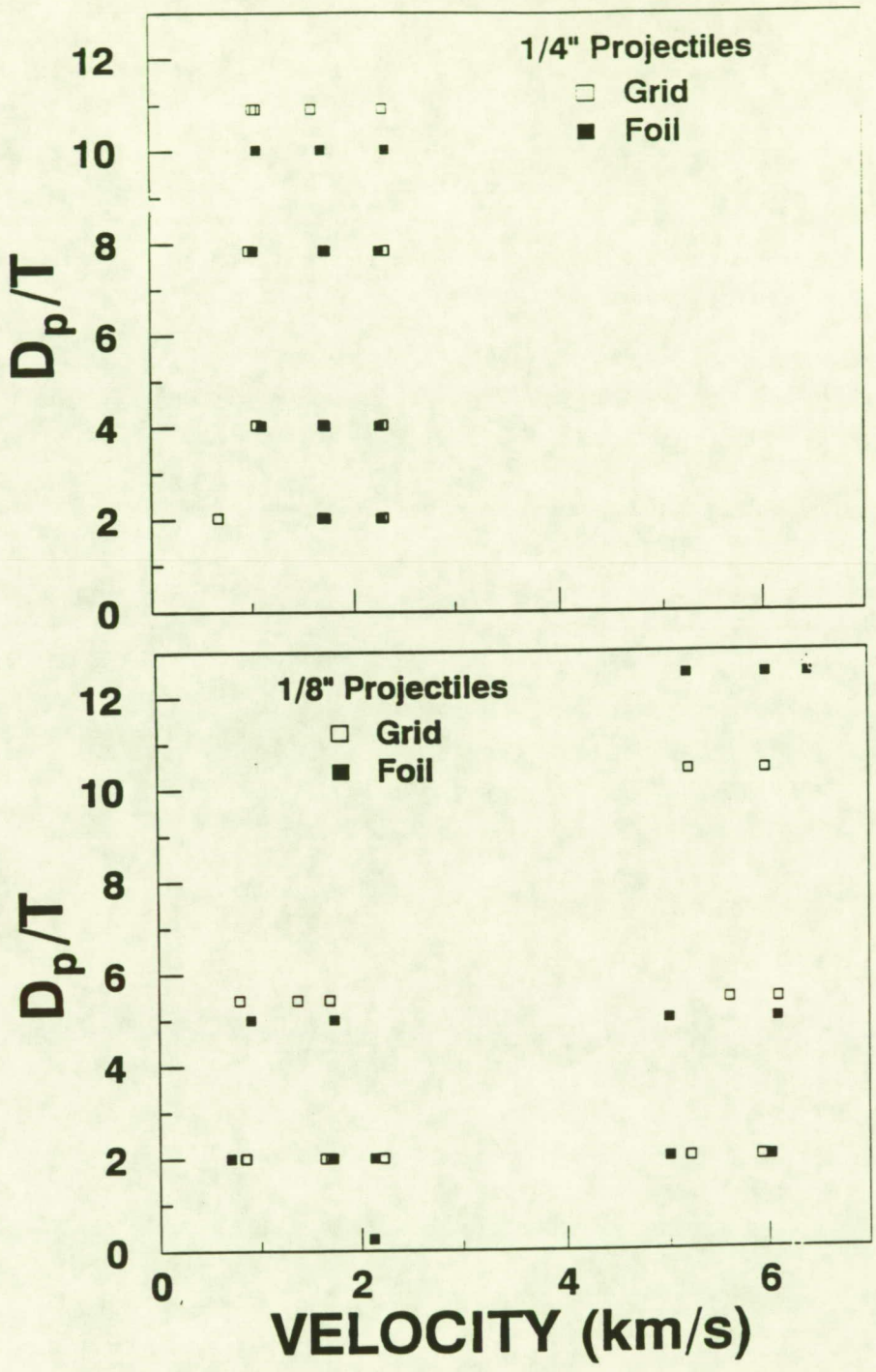

FIGURE 14. Visual display of the (major) initial conditions of all experiments conducted in this study and how these conditions fit the parametric matrix of interest. (A) Illustrates 1/4 " (6.3 mm) projectiles and (B) those employing 1/8" (3.2 mm) glass spheres. These figures may aid when studying the detailed photographic products to follow, because they rapidly convey the relationship among diverse variables. Detailed conditions and supporting data are listed in Table 1.

Continuous Bumper Targets

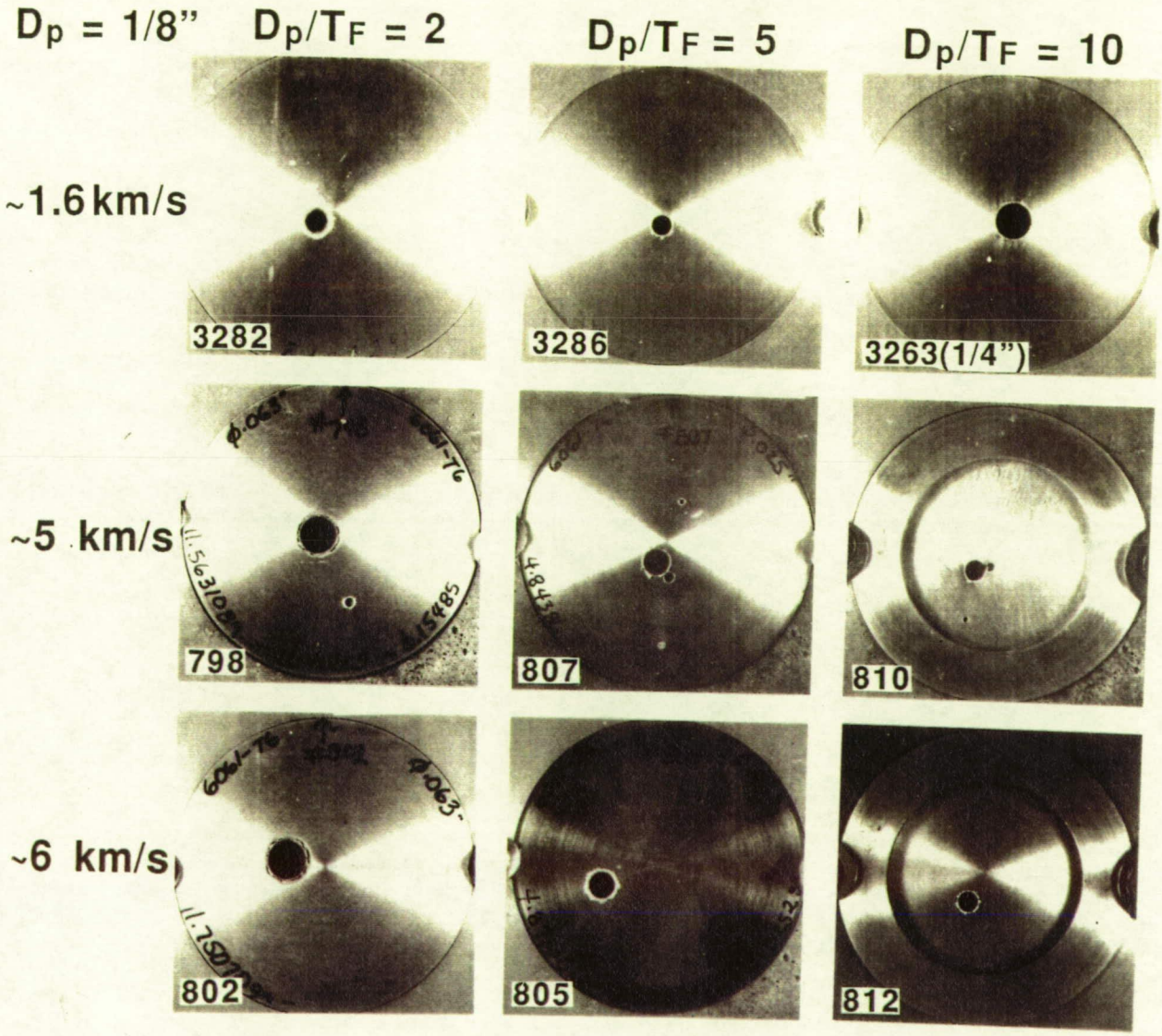

FIGURE 15A. Photodocumentation of representative penetration holes in continuous targets made from aluminum 6061-T6 sheet stock. All experiments, except 3263, employed 1/8" impactors (see text for detailed discussions and interpretations).

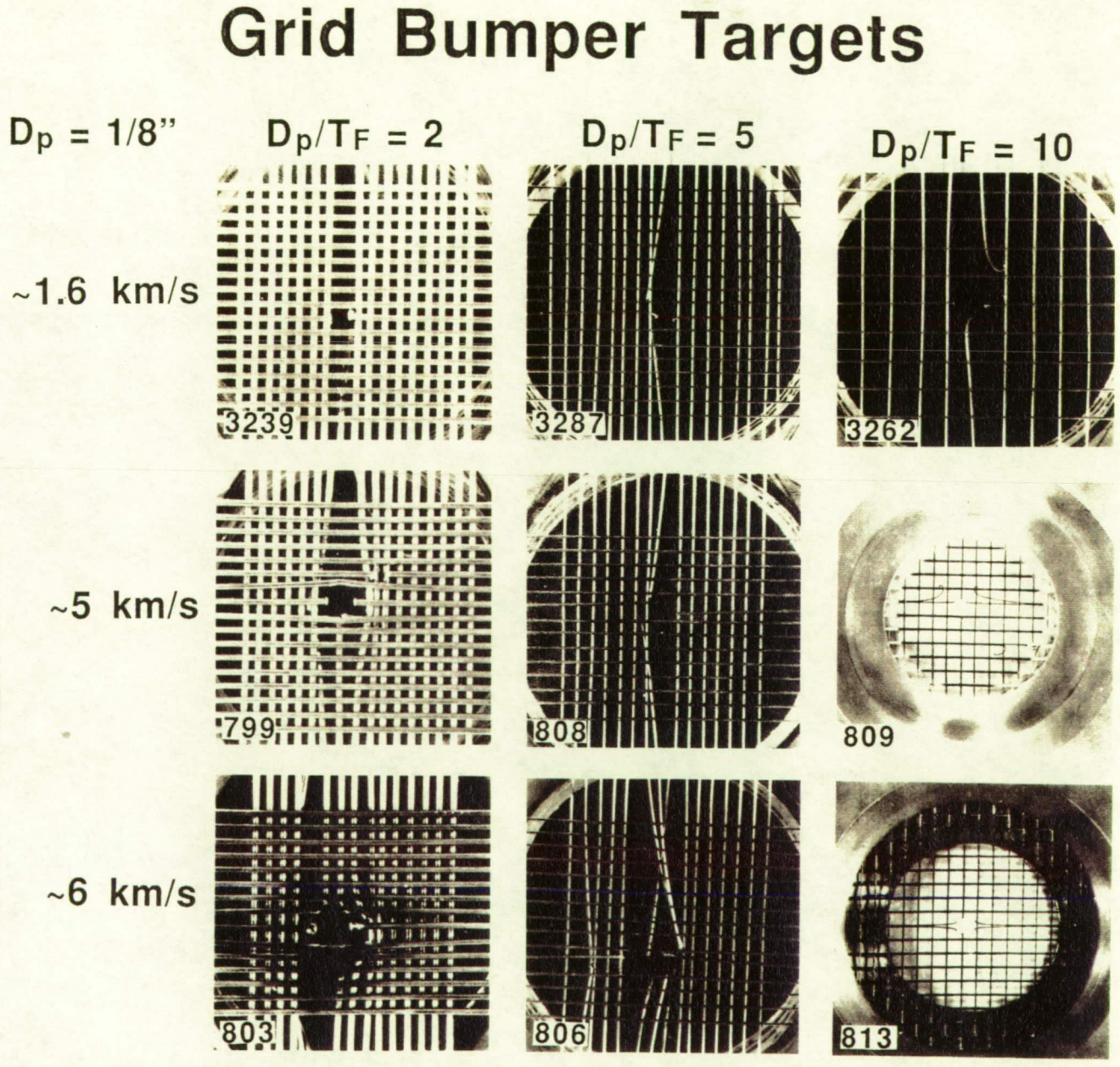

FIGURE 15B. Photodocumentation of representative grid-targets illustrating the nature of penetrations and the extend of damage to neighboring grid elements at experimental conditions that are equivalent to those of Figure 15A (see text for detailed discussions and interpretations).

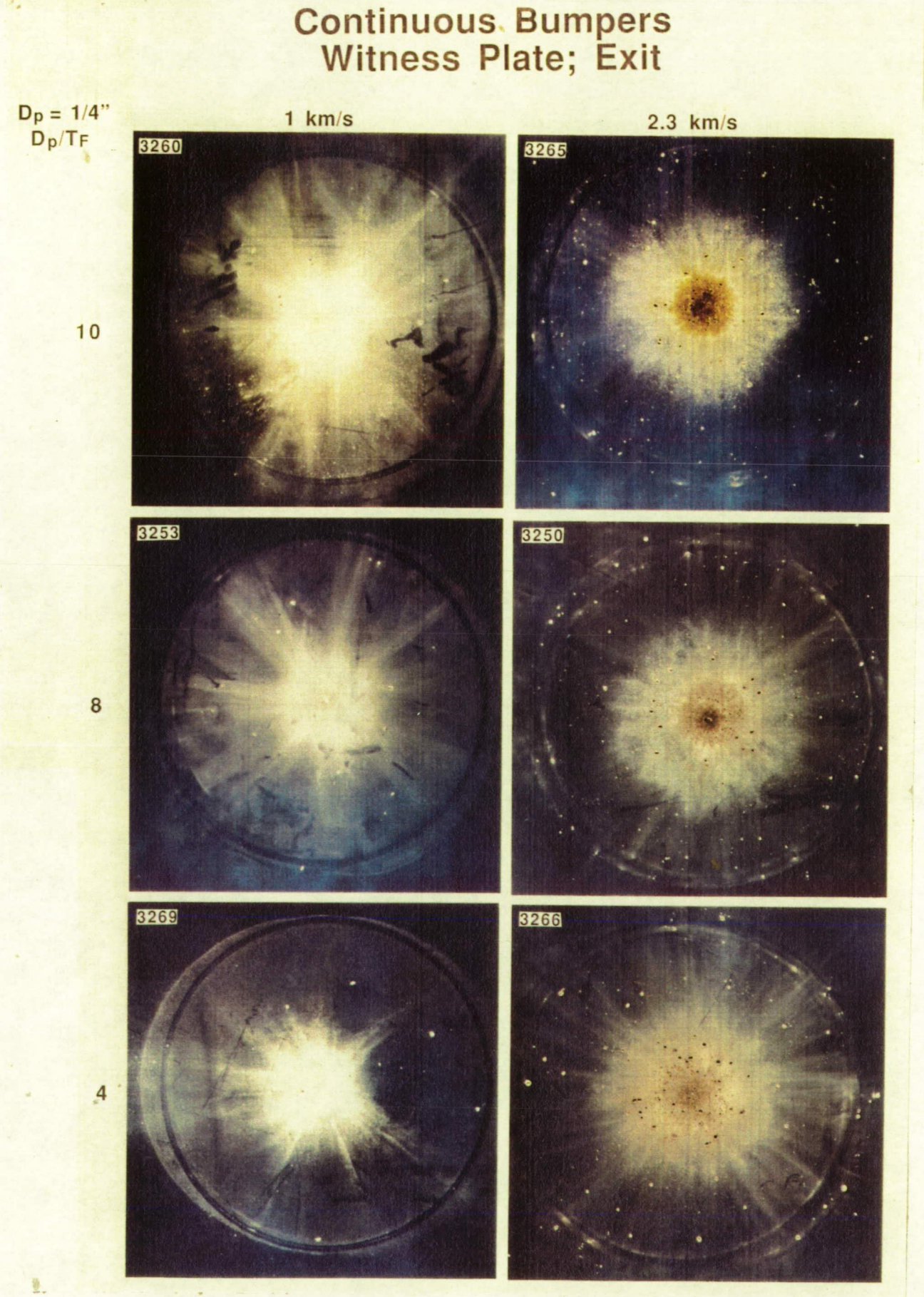

FIGURE 16A. Photodocumentation of Exit Plates employing continuous targets at low velocity and 1/4" diameter impactors (for details see text).

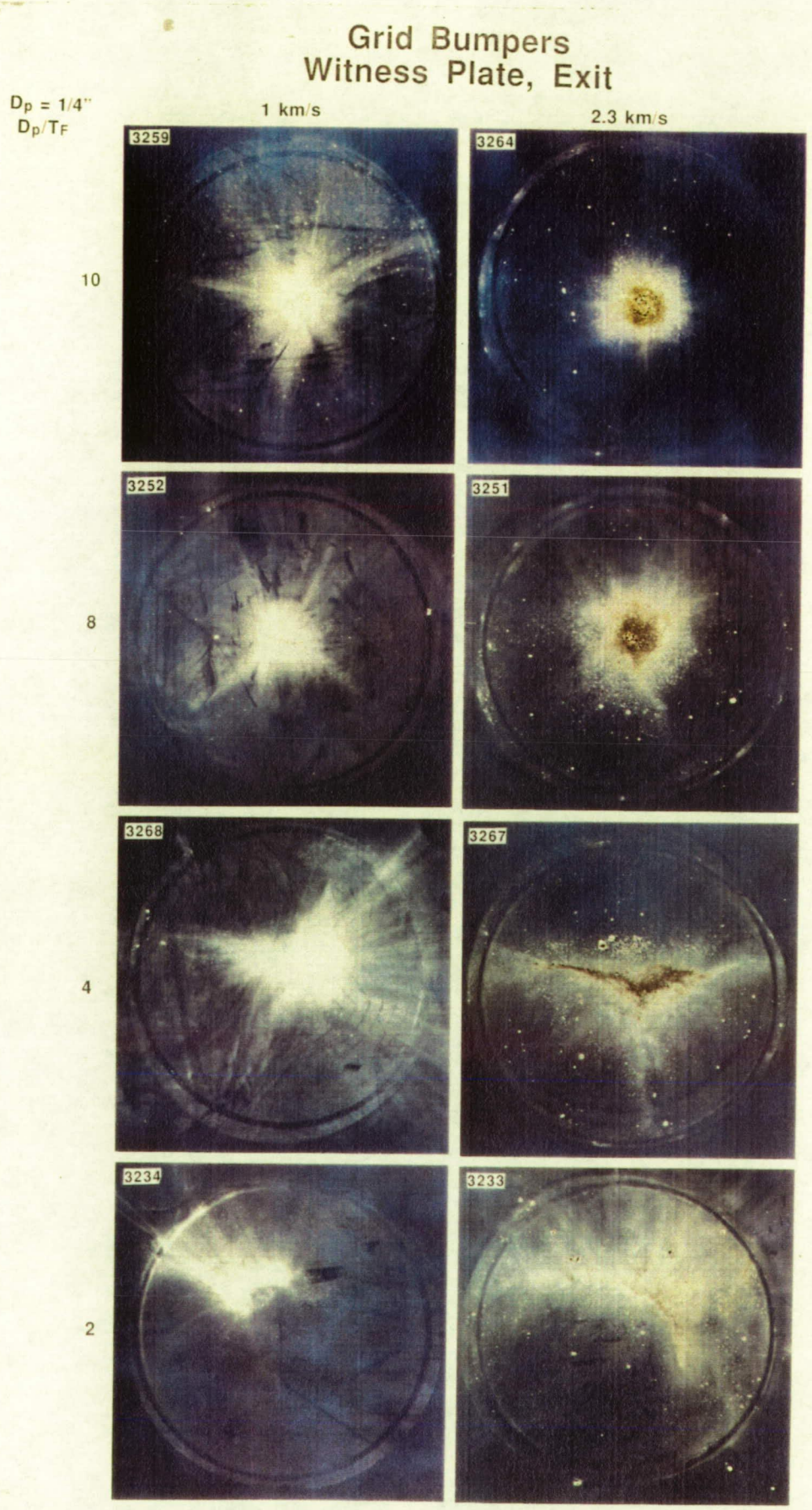

FIGURE 16B. Photodocumentation of Exit Plates employing grid-targets at experimental conditions that duplicate those of Figure 16A, save the $D_p/T=2$ case, which was not conducted with the continuous membranes.

Continuous Bumpers
Witness Plate; Exit

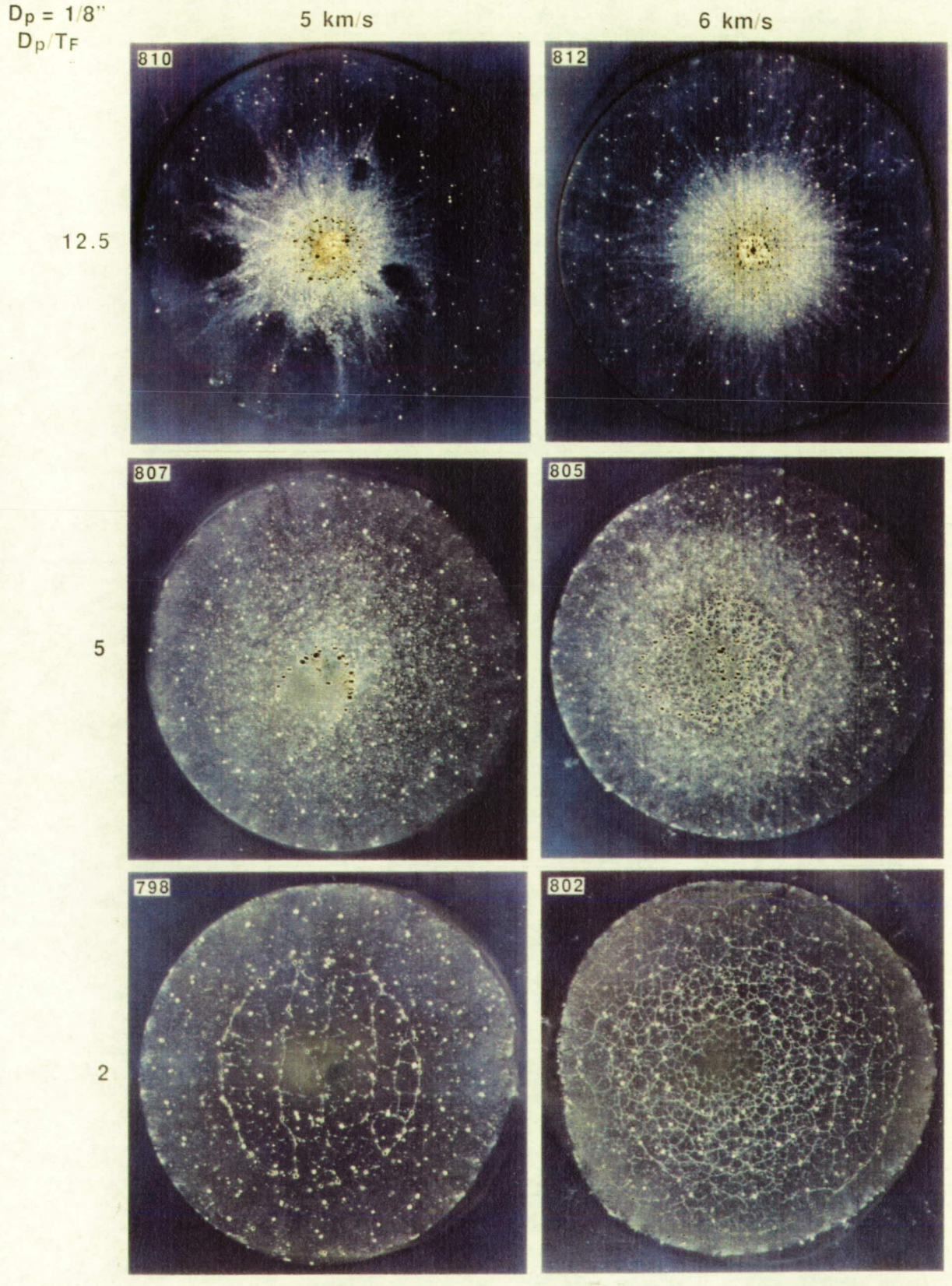

FIGURE 17A. Photodocumentation of Exit Plates employing continuous targets at 5 and 6 km/s, using 1/8" diameter projectiles (for details see text).

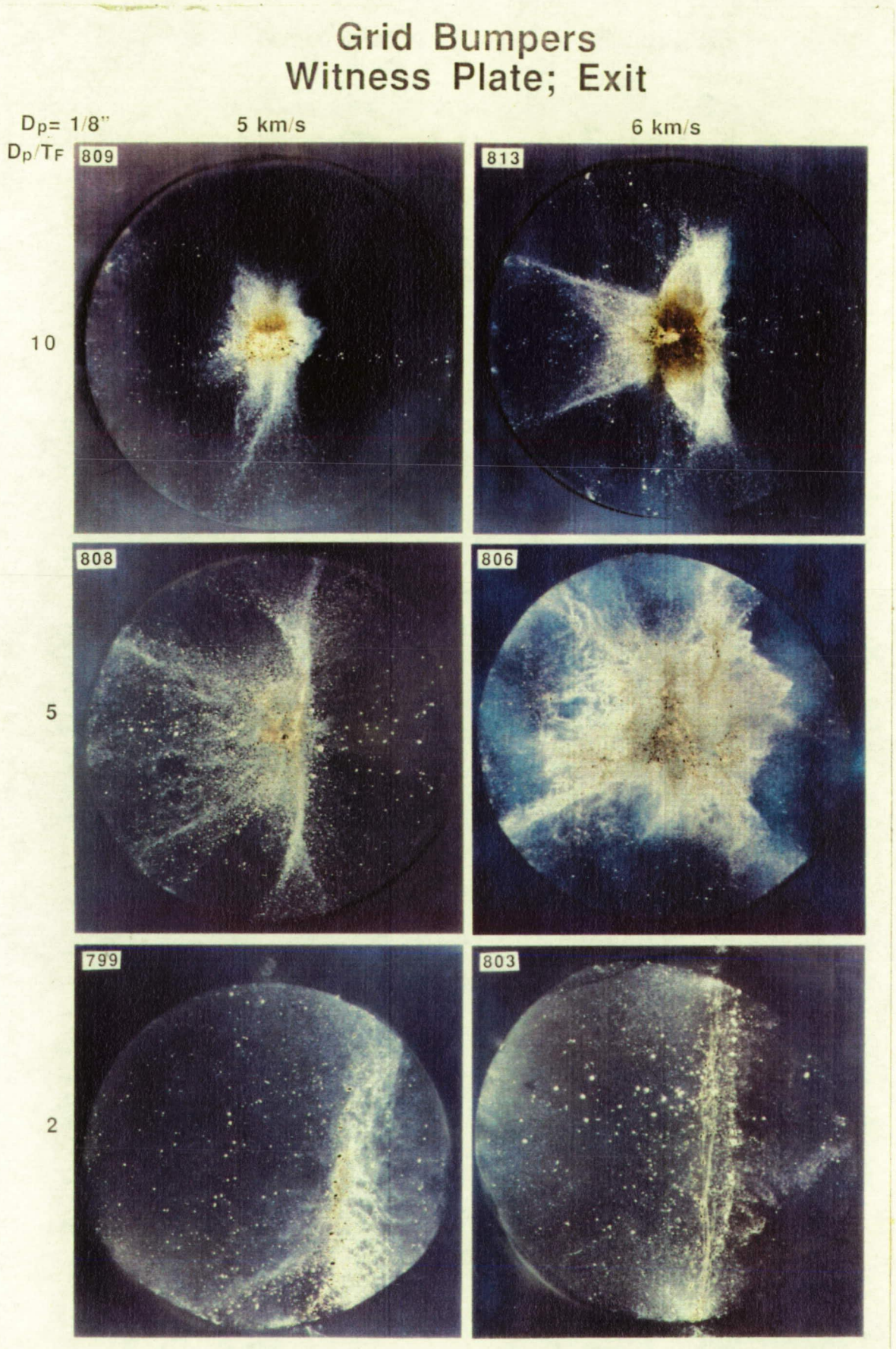

FIGURE 17B. Photodocumentation of Exit Plates employing grid-targets at experimental conditions that essentially duplicate those of Figure 17A (unfortunately 806 is an enlargement, somewhat out of scale)

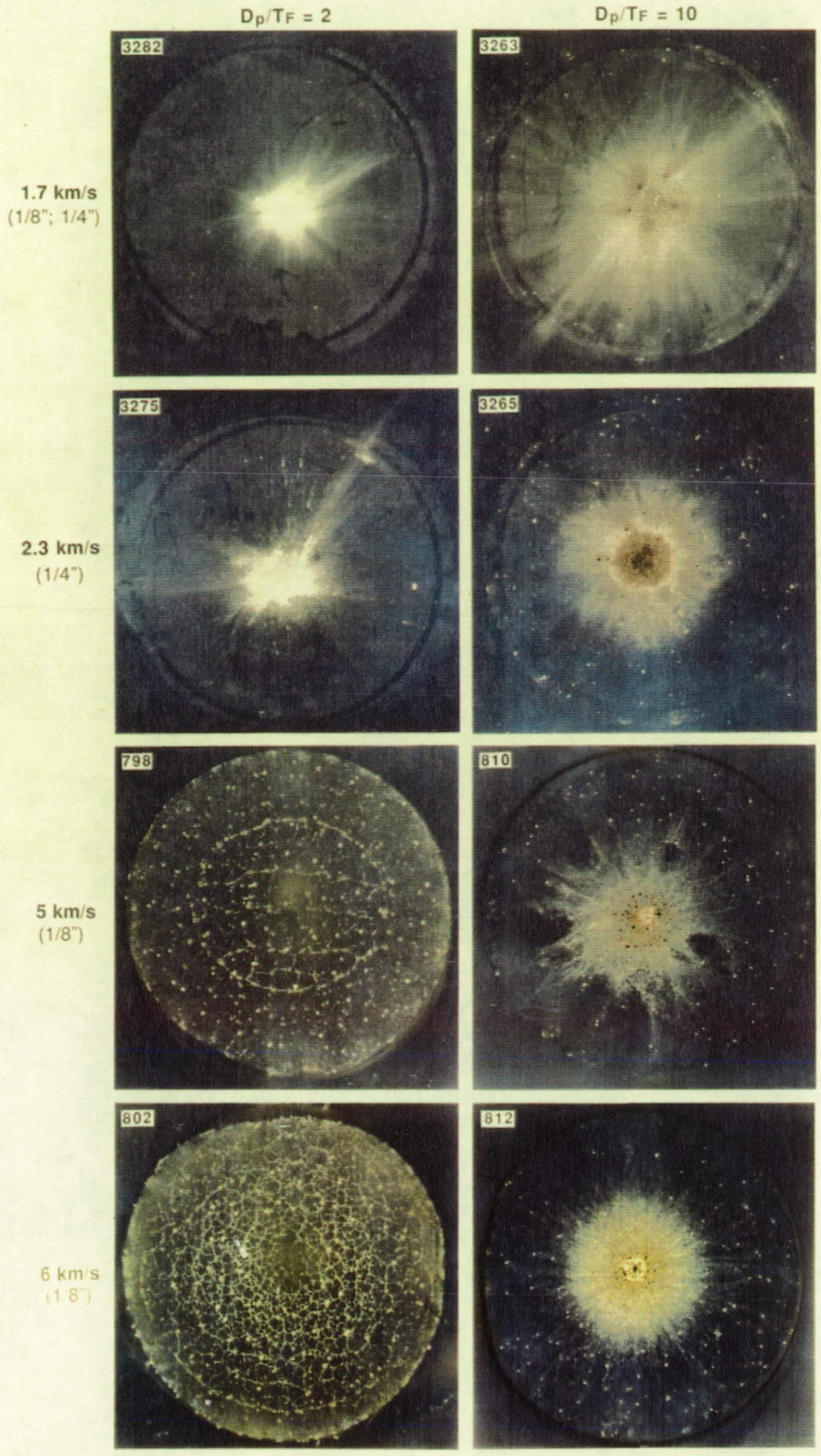

FIGURE 18A. Photodocumentation of Exit Plates employing continuous targets that illuminate the effects of velocity for two target thicknesses (for details see text).

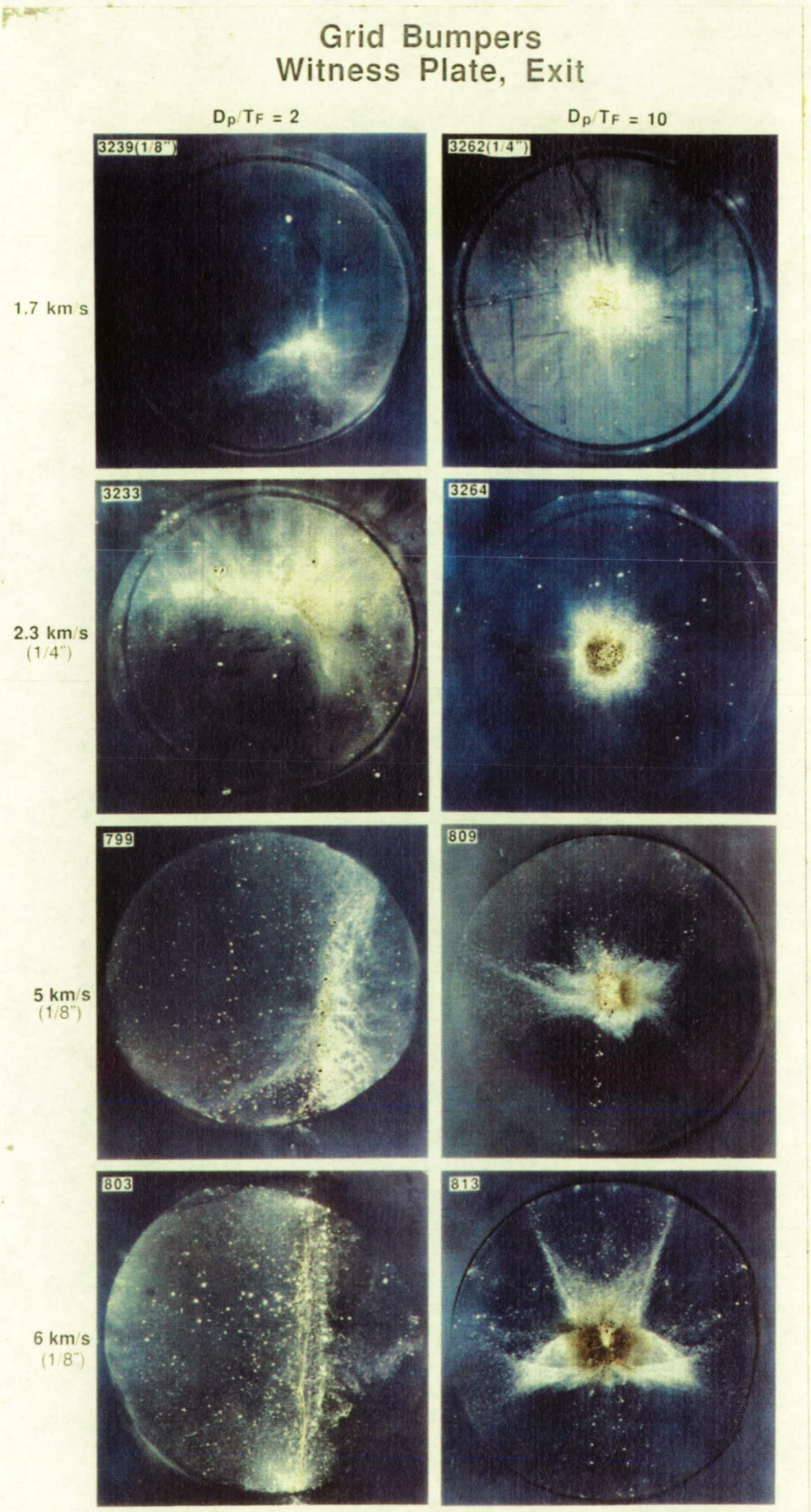

FIGURE 18B. Photodocumentation of Exit Plates employing grid-targets at experimental conditions that essentially duplicate those of Figure 18A.

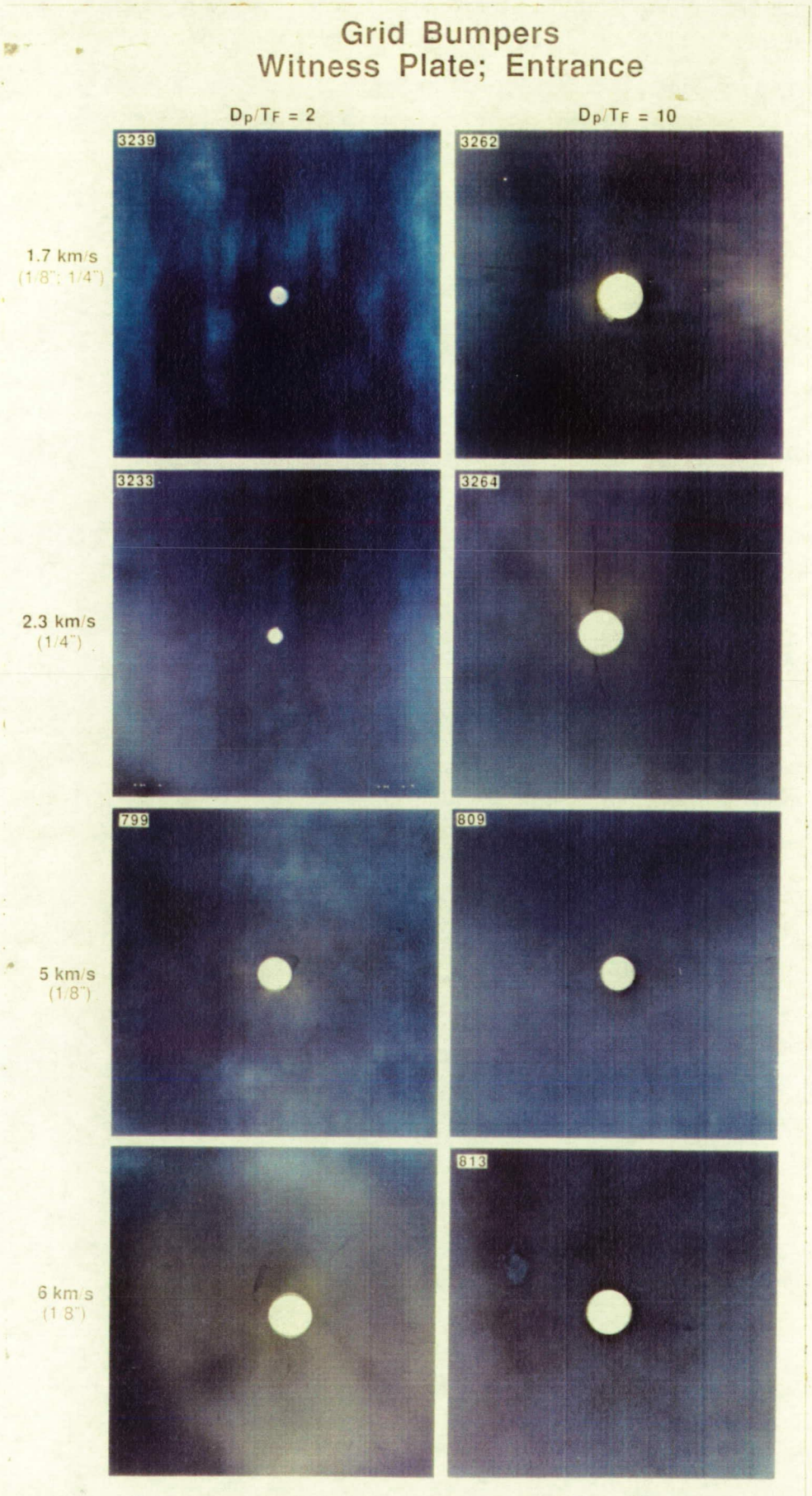

FIGURE 19. Photodocumentation of Entrance plates for grid-targets that illuminate the effects of velocity for two target thicknesses (for details see text).

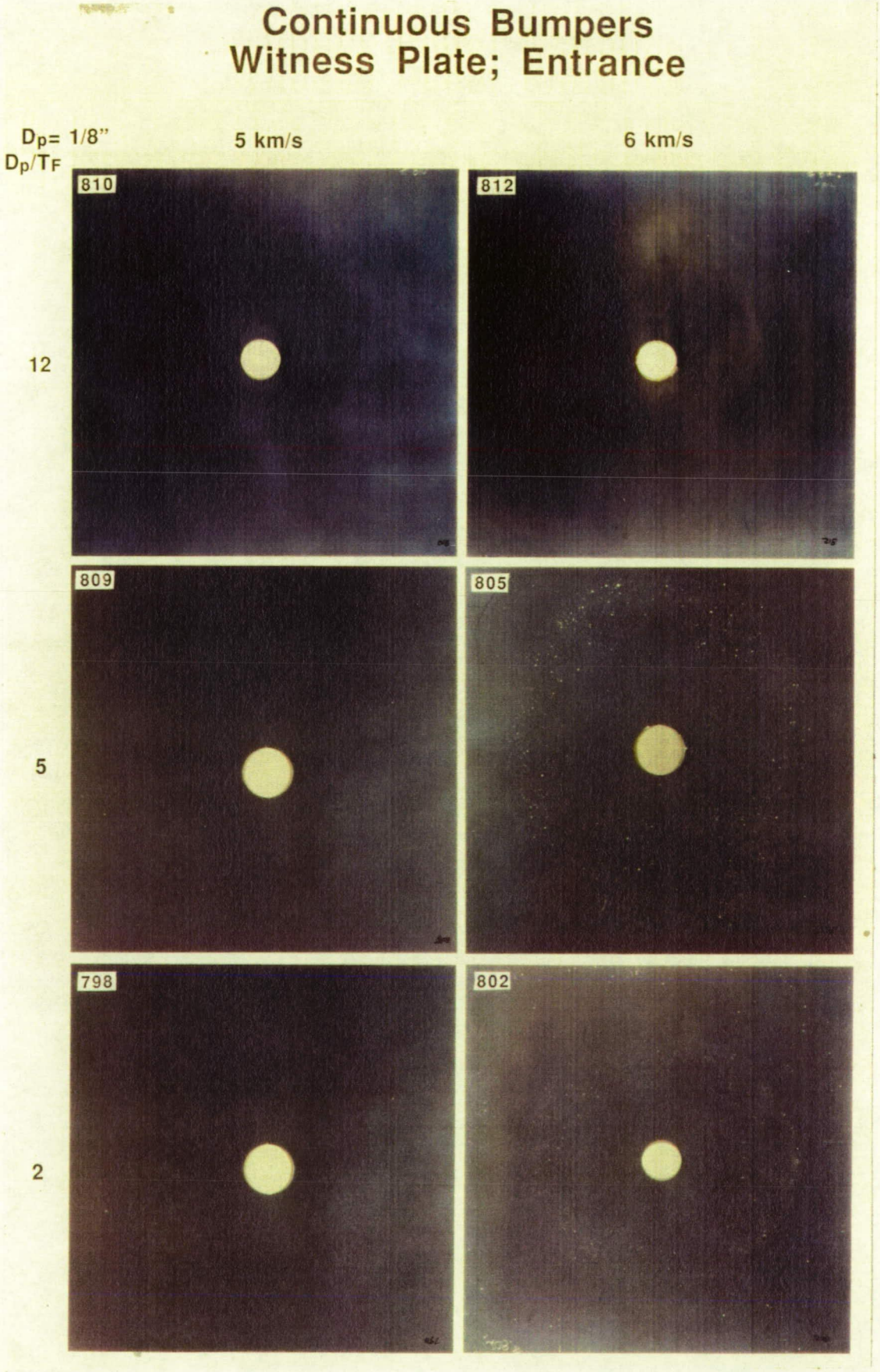

FIGURE 20A. Photodocumentation of Entrance Plates for high velocity impactors encountering continuous targets of three different thicknesses (for details see text).

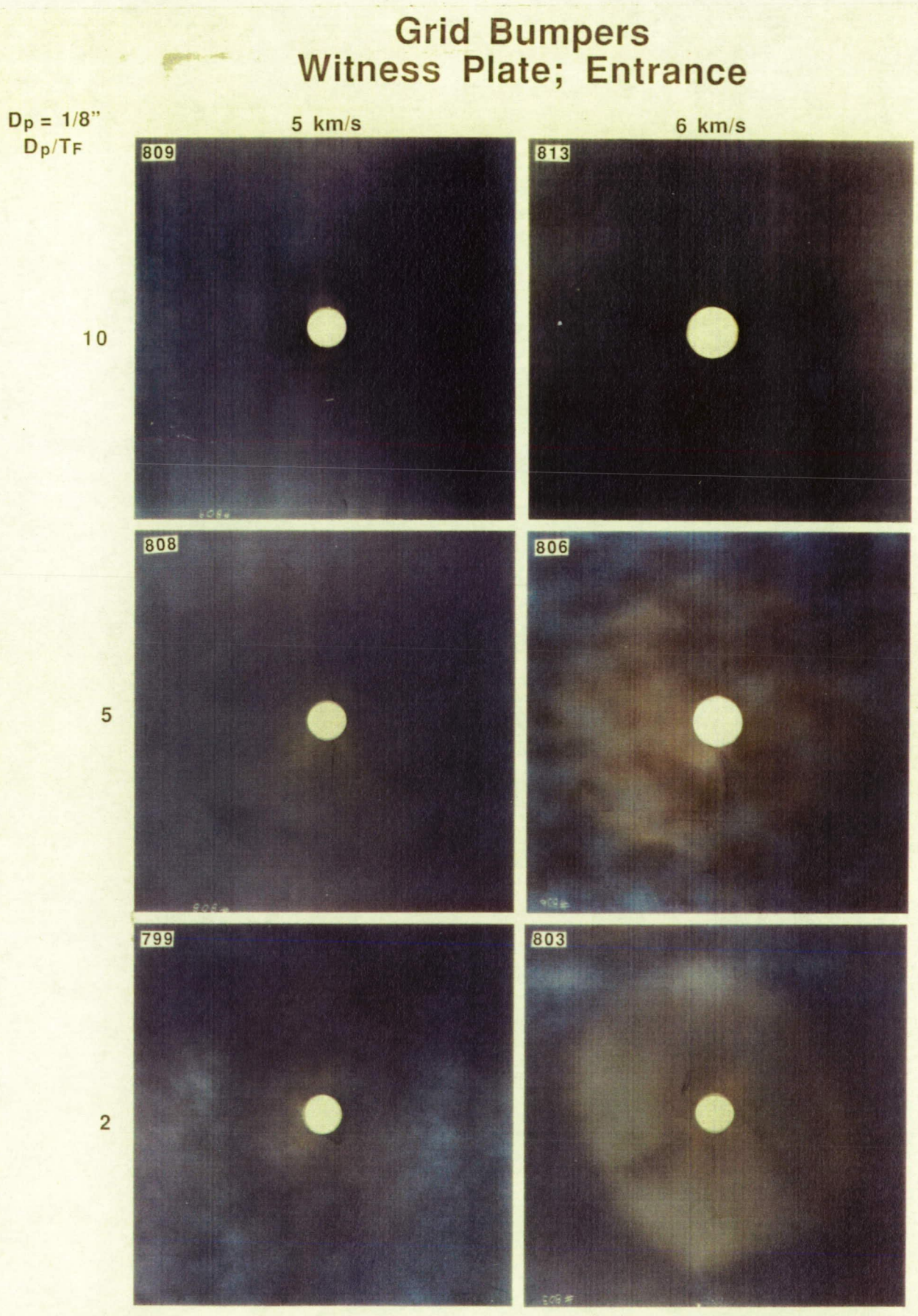

FIGURE 20B. Photodocumentation of Entrance Plates for grid-targets at experimental conditions that essentially duplicate those of Figure 20A.

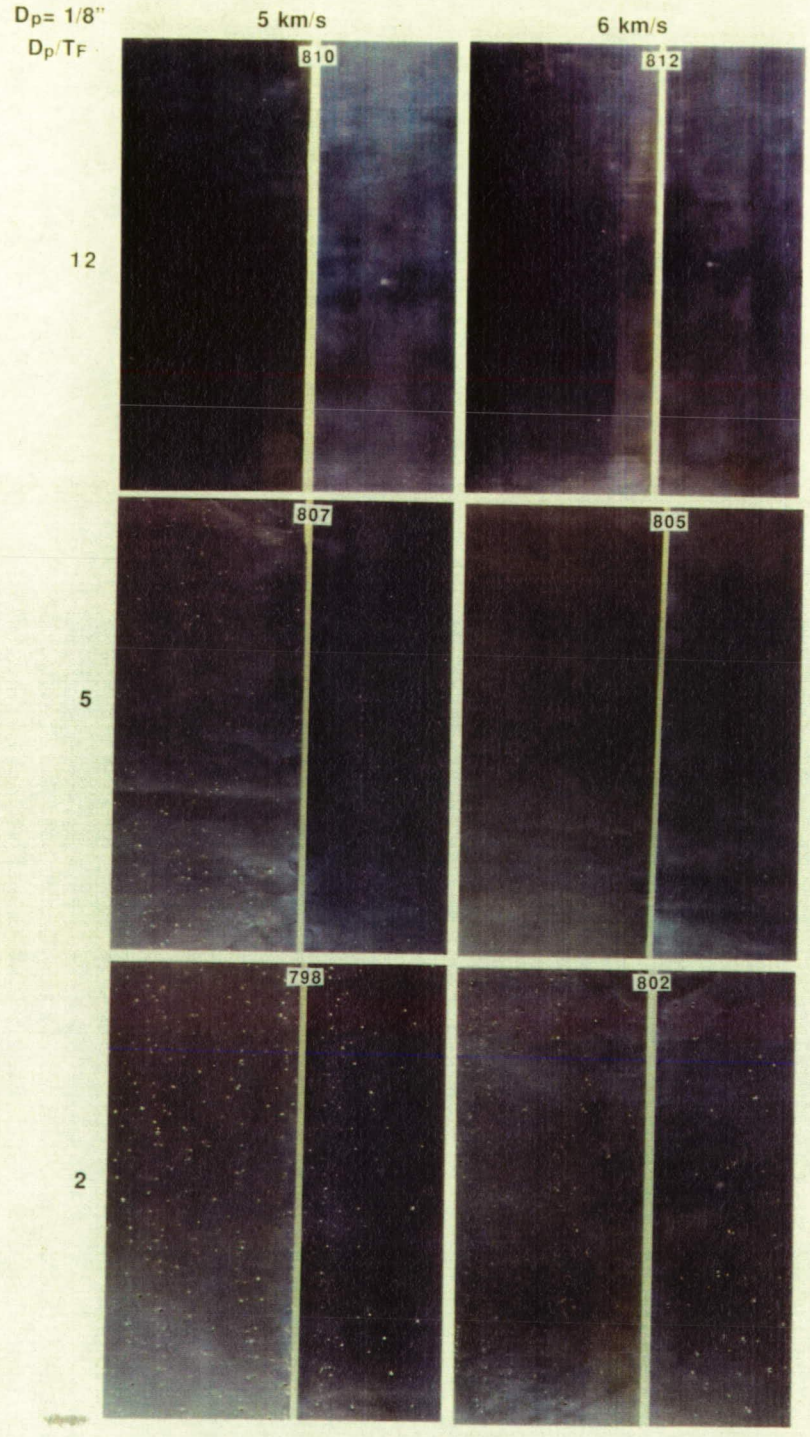

FIGURE 21A. Photodocumentation of the cylindrical witness plates following penetration of continuous targets by high-velocity impactors (for detail see text).

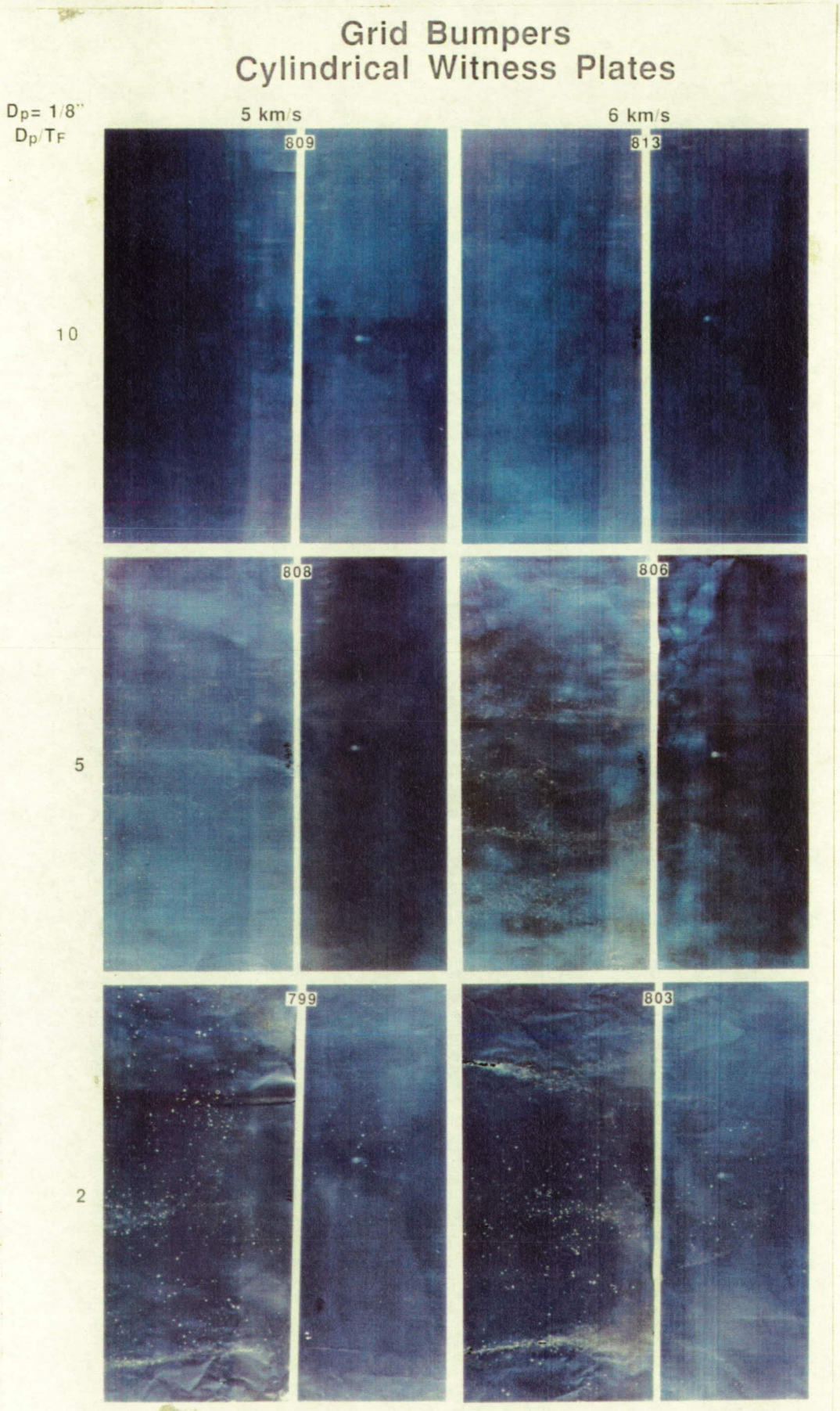

Figure 21B. Photodocumentation of the cylindrical witness plates employing grid-targets at experimental conditions that essentially duplicate those of Figure 21A.

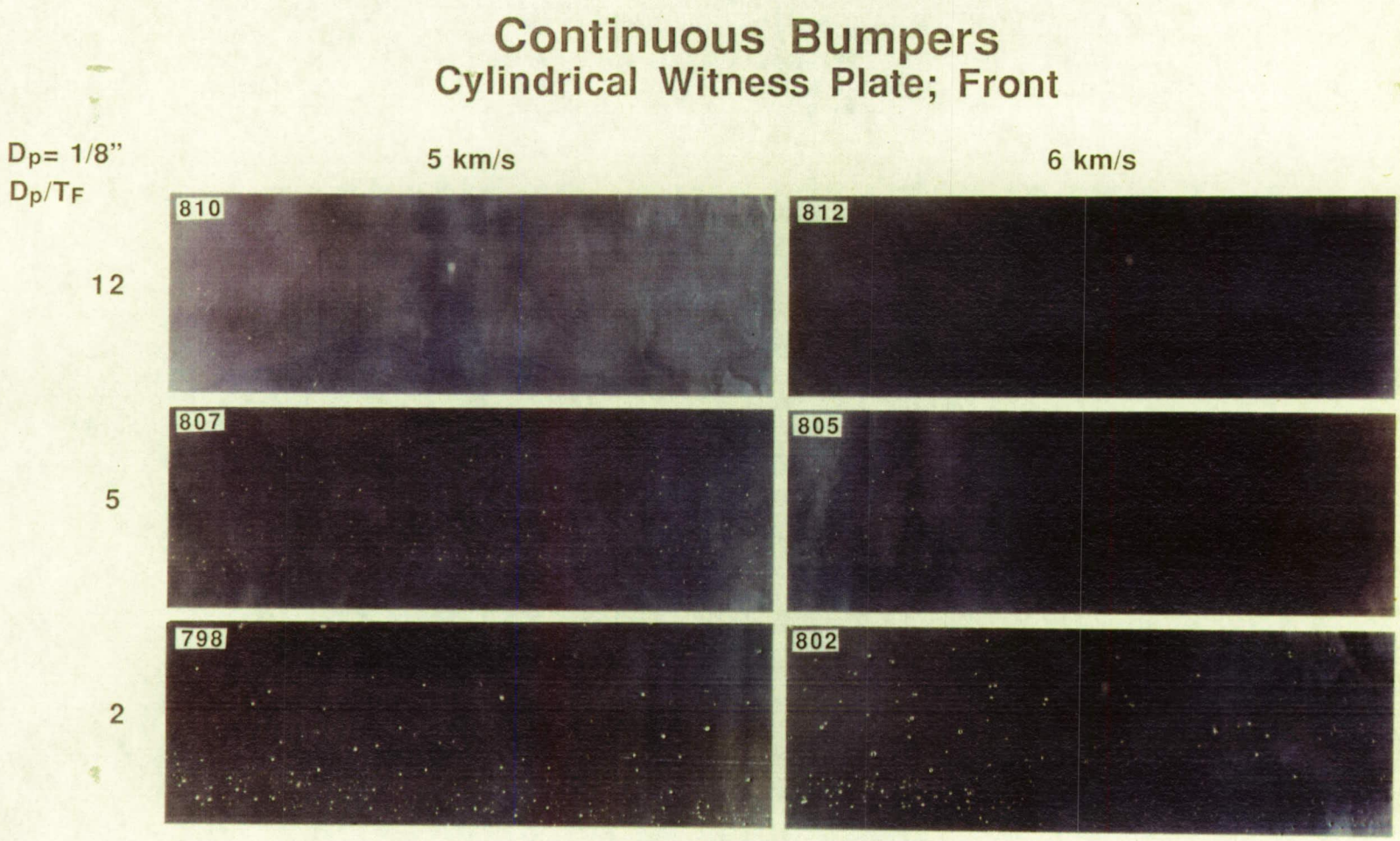

FIGFIGURE 22A. Details of the cylindrical Front Plate employing continuous targets and high-velocity impactors (for details see Text).

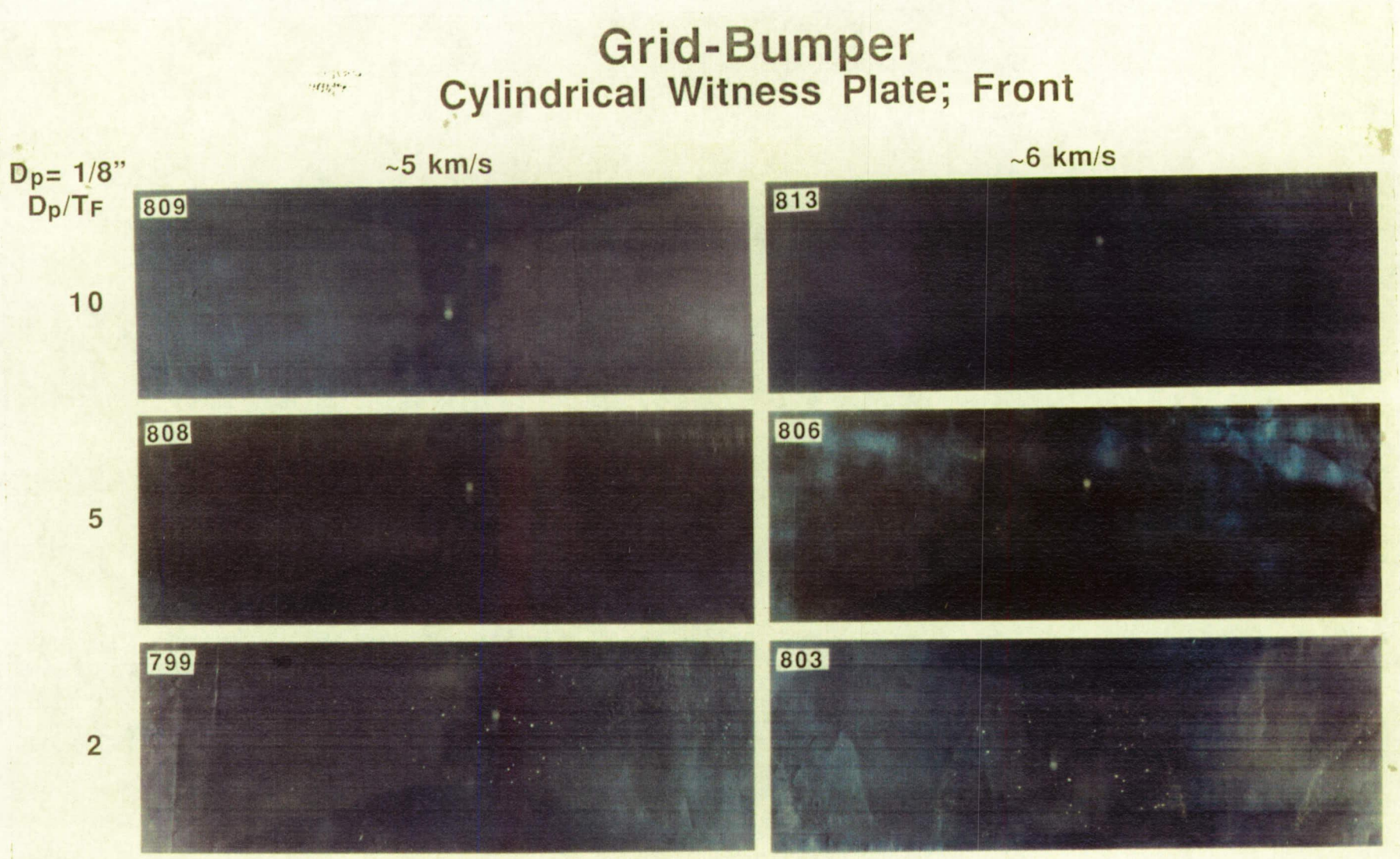

FIGURE 22B. Details of the cylindrical Front Plate employing grid-targets at experimental conditions that essentially duplicate those of Figure 22A.

Continuous Bumpers
Cylindrical Witness Plate; Rear

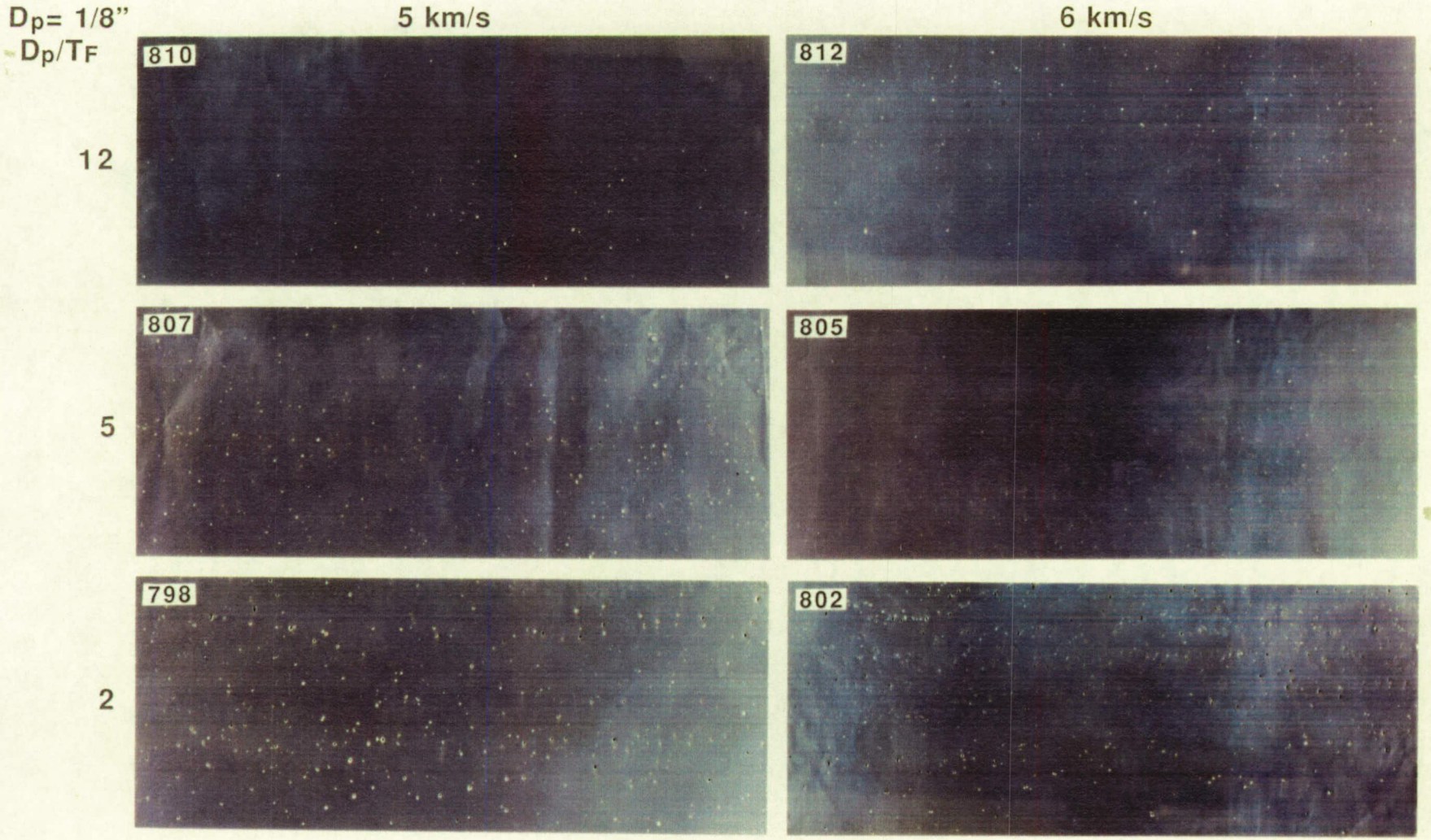

FIGURE 23A. Details of the cylindrical Rear Plates employing continuous targets and high-velocity impactors; these plates are complementary to the front plates illustrated Figure 22A.

Grid Bumper
Cylindrical Witness Plate; Rear

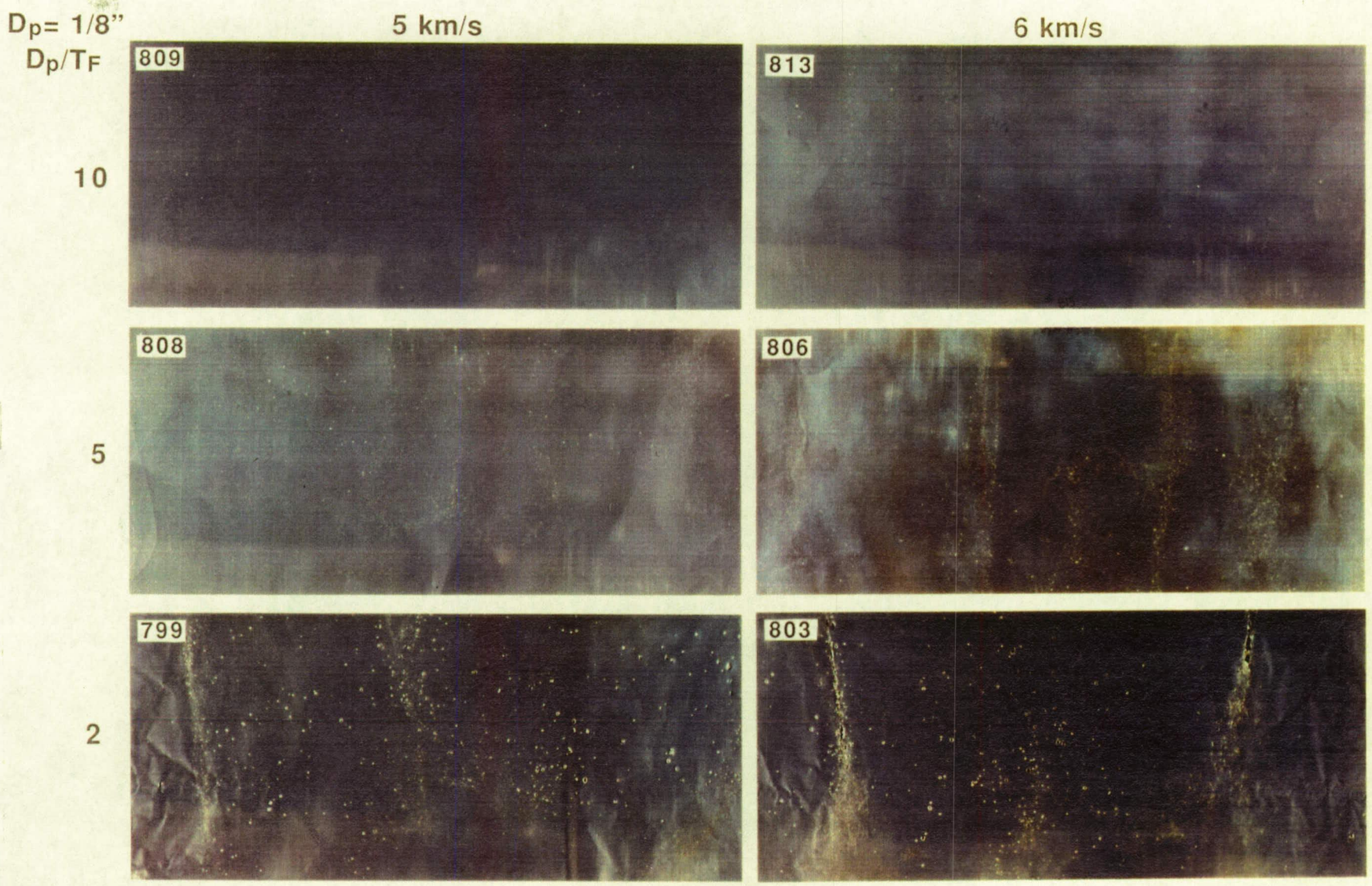

FIGURE 23B. Details of the cylindrical Rear Plates employing grid-targets and high-velocity impactors at experimental conditions that essentially duplicate those of Figure 22A and which are complementary to Figure 21B.

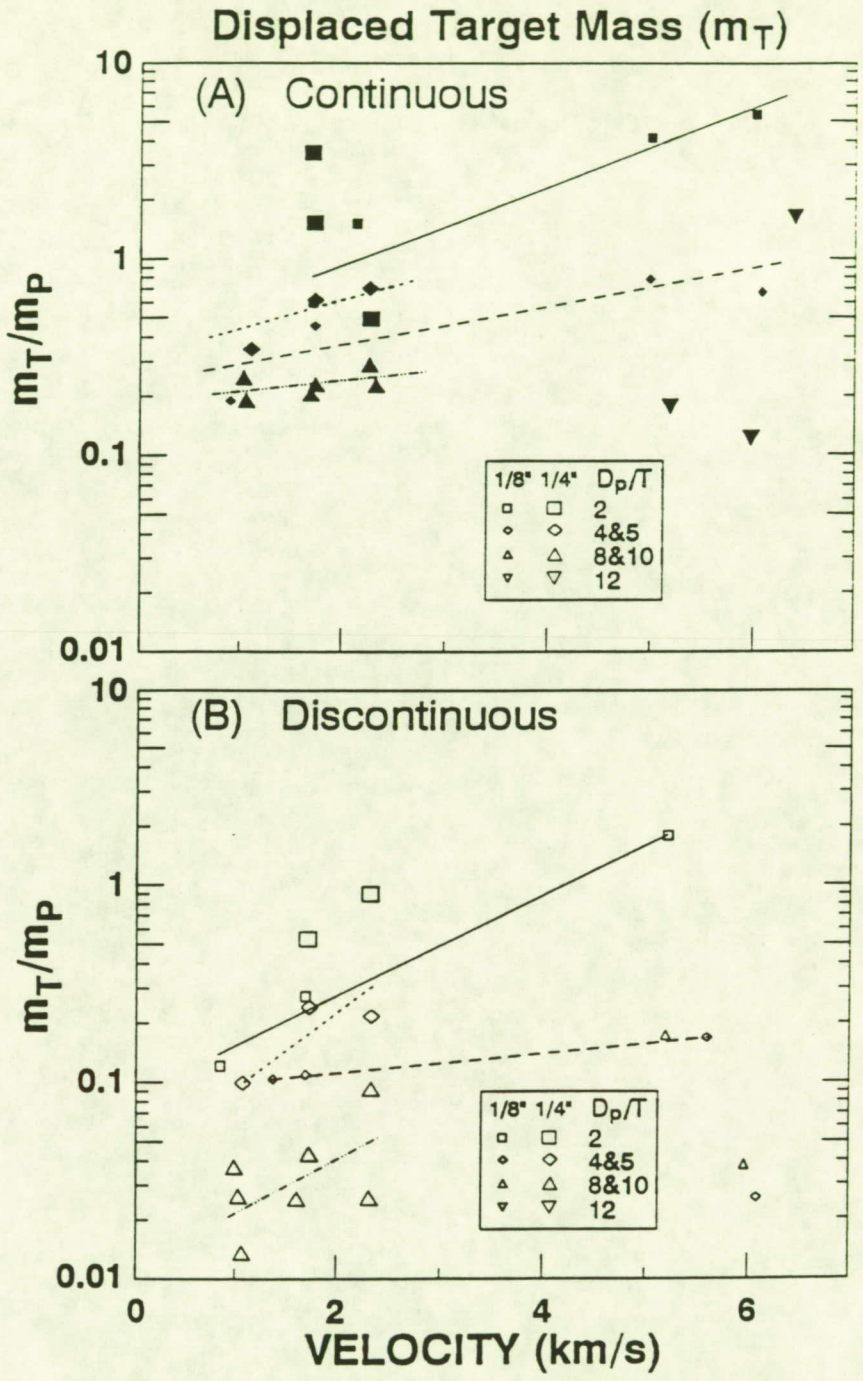

FIGURE 24. Total mass (m_T) displaced from continuous (A) and discontinuous (B) targets, normalized to projectile mass (m_P), as a function of impact velocity. Note that m_T is entirely controlled by D_P/T and depends on velocity as well. Also note that m_T is always larger for the continuous targets compared to grids and that this difference is readily a factor of 5 in many cases. Connecting lines are strictly to aid visualization of trends; they are not quantitative fits.

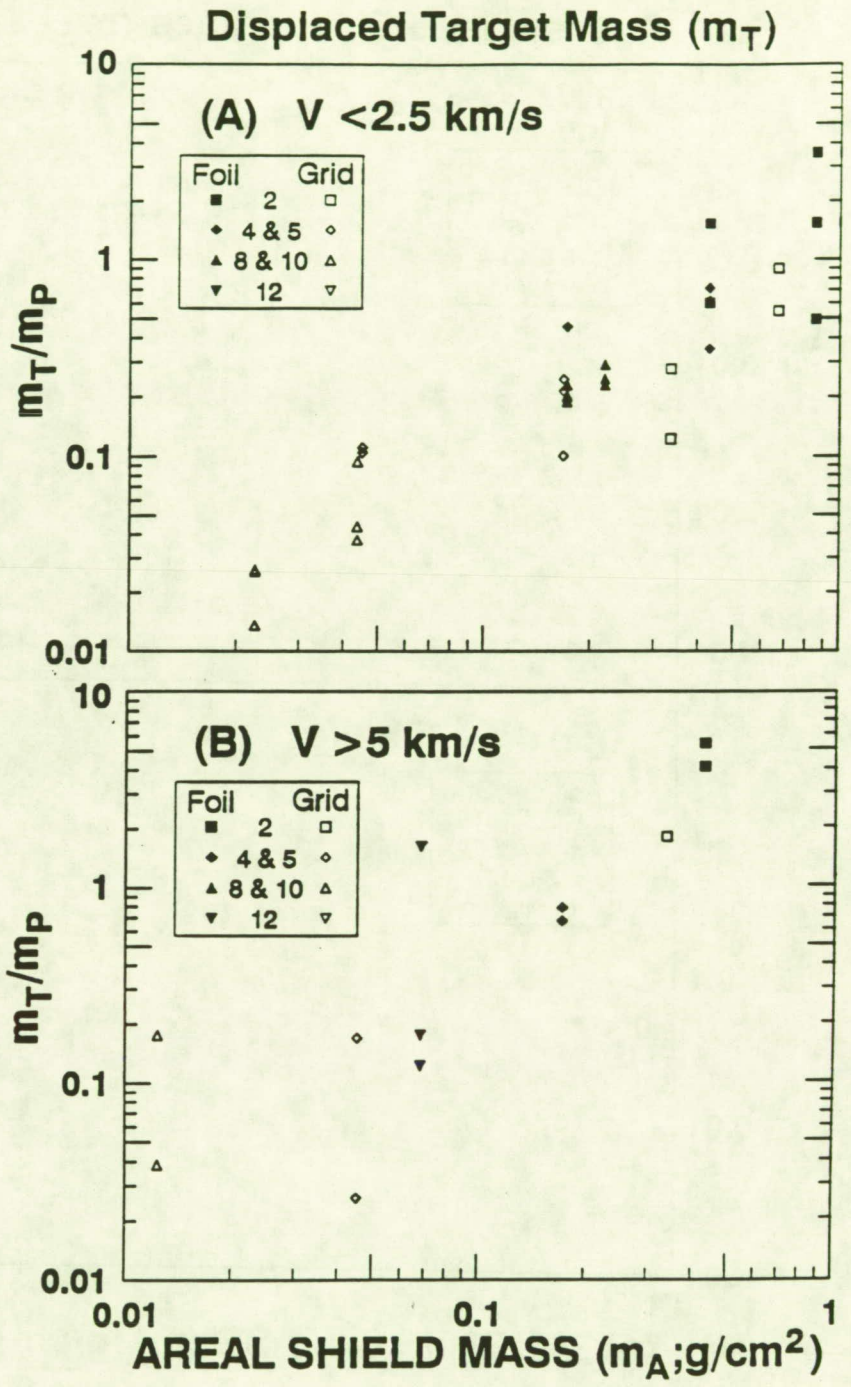

FIGURE 25. Comparisons of target mass (m_T/m_P) displaced from continuous and discontinuous targets, expressed as a function of absolute areal shield mass (m_A), separated into low- (A) and high- (B) velocity experiments. Vertical position reflects in part the difference in actual impact velocity, and in part genuine data scatter. Note the systematic trends that merely depend on m_A, but not on specific shield design.

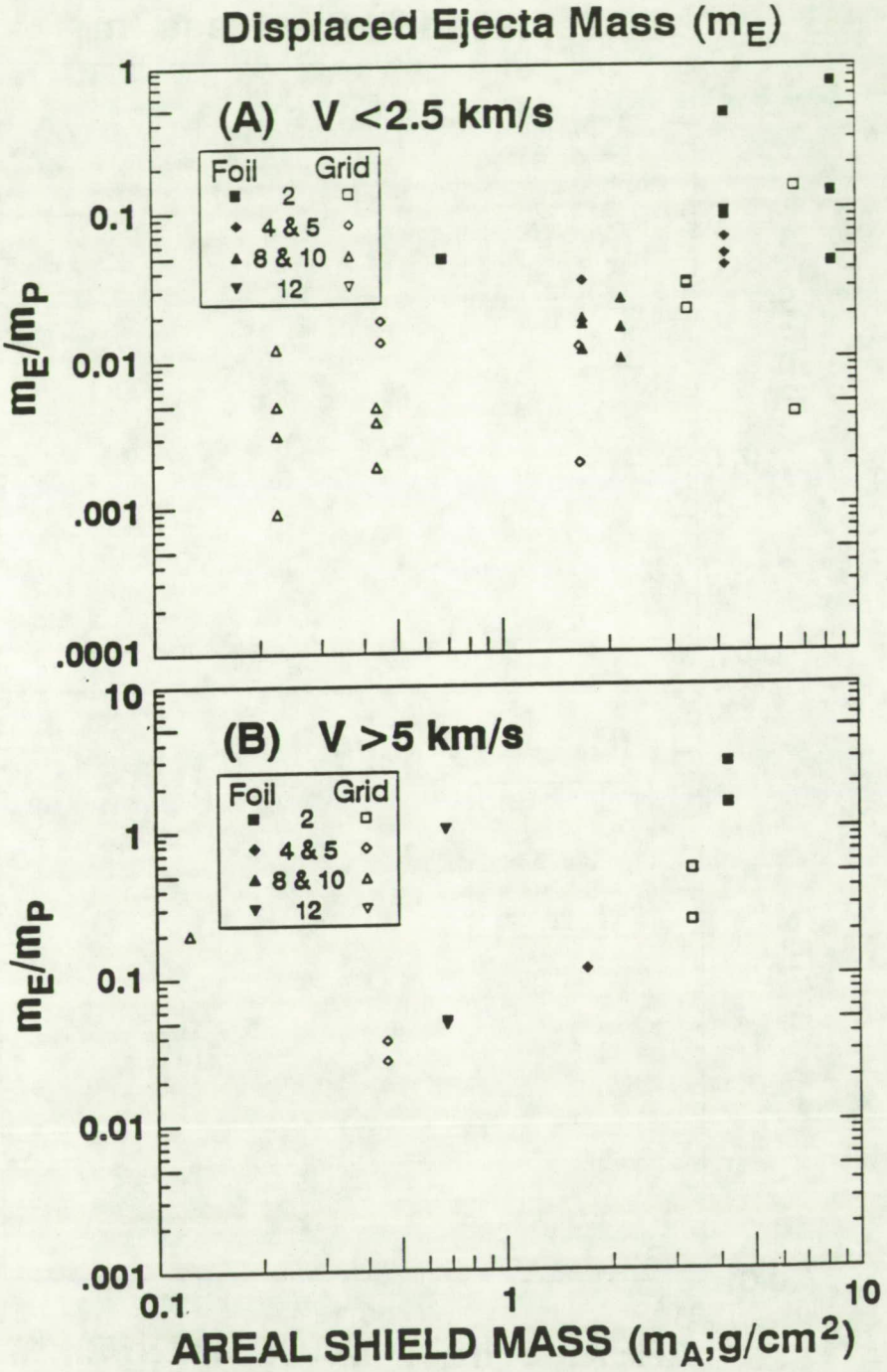

FIGURE 26. Comparison of the mass recovered in the uprange box-compartment (m_E), normalized to projectile mass (mp), that was dislodged from continuous and discontinuous targets and their witness plates versus areal shield mass (m_A), separated into low- (A) and high- (B) velocity experiments. Vertical position is in part caused by modest difference in impact velocity and in part by genuine data scatter. Note the systematic trends that depend on m_A only, and not on shield design.

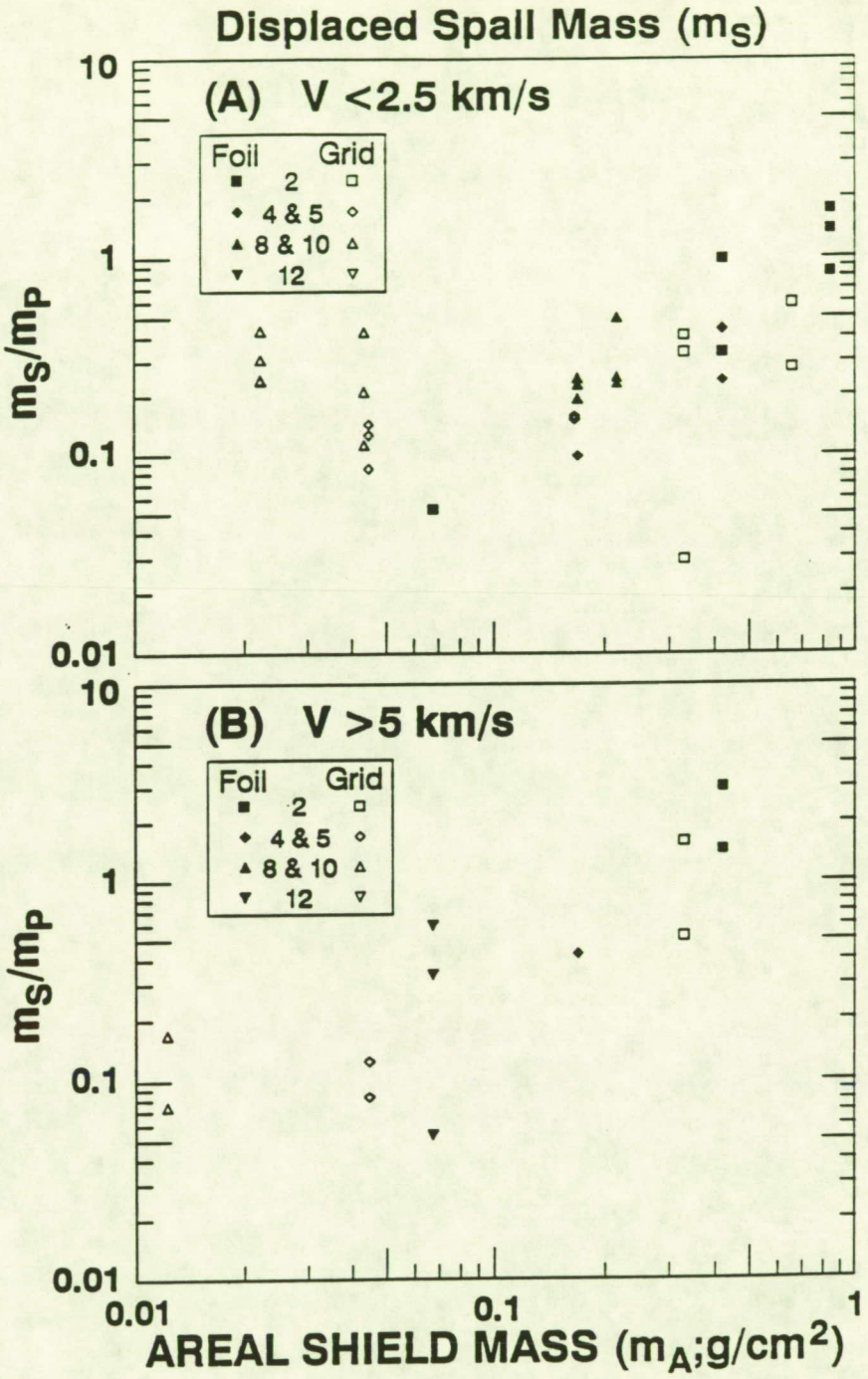

FIGURE 27. Comparison of the mass recovered in the downrange box compartment (m_S), normalized to projectile mass (m_P), that was dislodged from continuous and discontinuous targets and their witness plates as a function of areal shield mass (m_A), separated into low- (A) and high- (B) velocity experiments. Vertical position is in part velocity dependent, and in part true data scatter. Note the systematic trends that seemingly depend on m_A only, but not on specific bumper design.

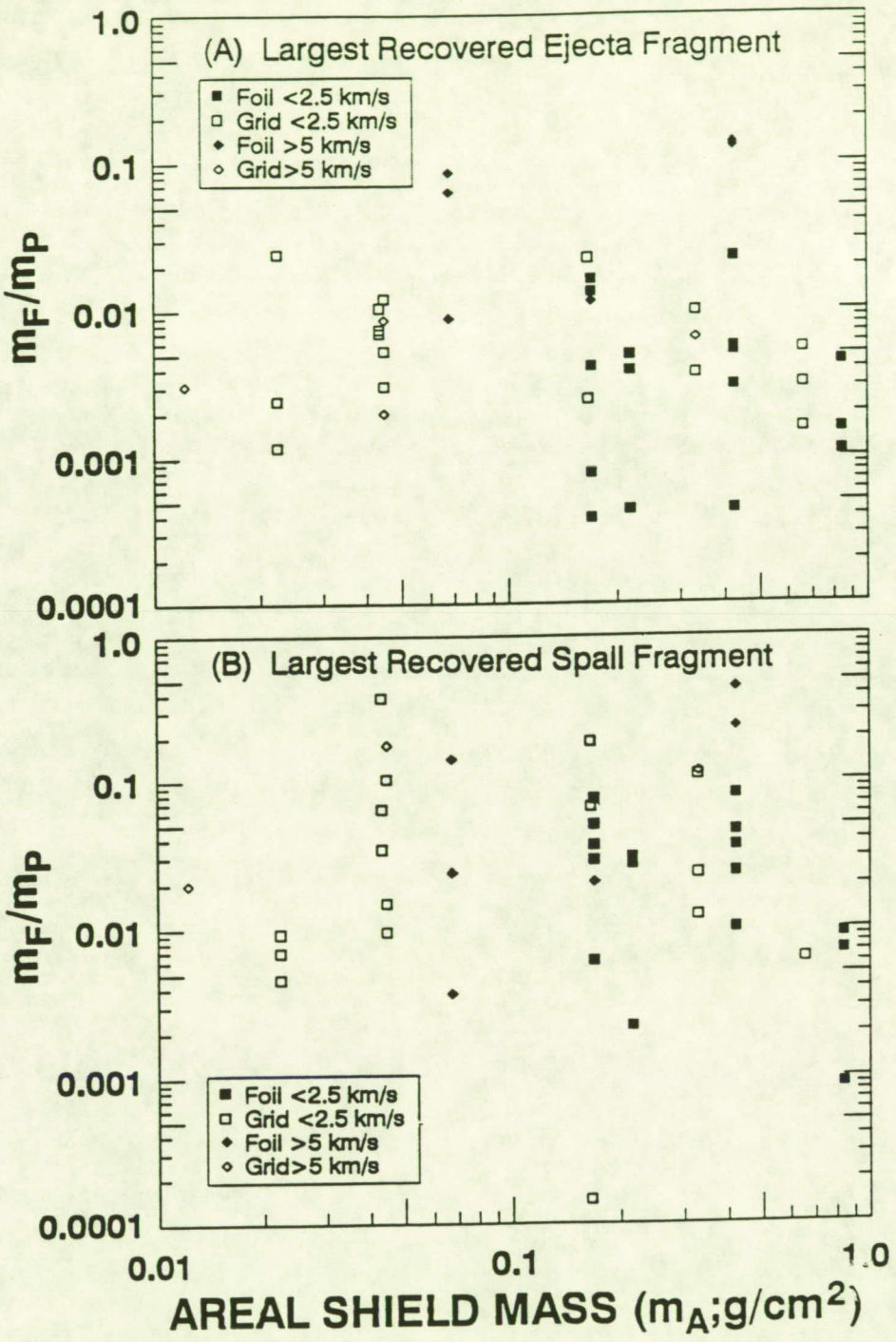

FIGURE 28. Relative mass (m_F/m_P) of the largest fragment recovered as "ejecta" (A) and "spall" (B) during penetration of continuous and discontinuous targets, but which are most likely dislodged from witness plates. Note that (1) the two bumper designs do not produce systematically different fragments, (2) the ejecta are (modestly) less massive than the spalls (3) vertical"scatter" at equivalent m_A reflects different velocity experiments, and (4) there seems to be no dependency on m_A, unlike Figures 25-27.

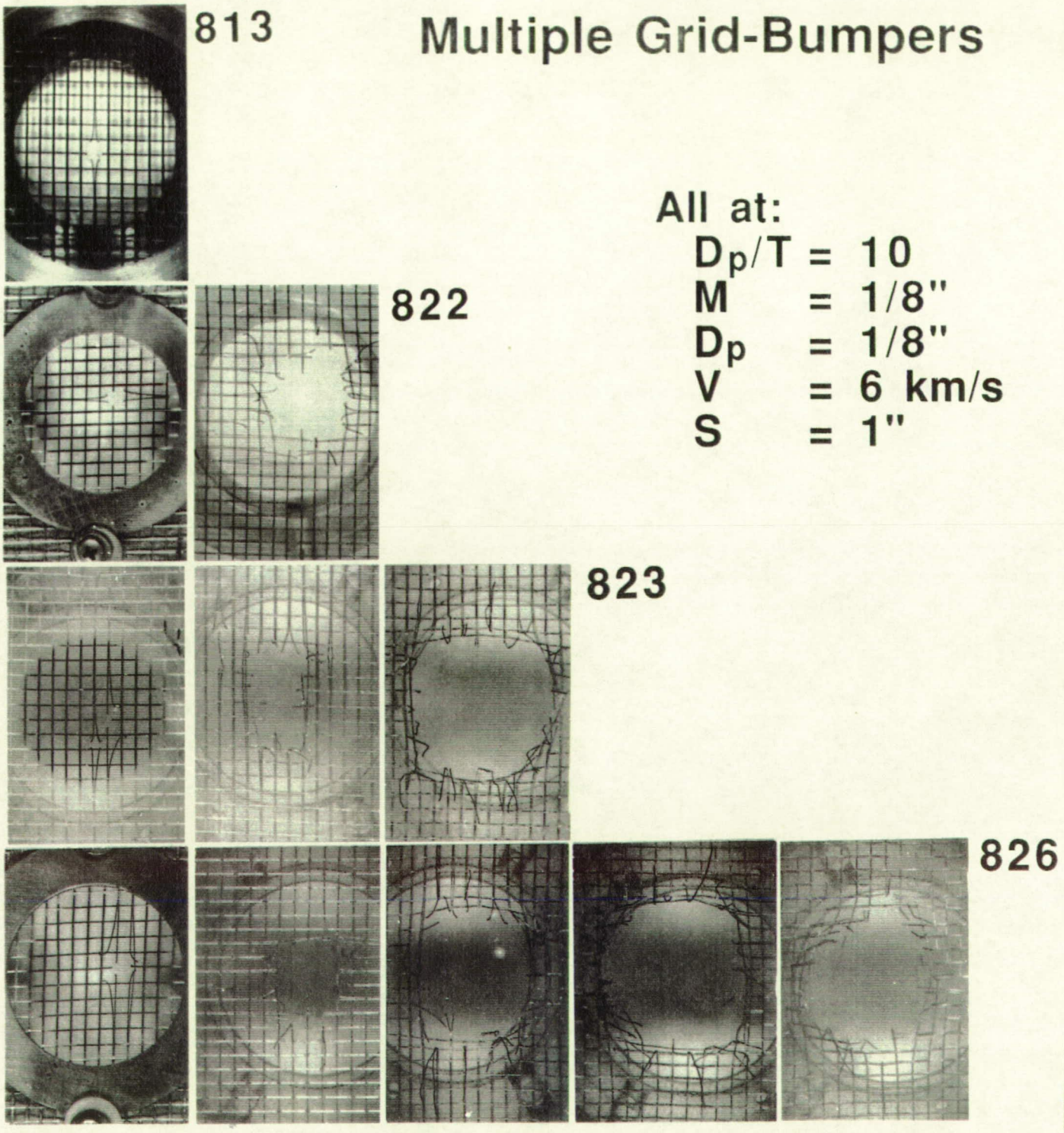

FIGURE 30. Photodocumentation of all grids employed in the multiple mesh experiments using 1/8" impactors at a nominal 6 km/s. Note the progressive enlargement of grids 2 and 3, where applicable, and that the damage (hole diameters) during experiment 826 was less on the fifth grid, than on the preceeding stack members. Also note that many wires are simply deformed, rather than dislodged. Also, experiment 823, unfortunately, was contaminated with a small piece of gun debris (small penetration on mesh 1), that produced a noncentro-symmetric area of damage on grid 2, possibly affecting grid 3 as well.

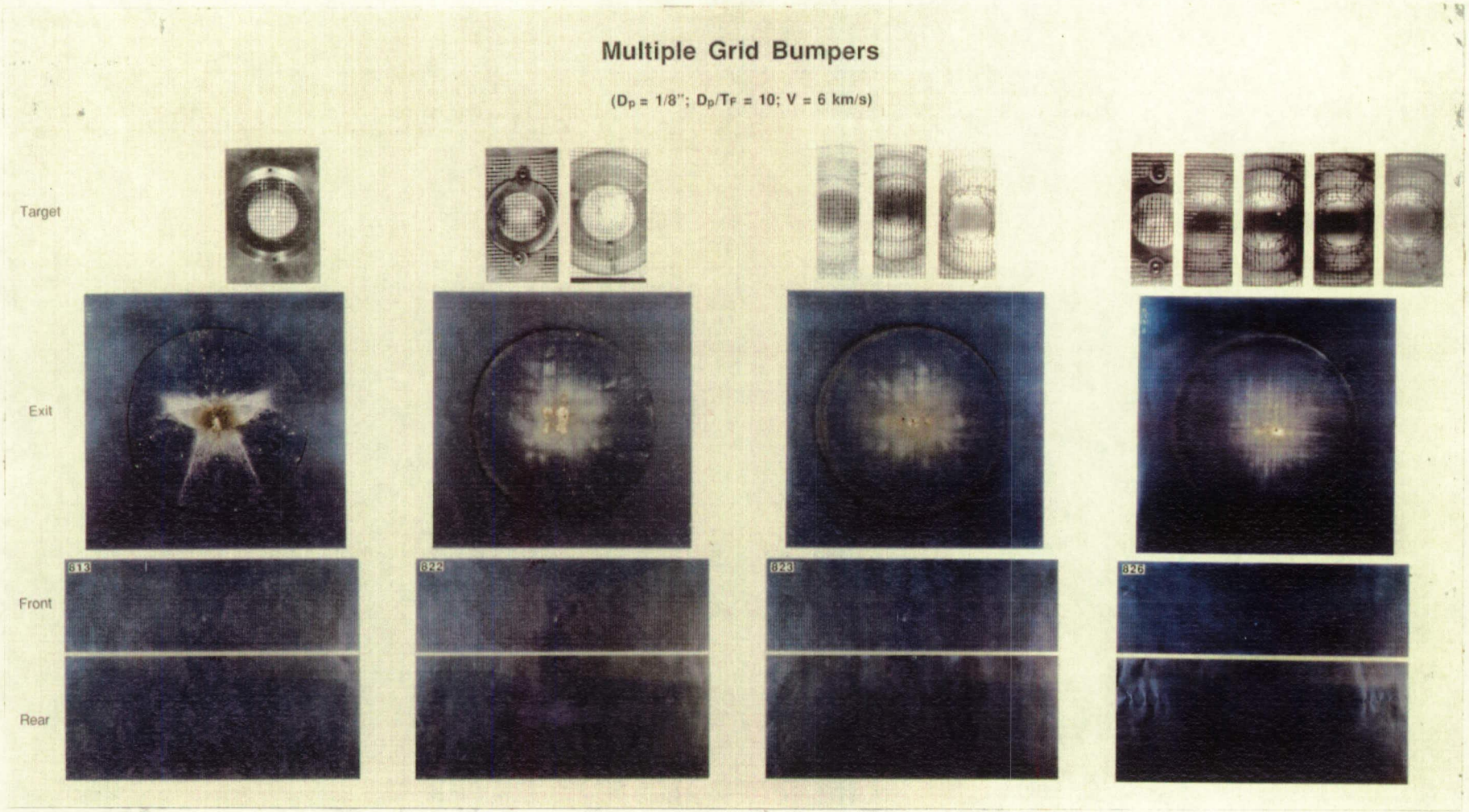

FIGURE 29. Overview of the multiple-grid experiments employing 1, 2, 3 and 5 grids, each of $D_p/T=10$, separated by 1" (2.5 cm). The progressive role of successive grids is well illustrated, as is the relatively undamaged nature of the cylindrical Front and Rear Plates; note that the "worst case" experiment (813) was introduced and illustrated in many of the preceding figures that address single grid penetrations.

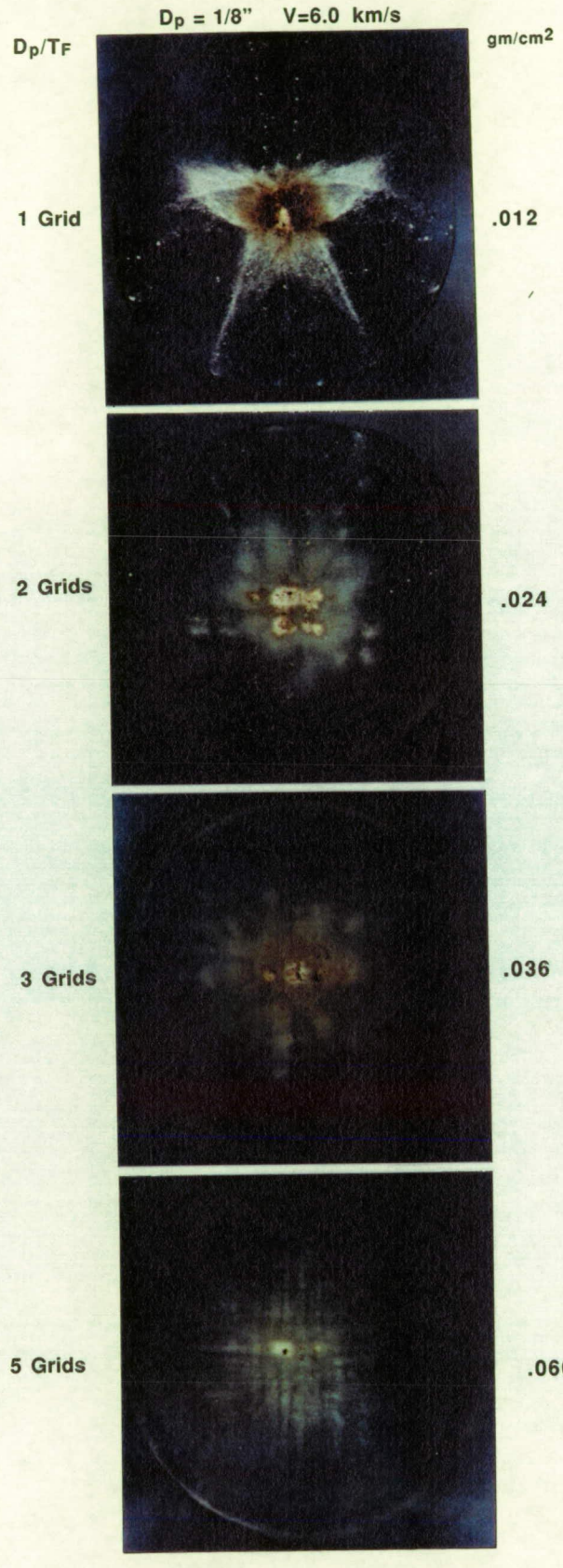

FIGURE 31. Photodocumentation of Exit Plate spray patterns following penetrations of 1, 2, 3 and 5 mesh-bumpers, each of $D_p/T=10$. Note the progressive elimination of undesirable debris clusters, the increased comminution of debris fragments, and the decreased overall dispersion for the 5-mesh case, all favorable performance criteria for any bumper design.

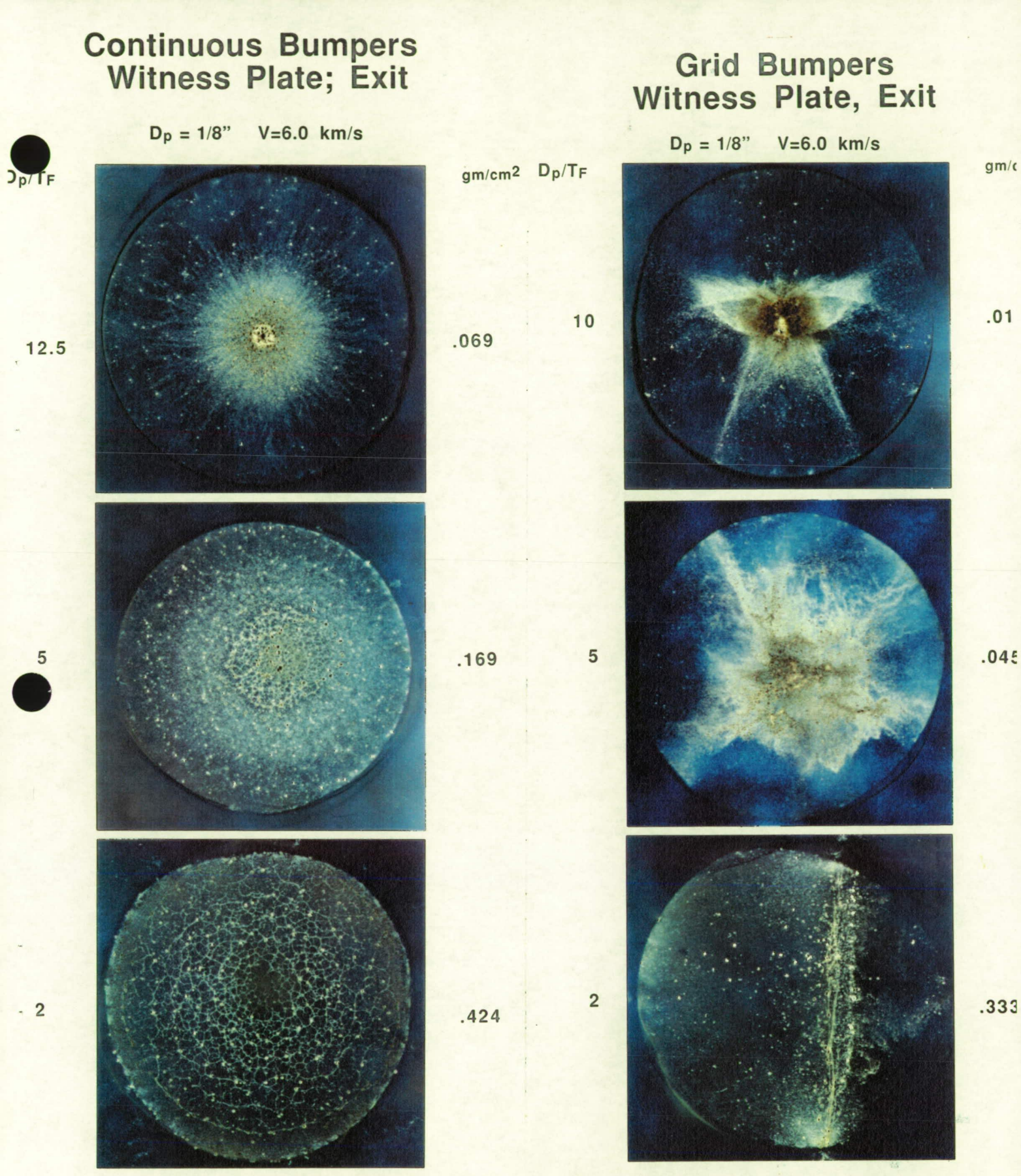

FIGURE 32. Summary type documentation of Exit Plate spray patterns of continuous and single grid penetrations, generated under essentially identical conditions that are comparable to those of Figure 31 (*i.e.*, all at 6 km/s, employing a 1/8" projectile and different D_p/T or m_A [g/cm^2] that overlap among the three concepts investigated). Note the difference between equivalent D_p/T and associated m_A values and that the multiple grid-bumper out performs the other designs at very modest shield mass.

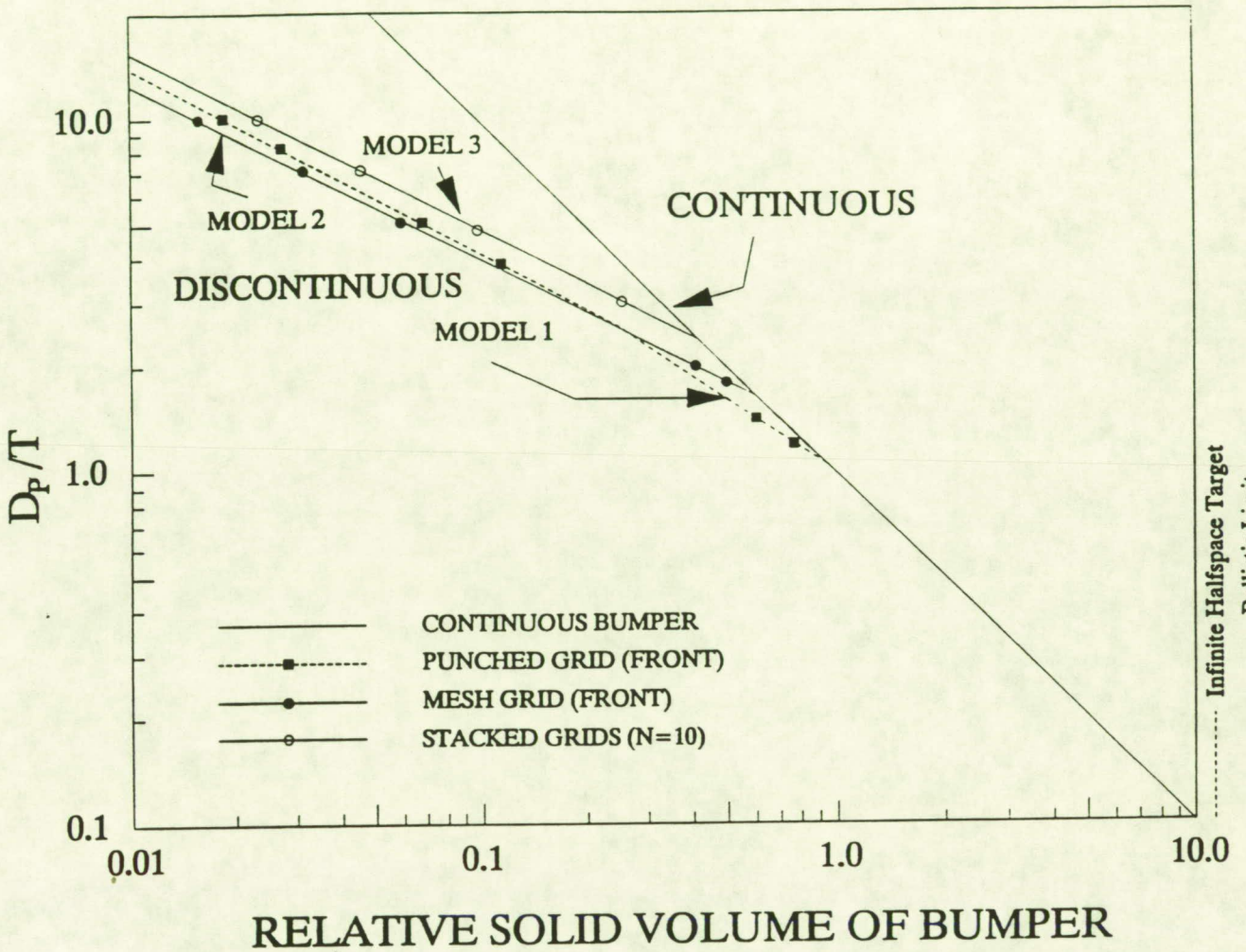

FIGURE 33. Relative volumes of various bumper designs, based on strictly geometric designs and arguments; if the bumpers were manufactured from material of identical density, the volume relations would translate directly into mass relations. "Unity" is defined as the volume represented by a bumper of thickness D_p ($D_p/T=1$). Note that any weave, employing round wire profiles (dots; Model 2)) contains more mass than a continuous sheet at $D_p/T<2.5$, due to wire overlaps and mass duplication at intersections. The square symbols (Model 1) represent square grid members and thus deviate from the continuous sheet at all $D_p/T>1$. However, round profiles/cross sections scale with πr^2, while squares scale with $4r^2$, the reason why thin round wires become more favorable at large D_p/T, after compensating for the overlap-related, excess mass. The third line (Model 3) of the discontinuous bumpers represents a ten-member bumper stack, with each bumper scaled according to Figure 1.

TABLE 1. Lists of the detailed initial experimental conditions sorted by experiment number. V=Projectile Velocity, D_p=Projectile Diameter, T=Thickness of Bumper, M_c=Mesh Dimensions (center-to-center distance), m_A=Areal shield mass, m_P=Projectile mass, m_T=Target mass displaced, m_E=Recovered ejecta mass (uprange), and m_S=Recovered spall mass (downrange).

	Shot	V	D_p	T	M_c	D_p/T	m_A	m_P	m_T	m_E	m_S
		Km/s	inches	inches	inches		g/cm^2	grams	grams	grams	grams
FOIL	798	5.00	0.125	0.063		2.00	0.424	0.0373	0.1549	0.0568	0.0542
GRID	799	5.20	0.125	0.063	0.125	2.00	0.333	0.0364	0.0661	0.0198	0.0190
FOIL	802	6.02	0.125	0.063		2.00	0.424	0.0303	0.1655	0.0885	0.0919
GRID	803	5.91	0.125	0.063	0.125	2.00	0.333	0.0373		0.0089	0.0592
FOIL	805	6.08	0.125	0.025		5.00	0.170	0.0373	0.0252	0.0000	0.0000
GRID	806	6.08	0.125	0.023	0.125	5.43	0.045	0.0374	0.0010	0.0010	0.0031
FOIL	807	5.00	0.125	0.025		5.00	0.170	0.0373	0.0294	0.0042	0.0160
GRID	808	5.60	0.125	0.023	0.125	5.43	0.045	0.0374	0.0064	0.0014	0.0046
GRID	809	5.19	0.125	0.012	0.125	10.42	0.012	0.0374	0.0066	0.0000	0.0063
FOIL	810	5.19	0.125	0.010		12.50	0.068	0.0373		0.0018	0.0020
FOIL	812	5.98	0.125	0.010		12.50	0.068	0.0375	0.0046	0.0018	0.0126
GRID	813	5.96	0.125	0.012	0.125	10.42	0.012	0.0373	0.0014	0.0074	0.0028
FOIL	815	6.41	0.125	0.010		12.50	0.068	0.0373		0.0389	0.0223
GRID	3231	1.71	0.250	0.125	0.250	2.00	0.666	0.2990	0.1634	0.0000	0.0000
GRID	3233	2.31	0.250	0.125	0.250	2.00	0.666	0.2990	0.2688	0.0431	0.1756
GRID	3234	0.68	0.250	0.125	0.250	2.00	0.666	0.2990		0.0013	0.0827
GRID	3239	1.63	0.125	0.063	0.125	2.00	0.333	0.0379		0.0008	0.0154
FOIL	3245	1.73	0.250	0.063		4.00	0.424	0.2990	0.1840	0.0153	0.1300
FOIL	3246	1.73	0.250	0.125		2.00	0.848	0.2990	0.4636	0.0400	0.4144
GRID	3247	1.72	0.250	0.063	0.250	4.00	0.166	0.2990	0.0733	0.0000	0.0000
FOIL	3248	1.74	0.250	0.032		7.81	0.217	0.2990	0.0684	0.0049	0.0747
GRID	3249	1.73	0.250	0.032	0.250	7.81	0.044	0.2990	0.0131	0.0014	0.0626
FOIL	3250	2.27	0.250	0.032		7.81	0.217	0.2990	0.0871	0.0077	0.0694
GRID	3251	2.33	0.250	0.032	0.250	7.81	0.044	0.2990	0.0282	0.0011	0.0335
GRID	3252	0.99	0.250	0.032	0.250	7.81	0.044	0.2990	0.0112	0.0006	0.1265
FOIL	3253	1.03	0.250	0.032		7.81	0.217	0.2990	0.0740	0.0030	0.1502
GRID	3259	1.07	0.250	0.023	0.250	10.87	0.023	0.2990	0.0041	0.0003	0.0920
FOIL	3260	1.07	0.250	0.025		10.00	0.170	0.2990	0.0567	0.0035	0.0679
GRID	3261	1.03	0.250	0.023	0.250	10.87	0.023	0.2990	0.0079	0.0015	0.1291
GRID	3262	1.62	0.250	0.023	0.250	10.87	0.023	0.2990	0.0076	0.0009	0.0724
FOIL	3263	1.70	0.250	0.025		10.00	0.170	0.2990	0.0609	0.0052	0.0735
GRID	3264	2.32	0.250	0.023	0.250	10.87	0.023	0.2990	0.0077	0.0036	0.0715
FOIL	3265	2.34	0.250	0.025		10.00	0.170	0.2990	0.0687	0.0057	0.0576
FOIL	3266	2.27	0.250	0.063		4.00	0.424	0.2990	0.2119	0.0198	0.1310
GRID	3267	2.31	0.250	0.063	0.250	4.00	0.166	0.2990	0.0640	0.0036	0.0467
GRID	3268	1.06	0.250	0.063	0.250	4.00	0.166	0.2990	0.0300	0.0006	0.0450
FOIL	3269	1.11	0.250	0.063		4.00	0.424	0.2990	0.1047	0.0128	0.0717
FOIL	3275	2.28	0.250	0.125		2.00	0.848	0.2990	0.1484	0.0135	0.2535
FOIL	3276	1.70	0.250	0.125		2.00	0.848	0.1280	0.4543	0.0972	0.2227
FOIL	3282	1.72	0.125	0.063		2.00	0.424	0.0379	0.0227	0.0038	0.0127
GRID	3285	1.69	0.125	0.063	0.125	2.00	0.333	0.0379	0.0105	0.0012	0.0011
FOIL	3286	1.74	0.125	0.025		5.00	0.170	0.0379	0.0173	0.0000	0.0000
GRID	3287	1.69	0.125	0.023	0.125	5.43	0.045	0.0379	0.0042	0.0007	0.0048
GRID	3288	1.37	0.125	0.023	0.125	5.43	0.045	0.0379	0.0040	0.0000	0.0032
FOIL	3289	0.91	0.125	0.025		5.00	0.170	0.0379	0.0072	0.0013	0.0037
GRID	3290	0.79	0.125	0.023	0.125	5.43	0.045	0.0379	0.0001	0.0005	0.0054
GRID	3293	0.84	0.125	0.063	0.125	2.00	0.333	0.0379	0.0047	0.0000	0.0000
FOIL	3294	0.70	0.125	0.063		2.00	0.424	0.0379	0.0005	0.0178	0.0000
FOIL	3300	2.14	0.125	0.063		2.00	0.424	0.0379	0.0581	0.0035	0.0375
GRID	3313	2.22	0.125	0.063	0.125	2.00	0.333	0.0379		0.0013	0.0126
FOIL	3355	2.12	0.125	0.500		0.25	3.391	0.0379		0.0043	0.0000

REPORT DOCUMENTATION PAGE

Form Approved
OMB No. 0704-0188

1. AGENCY USE ONLY *(Leave blank)*

2. REPORT DATE
April 1992

3. REPORT TYPE AND DATES COVERED
Technical Memorandum

4. TITLE AND SUBTITLE
Comparison of Continuous and Discontinuous Collisional Bumpers: Dimensionally Scaled Impact Experiments Into Single Wire Meshes

5. FUNDING NUMBERS

6. AUTHOR(S)
Friedrich Hörz, Mark Cintala, Thomas See, Ronald Bernhard, Frank Cardenas, William Davidson, Jerry Haynes

7. PERFORMING ORGANIZATION NAME(S) AND ADDRESS(ES)
Solar System Exploration Division
National Aeronautics and Space Division
Johnson Space Center
Houston, Texas 77058

8. PERFORMING ORGANIZATION REPORT NUMBER
S-676

9. SPONSORING / MONITORING AGENCY NAME(S) AND ADDRESS(ES)
National Aeronautics and Space Administration
Washington, D.C. 20546-001

10 SPONSORING / MONITORING AGENCY REPORT NUMBER
NASA-TM-104749

11. SUPPLEMENTARY NOTES
Friedrich Hörz and Mark Cintala: Johnson Space Center, Houston, Texas; Thomas See, Ronald Bernhard, Frank Cardenas, William Davidson, and Jerry Haynes: Lockheed Engineering and Sciences Company, Houston, Texas

12a. DISTRIBUTION / AVAILABILITY STATEMENT
Unclassified/Unlimited Publicly Available
Subject Category 39

12b. DISTRIBUTION CODE

13. ABSTRACT *(Maximum 200 words)*

An experimental inquiry into the utility of discontinuous bumpers was conducted to investigate the collisional outcomes of impacts into single grid-like targets and to compare the results with more traditional bumper designs that employ continuous sheet stock. We performed some 35 experiments using 6.3 and 3.2 mm diameter spherical soda lime glass projectiles at low velocities (<2.5 km/s) and 13 at velocities between 5 and 6 km/s, using 3.2 mm spheres only. The thrust of the experiments related to the characterization of collisional fragments as a function of target thickness or areal shield mass of both bumper designs. The primary product of these experiments was witness plates that record the resulting population of collisional fragments. Substantial interpretative and predictive insights into bumper performance were obtained. All qualitative observations (on the witness plates) and detailed measurements of displaced masses seem simply and consistently related only to bumper mass available for interaction with the impactor. This renders the grid bumper into the superior shield design. These findings present evidence that discontinuous bumpers are a viable concept for collisional shields, possibly superior to continuous geometries.

14. SUBJECT TERMS
Collisional Bumpers, Penetration, Whipple Shields, Mesh-Bumpers

15. NUMBER OF PAGES

16. PRICE CODE

17. SECURITY CLASSIFICATION OF REPORT	18. SECURITY CLASSIFICATION OF THIS PAGE	19. SECURITY CLASSIFICATION OF ABSTRACT	20. LIMITATION OF ABSTRAC
Unclassified	Unclassified	Unclassified	